Investigating New Materials and Understanding the Ambipolar Qualities of Organic Small Molecules for use in Organic Photovoltaics.

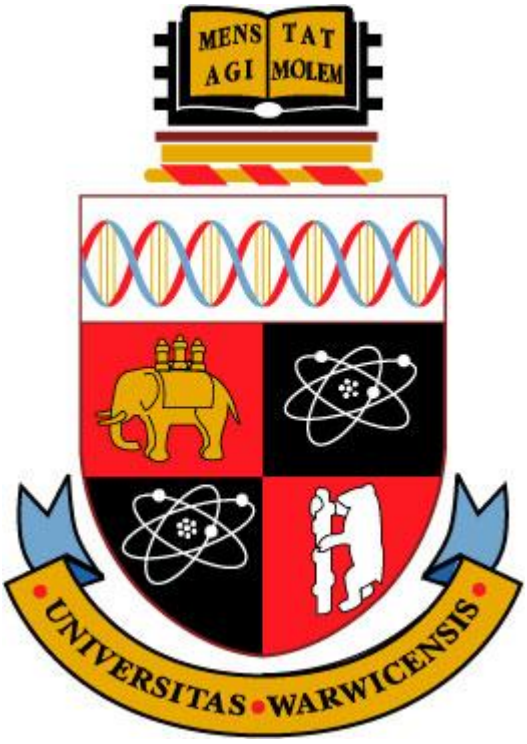

By Nicola Louise Beaumont

A thesis submitted for the degree of Doctor of Philosophy

Department of Chemistry

University of Warwick

May 2013

Abstract

Organic photovoltaics (OPVs) have huge potential for competing with current inorganic photovoltaics in the search for a reliable, renewable source of energy. It is thought that only ~ 10 % efficiency is necessary for commercialisation and also allows avenues towards flexible, compact, lightweight optoelectronics, with current certified efficiencies already at 12 %! Although the current efficiencies have surpassed expectations in order to continue the high progress new materials need to be investigated. Through understanding current materials and utilising new donor and acceptor materials the hopes of achieving higher efficiencies are realistic.

Halogenation as a method to modify current organic semiconductors materials has successfully been demonstrated with minimal change to the optical properties. Successful modification of copper phthalocyanines (CuPc) to the fluorinated F_{16} CuPc derivative resulted in a large change in ionisation potential allowing for its use as an acceptor. This thesis will discuss the modification of 6,13-bis(triisopropylsilylethynyl)pentacene (TIPSEpent) via chlorination in the hopes of achieving a more efficient donor material in single heterojunction devices. Through addition of electron withdrawing groups, the molecular frontier orbitals can be tuned to allow for improved stability towards C_{60} in solution, larger ionisation potentials which allow for larger interface gaps when used in devices, resulting in improvements in open circuit voltage (V_{oc}), short circuit current (J_{sc}) and power conversion efficiency.

The second part of the thesis will concentrate on the ambipolar qualities of (sub)phthalocyanines and their use as acceptors in conjunction with both the underused acene, tetracene (**Chapter 5**) and the more widely studied pentacene (**Chapter 6**). To obtain a strong understanding of using boron subphthalocyanine chloride (SubPc), Cl_6-SubPc and ClAlPc as acceptors, UV –Vis absorption, atomic force microscopy (AFM), photoluminescence (PL), photoelectron spectroscopy (PES), space charge limited current (SCLC) theory to gain charge mobilities and devices were explored.

Contents

Declaration

I declare that this thesis contains an account of my research carried out in the Department of Chemistry at the University of Warwick between July 2009 and Dec 2012 under the supervision of Prof. Tim Jones and Dr. Ross Hatton. The research reported here has not been submitted, either wholly or in part, in this or any other academic institution for admission to a higher degree.

The TIPSE – pentacene derivatives were synthesised by Dr. Amelie Duraud under supervision of Professor Mike Shipman from the Department of Chemistry at the University of Warwick. All data on the solutions, thin film characterisation and device manufacture was collected by the author. Preliminary work on the TIPSEpent parent acene was done in collaboration with Dr. L-J. Pegg and Dr. R. Da Campo.

The synchrotron based experiments were performed at Beamline X1B, National Synchrotron Light Source, Brookhaven National Laboratory in collaboration with Boston University. Assistance with data collection was provided by Dr. Sang Wan Cho, Dr. Alex deMasi, Dr. Andrew Preston and David Newby. All of the remaining data collection was performed by the author. The data analysis and interpretation was all performed by the author.

Acknowledgements

First and foremost I would like to thank my supervisors as without their help I would never have reached the end!

A massive thank you must go to Professor Tim Jones who allowed me to conduct the research I was interested in and allowed me to travel to France, Belgium, America and Australia during my PhD to present my findings! Without his support and guidance I would not have been able to finish. Thanks to Dr. Ross Hatton for his help and support from my MChem project to the end. Thanks must go to Professor Kevin Smith, Dr. Sang Wan Cho, Dr Andrew Preston, Dr. Alex De Masi and Dave Newby from Boston University for allowing me to join their group at Brookhaven National Laboratory and for making my short time their enjoyable! Also, to our collaborators at Warwick, Dr. Amelie Duraud and Prof. Mike Shipman, thank you for the opportunity to be involved in something new and exciting!

A great amount of thanks must go to the group, in particular Paul, Ian, Stefan, Tom and Raff, who supported me and my insanity from start to finish. You guys adopted me in my Mchem (after chucking tea over me of course) and have helped me with my work and coping in general throughout the time I've known you so thank you so much for that! Luke and Edd: You two have had to put up with me not only through undergrad but also through a PhD! Edd you even lived with me in fourth year - I don't know how you have managed to put up with me but I appreciate it all! Chloe, I haven't been able to shake you since your MChem but I wouldn't have it any other way! Nat and Gavin you guys have not nearly known me as long but I am thankful for all the amusing moments we have shared in that short time! Good luck with the write ups!

Dawn and Ricky: I wish you guys all the best in finishing and I hope you enjoy your PhDs as much as I enjoyed mine!

Last but not least, I'd like to thank my Mike, my parents and my brother. Without your unconditional love and support I wouldn't be where I am today!

List of publications

Increased efficiency in small molecule organic photovoltaic cells through electrode modification with self-assembled monolayers, **N. Beaumont,** I. Hancox, P. Sullivan, R. A. Hatton and T. S. Jones, **Energy Environ. Sci**., 2011, **4**, 1708-1711

Boron Subphthalocyanine Chloride as an Electron Acceptor for High-Voltage Fullerene-Free Organic Photovoltaics, **N. Beaumont**, S. W. Cho, P. Sullivan, D Newby, K. E. Smith, Tim. S. Jones. **Adv. Funct. Mater.** 2012, **22** (3), 561 - 566

Other authorships

The effect of a MoO_x hole-extracting layer on the performance of organic photovoltaic cells based on small molecule planar heterojunctions, I. Hancox, P. Sullivan, K.V. Chauhan, **N. Beaumont,** L.A. Rochford, R.A. Hatton and T.S. Jones, **Organic Electronics**, 2010, **11**, 2019-2025.

Halogenated Boron Subphthalocyanines as Light Harvesting Electron Acceptors in Organic Photovoltaics, Paul Sullivan, Amelie Duraud, lan Hancox, **Nicola Beaumont,** Giorgio Mirri, James H.R. Tucker, Ross A. Hatton, Michael Shipman, Tim S. Jones, **Advanced Energy Materials**, 2011, **1**, 352.

Submitted or *in prep*.

Ambipolar characteristics of Subphthalocyanines in Organic Photovoltaics. **N.Beaumont,** J. S. Castucci, P. J. Sullivan, I. Hancox, Z-H. Lu, T. P. Bender and Tim. S. Jones

Phthalocyanines as Electron Acceptors in Fullerene Free Pentacene Organic Photovoltaics**. N. Beaumont,** I. M. Hancox, P. Sullivan and Tim. S. Jones

Stability mechanisms in Fullerene Free Pentacene cells **N. Beaumont,** I. Hancox, P. Sullivan and T. S. Jones.

Chlorinated 6,13-Bis(triisopropylsilylethynyl)pentacene Derivatives as Electron Donors for Organic Photovoltaics **N. Beaumont,** A. Duraud, L-J. Pegg, R.Da Campo, R. A. Hatton, M. Shipman, and Tim S. Jones

Increased photocurrent in small molecule organic solar cells through a dual heterojunction cascade structure. E.New, **N.Beaumont**, P.J.Sullivan and T. S. Jones.

High voltage hybrid organic photovoltaics using a zinc oxide acceptor alongside a boron subphthalocyanine chloride donor. C. Dearden, M. Walker, I.Hancox, **N. Beaumont**, J. Mudd, P. Sullivan, C. McConville and T. S. Jones.

Exciton Diffusion Length Measurement on Boron Subphthalocyanine Chloride and derivatives. T. Howells, **N. Beaumont** and T.S. Jones

List of abbreviations

- AFM Atomic force microscopy
- AM Air mass
- AO Atomic orbital
- BE Binding energy
- BHJ Bulk heterojunction
- CB Conduction band
- CT Charge transfer
- CV Cyclic voltammetry
- CELIV Charge extracted by linearly increasing voltage
- D/A Donor/Acceptor
- DSSC Dye-sensitised solar cell
- EA Electron affinity
- EM Electron microscopy
- ES Excited state
- FEG Field emission gun
- (O)FET (Organic) field effect transistor
- FRET Förster resonance energy transfer
- GS Ground state
- (S)HJ (Single) Heterojunction
- HOMO Highest occupied molecular orbital
- HV High vacuum
- IL Interfacial layer
- IC Internal conversion

List of abbreviations

- AFM Atomic force microscopy
- AM Air mass
- AO Atomic orbital
- BE Binding energy
- BHJ Bulk heterojunction
- CB Conduction band
- CT Charge transfer
- CV Cyclic voltammetry
- CELIV Charge extracted by linearly increasing voltage
- D/A Donor/Acceptor
- DSSC Dye-sensitised solar cell
- EA Electron affinity
- EM Electron microscopy
- ES Excited state
- FEG Field emission gun
- (O)FET (Organic) field effect transistor
- FRET Förster resonance energy transfer
- GS Ground state
- (S)HJ (Single) Heterojunction
- HOMO Highest occupied molecular orbital
- HV High vacuum
- IL Interfacial layer
- IC Internal conversion

- UPS Ultra violet photoelectron spectroscopy
- UV ultra violet
- PES Photoelectron spectroscopy
- PL Photoluminescence
- TCO Transparent conducting oxide
- TMO Transition metal oxide
- TP(C)/V Transient photo(current) / voltage
- TAS Transient absorption spectroscopy
- TM Tapping mode
- ToF Time of Flight
- SCLC Space charge limited current

List of symbols / notation

- φ Workfunction
- Å Angstrom (1 Å = 0.1 nm)
- *c* Concentration
- *d* Actual film thickness
- *dhkl* Lattice plane spacing or interplanar spacing of plane *(hkl)*
- *D* Diffusion coefficient
- ε Dielectric constant
- E_B Exciton binding energy
- E_{cutoff} Secondary electron cutoff
- E_F (Fermi) energy
- E_g Energy gap
- E_m / R_e Emitter / Receiver

- EQE External quantum efficiency
- E_{Vac} Vacuum energy level
- *f(E)* Fermi-Dirac distribution
- *FF* Fill factor
- $HOMO_{onset}$ Onset of the HOMO level in OSC
- I_g Interface gap
- *(hkl)* Miller indices
- ϕAM Incident angle (sun light)
- *J(dark,ph)* Dark current density, photo current density
- $J_{(SC)}$ (Short-circuit) current density
- *Jmp* Current density at maximum power point
- *J-V* Current density-voltage
- λ Wavelength
- L_D Exciton diffusion length
- *η(abs,ed,ct,cc)* Quantum efficiency of photon absorption and exciton formation, exciton diffusion, charge transfer, charge collection
- P_{inc} Incident radiation power density
- *Pmp* Operational maximum power output
- *PCE* Power conversion efficiency
- *r(B,C)* Bohr radius, Coulomb radius
- *R(l,s,sh)* Load resistance, series resistance, shunt resistance
- R_q Surface roughness parameter
- *r.t.p* Room temperature and pressure
- t Step edge thickness, actual film thickness
- *S(0,1)* First singlet ground state, excited state

- θ Angle of incidence (XRD)
- *T* Temperature
- *T(λ)* Transmission
- *τ* Life time
- *γ A*ctivation parameter
- $V_{(OC)}$ (Open-circuit) voltage
- V_{mp} Voltage at maximum power point
- A(*m*)/B(*n*) Layer of compound A with the actual thickness *m* in brackets covered by a layer of compound B with an actual thickness *n*

List of compounds

- (M)Pc (Metal) phthalocyanines
- BCP 2,9-dimethyl-4,7-diphenyl-1,10-phenantroline (bathocuproine)
- BODIPY Borondipyrromethane
- BP benzoporphyrine
- C_{60} Buckminster fullerene
- Cl_6 - SubPc Hexa - Chloro boron subphthalocyanine chloride
- ClAlPc Chloroaluminium phthalocyanine
- CP bicycloporphyrin
- CuPc Copper phthalocyanines
- DPP Diketopyrrolopyrroles
- Fc / Fc^+ Ferrocene / Ferrocenium ion
- H - SubPcs Halogenated Subphthlaocyanines
- H_2Pc Metal-free phthalocyanine
- ITO Indium-tin oxide

- MC Merocyanine
- MEH-PPV Poly(2-methoxy-5-(2'-ethyl-hexyloxy)-p-phenylene vinylene)
- MoO_x Molybdenum oxide
- Pent Pentacene
- P_3HT Poly(3-hexylthiophene)
- PCBM Phenyl-C61-butyric acid methyl ester
- PEDOT:PSS Poly(3,4-ethylenedioxythiophene) poly(styrene sulfonate)
- PPI Perylene diimides
- PPV Poly(phenylene)vinylene
- PTCBI perylenetetracarboxylic bis-benzimidazole
- PTCDA perylene-3,4,9,10-tetracarboxylic dianhydride
- SIMEF 1,4-bis(dimethylphenylsilylmethyl)[60] fullerene
- SubNPc SubNaphthalocyanine
- SubPc Boron subphthalocyanine chloride
- SQ Squaraine
- TBAFP Tetra-n-butylammonium fluoride phosphate
- Tc Tetracene
- TIPSEpent 6,13-bis(triisopropylsilylethynyl)pentacene
- V_2O_x Vandium oxide
- VOPc Vanadyl phthalocyanines
- WO_x Tungsten oxide
- ZnPc Zinc phthalocyanine

Chapter 1

Introduction

This chapter provides a general overview for the requirement of renewable energy and photovoltaics (PV), in particular organic photovoltaics (OPV) with a specific discussion of the historical background and scientific theory behind this technology. Second to the need for renewables and PV, this section discusses the unique properties of organic semiconductors that allow for their exploitation in electronics. The discussion delves into the need for an increased number of small molecule organic semiconductors, especially acceptor materials, and the inherent challenges with new materials, and the final section gives an outline for the remaining thesis chapters.

1.1. Overview

1.1.1. The need for renewable energy.

Arguably, energy has played one of the most important roles in human and economic development since society began and much has changed since wood was first used to heat homes. Since most of the heat and electricity has come from fuel combustion, this has led to a gargantuan increase in the demand for fossil fuels such as oil, coal and natural gas which are limited resources.[1] Unfortunately, another disadvantage to fossil fuels is the amount of pollution caused through burning. 21.3 billion tonnes of carbon dioxide (CO_2) are estimated to be produced from the burning of fossil fuels each year (with half being absorbed by natural processes).[2] CO_2 is a known contributor to the greenhouse effect (i.e. the process of absorption / emission of infrared light which warms the planet's surface and lower atmosphere) and the increase in CO_2 emissions since the industrial revolution is thought to play a large part in global warming.[2]

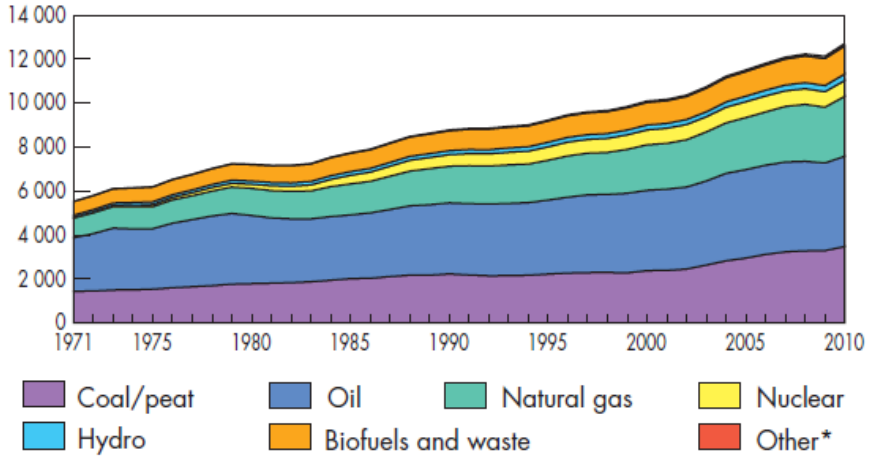

Figure 1.1 World total primary energy supply from 1971 to 2010 by fuel (Mtoe – Million tons of oil equivalent vs year). Graphic taken from the International Energy Agency.[2]

The evolution of the total production of energy in the world from 1971 to 2010 is shown in **Figure 1.1** and clearly shows a large increase in energy usage and a clear, heavy dependence on oil and coal even today. Over 80 % of the world's energy is still supplied by fossil fuels (oil, coal and gas) (as shown in **Figure 1.2**) and other sources, including renewables such as geothermal and solar, reach a mere 0.9 % of the total supply. The global primary energy demand will continue to grow in the next 25 years, with non-OECD (organisation of economic co-operation and development) countries accounting for the majority (~ 90%) of the increase.[2]

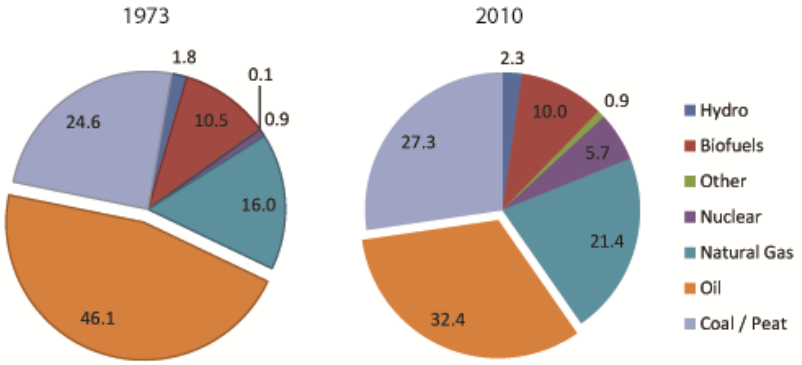

Figure 1.2 1973 and 2010 fuel shares of total primary energy supply. Information taken from the International Energy Agency.[2] **other includes geothermal, solar, wind, heat etc.*

To cope with the high demand it is expected that a broad range of energy sources are required, and in this renewable energies will play an important role, in particular for finding a clean source of energy. The sun is the only likely non – polluting energy source available to potentially cover both the present and future energy demand on Earth with a total power of 89, 300 TW striking the Earth.[3] This theoretical potential represents more energy striking the earth's surface every 1.5 hours than worldwide energy consumption in 2001.[3] To convey whether this is actually realistic Figure 1.3

shows a map of the U.S.A. The 8 green screens are solar farms consisting of only 6 % cells. This would be sufficient to meet the energy demand in the US. Using 1% cells in California (red square), you could supply the energy needs for the state or the whole of the US with 6 % cells. Although these values are merely theoretical it gives an idea of the grand energy source we could potentially harness in order to change the dependence on non – renewable, harmful fossil fuels.

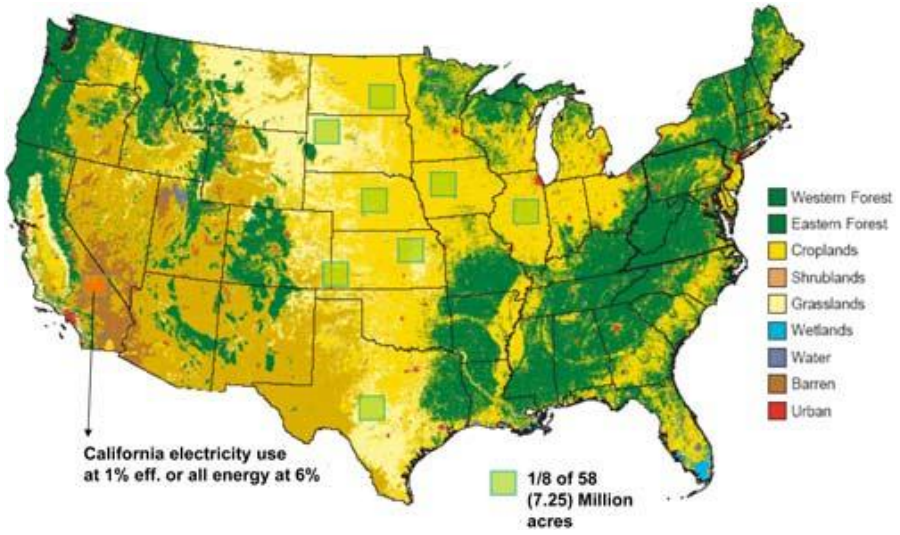

Figure 1.3. USA depicting areas for 6 % cell use or 1 % cell use. [from NREL website]

1.1.2. History of photovoltaics (PV).

The first major advancement in photovoltaics (PV) was in 1839 when scientist Edmond Becquerel discovered the photovoltaic effect by placing two electrodes into a conductive solution and monitoring the voltage generated when illuminating the semiconducting contact.[4] Over four decades later the first solid state solar cells, based on Selenium, were made with power conversion efficiencies (PCEs) of around 1 %.[5] This efficiency would take a good few decades to beat! In the 1950s Bell labs made huge progress with regards to PV, and after the discovery of the silicon transistor and p – n junctions, the silicon photovoltaic cell was developed with the

first devices achieving a PCE of 4.5 %.[6] Efficiencies were soon increased and in 1958 solar cells were integrated into the Vanguard I satellite.[7] Silicon cells became a huge success for use in space applications and are used today to power the International Space Station, a power generation of ~ 128kW.[7] Generally, conventional inorganic high efficiency solar cells are still based on silicon (either mono – or poly- crystalline p-n doped Si) with efficiencies reaching 25 %.[8] Due to the high energy input and fabrication costs they are not ideal for terrestrial, commercial applications. Multi crystalline and thin film silicon cells were investigated to reduce the use of high purity silicon ingots and reduce the amount of material needed. Their amorphous counterpart, α – Si:H, although much less costly, has a much lower efficiency of ~ 10 %.[9] **Figure 1.4** shows a summary of cell types and accredited efficiencies over the past 40 years.[10]

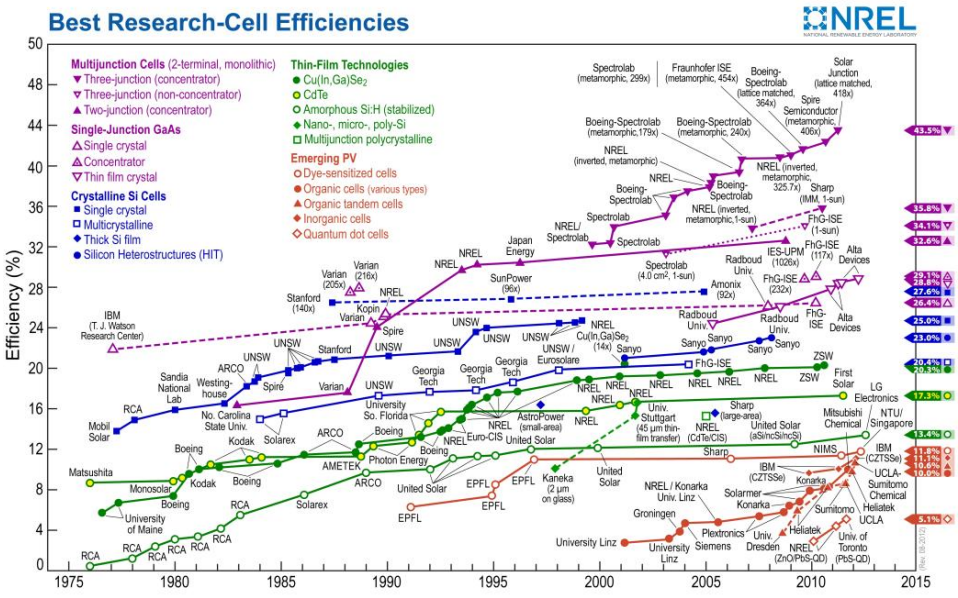

Figure 1.4 Development of PV devices quoting the efficiencies for different technologies from 1976 until 2012.[10]

As much of the cost with inorganic cells is the processing methods of the silicon itself (to ensure single crystal growth), other avenues were beginning to be explored. Interest in combining elements from groups III and V e.g. Gallium Arsenide (GaAs) and Indium Phosphide (InP), or II and VI such as Cadmium Sulphide (CdS), Cadmium Telluride (CdTe) and Cadmium Selenide (CdSe) steadily increased in the hopes of improving efficiencies.[11-15] Due to the precise growth of these materials, it enabled thin extremely controlled multi-layered structures, which could be tailored to the solar spectrum. Efficiencies as high as 36 % could be reached with multi-junction III-V cells, but although comparative to silicon cells in efficiency, the disadvantages include low abundance and high toxicity of the materials used as well as higher cost.[16]

As a further step to decrease the cost of photovoltaics, organic semiconductors (OSCs) became an interest due to their cheap production processes and thin layers but the efficiencies are significantly lower than conventional silicon cells. Nevertheless, they potentially provide a cheap alternative and could in theory begin to compete due to recent efficiencies reaching 12 %.[17]

Excitonic solar cells generally fall into three different categories, dye – sensitized solar cells (DSSCs), hybrid inorganic / organic cells, and polymer / small molecule solar organic cells. Primarily only solution and vacuum processed small molecule photovoltaics will be concentrated on in the following section.

1.1.3. History of small molecule organic photovoltaics (OPVs)

Until 1986, organic solar cells consisted of ~ 100 nm thick layers of a single material, generally an organic dye; such as phthalocyanines or conjugated polymers

sandwiched between a transparent electrode (often indium tin oxide (ITO)) and a back electrode.[18] Unfortunately, due to the large amount of recombination (with exciton dissociation mainly occurring at high electric field and / or trap sites) the efficiencies were extremely low, typically ~ 0.1 % (shown in **Figure 1.5a.-b**).[18]

Fortunately, in 1986 Tang had the revolutionary idea of creating a heterojunction (HJ) by combining two different materials with offset energy levels to create an interface to improve exciton dissociation (**Figure 1.5c**).[19] Tang used two semiconductors, copper phthalocyanine (CuPc) as the electron donating material and 3,4,9,10-perylenetetracarboxylic bis-benzimidazole (PTCBI), a perylene derivative, as the electron acceptor material.[19] The interface energy offset allowed for exciton dissociation to be heavily improved and improved charge transport. This improvement also resulted in decreased recombination due to having continuous charge specific layers direct from the interface to the electrodes. This increased efficiencies by an order of magnitude to 1 % (device structure shown in **Figure 1.5d**)

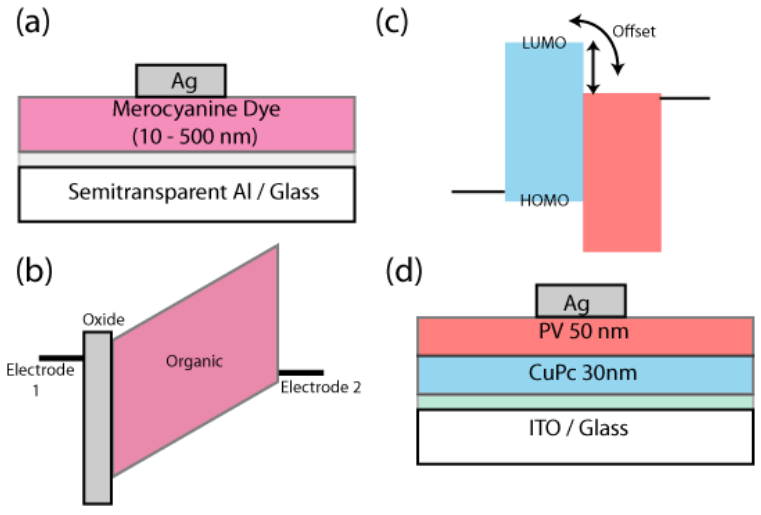

Figure 1.5 (a) Single cell device (b) under working conditions (c) Simple schematic of a heterojunction at open circuit and (d) Tang's HJ device structure[19]

To significantly improve efficiencies in small molecule HJs new materials were necessary, and with Kroto's discovery in 1985 of C_{60}, it soon became the new wonder electron acceptor material.[20] The use of C_{60} increased device performance from 0.95% to 3.5%.[21] New phthalocyanines, oligoacenes, improved vacuum depositing technology and new cell architectures (co-deposition and gradient cells) have seen PCEs in SHJs reaching above 5 %.[22-26]

Due to the limitations in SHJs, commercially viable efficiencies of 10 % are a hard target to reach. Problems with SHJ devices are predominantly due to the limited diffusion length of the organic semiconductor. Due to the short diffusion lengths (L_D) of most materials, layer thicknesses have to be kept small which will limit the total amount of light absorbed and this bottle neck can be avoided through clever cell architecture.[27] To push efficiencies higher, one solution was to blend or co-deposit organic materials similar to the polymer community.[25, 26, 28] This intermixing allows for a larger number of dissociation sites and a high probability of all excitons created reaching a dissociation site.[25] This was shown to be extremely promising with Sullivan *et al.* creating gradient intermixed cells improving short circuit current densities (J_{sc}) from ~4 to ~ 6 $mAcm^{-2}$ in CuPc / C_{60} cells in 2004, and more recently Holmes *et al.* showing an improvement in boron subphthalocyanine chloride (SubPc) / C_{60} cells.[22, 26] Through using 80% C_{60} content in the active layer, the J_{sc} increased to ~ 10 $mAcm^{-2}$, resulting in a PCE of 4.2 % – one of the highest efficiencies for a SubPc based SHJ cell.[26]

Another way around the limitations is via tandem cell architectures: the stacking of complementary single cells connected in series via a recombination layer.[29] This allows for the summation of the open circuit voltage, V_{oc}, values of the individual single cells and an increase in PCE. This recently has been shown to be one of the

major game changers in OPVs and high efficiencies have been demonstrated both for a fully solution processed cell by Saricifitci in 2007 reaching 6.5 % and for small molecules by Chenys *et al.* with 5.2 %.[30, 31] Earlier work by Riede *et al.* on tandem cells utilised fluorinated zinc phthalocyanine (F_4-ZnPc) with C_{60} with the complementary absorbing cell comprising of α,ω-bis-(dicyanovinyl-sexithiphene)-Bu(1,2,5,6) (DCV6T). Exploiting the p-i-n structure and optical spacers, the p-(n-) doped interlayers improve charge transport and collection efficiency and the spacing layer improves the light harvesting and the efficiency reached 6 % for a 2 cm^2 cell.[32] Recently, Heliatek have announced a tandem cell certified at 12 % although the precise structure is unknown.[17]

Recently, work by Mitshibushi has shown that small molecule SHJ systems can reach 10 % through interface modification of two materials.[33] The BP is made through thermal treatment of bicycloporphyrin (CP), as shown in **Figure 1.6.**

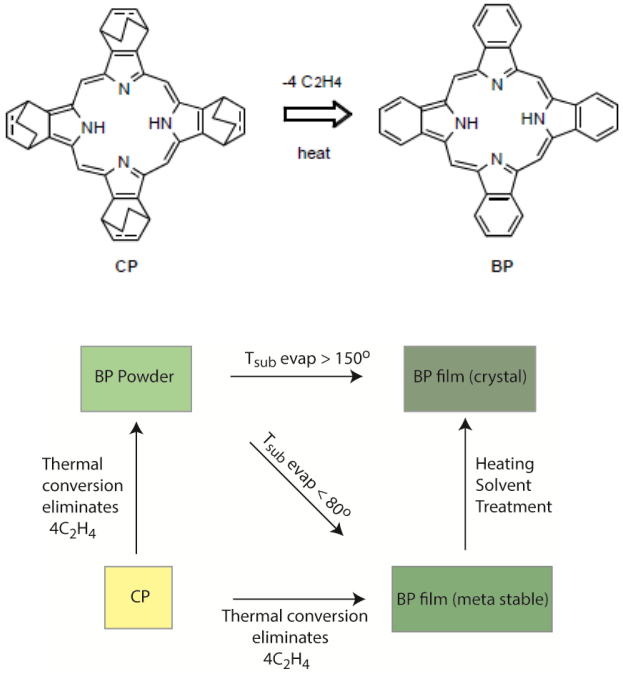

Figure 1.6 Conversion of CP to BP [adapted from ref. 34]

Via this process the 4 C_2H_2 units are removed, resulting in a BP powder which is further purified via heating. Where CP was readily soluble, the conversion to BP renders the new material insoluble and therefore, solution processed acceptor layers can be used without dissolving the donor layer. It is assumed that their recent 10 % device is based on earlier work on benzoporphyrine (BP) based devices published in 2008.[34]

Using a p-i-n based device structure (shown in **Figure 1.7**) and 1,4-bis(dimethylphenylsilylmethyl)[60] fullerene (SIMEF), a novel fullerene derivative, as the acceptor, efficiencies of 4.1 % were achieved.[34] Optimization of the nanostructured BP layer and infiltration of the acceptor material has allowed for further improvement to 10 % in 2011.[35]

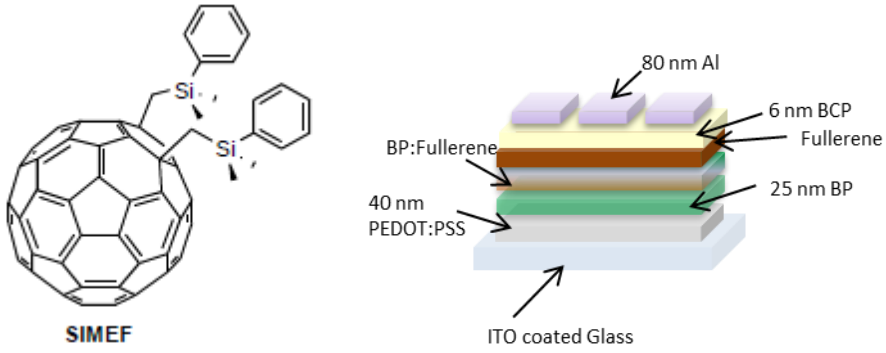

Figure 1.7 (a) Fullerene, SIMEF and (b) P-i-N Mitshibushi device structure

1.2. Semiconductor theory and principles of OPV device operation

This section will discuss the theory behind semiconductors, the main principles of OPV device operation and the potential losses and avenues around these losses to target improved performance. [36, 37]

1.2.1. Semiconductor theory

To fully understand materials it is important to begin with atomic orbitals and bonding. Singular atoms (N = 1) contain atomic orbitals (AOs) which consist of discrete energy levels. When two atoms come into contact to form a molecule (N = 2) the atoms form bonding and anti-bonding orbitals which are separated by a certain energy (shown in **Figure 1.8** for hydrogen). If you consider hydrogen (2 separate protons and 2 electrons) the lower energy orbitals has a greater electron density between the nuclei. This is the bonding molecular orbital (MO) and it is lower in energy than the 1s orbitals due to having an increased stability compared to the separate atomic orbitals. The upper MO has a node in the electronic work function and the electron density is low between the two positively charged nuclei and therefore is greater in energy than the 1s and is known as the anti-bonding orbital.

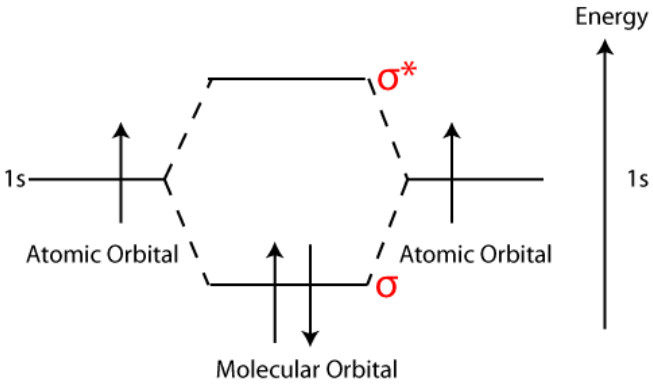

Figure 1.8 Example of a simple molecule (hydrogen) forming molecular orbitals

Expanding this molecule further with N = odd, non – bonding orbitals can also form between the bonding and anti-bonding orbitals. At N = 10 there are 5 bonding and 5 anti-bonding orbitals and as the number of atoms increases the gap between the anti - bonding and bonding orbitals decreases (shown in **Figure 1.9**). In the case of metals, as the number of atoms becomes extremely large (quasi-infinite) this gap disappears

entirely as the orbitals mix and a band is formed.

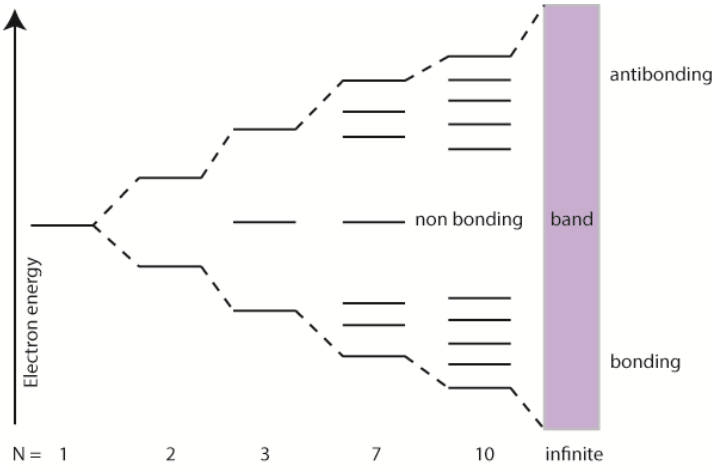

Figure 1.9 Example of a metal solid from one atom to quasi - infinite.

In the case of non – metals, such as semiconducting materials, two bands are formed separated by an energy gap (the band gap, E_g) known as the valence band (VB) and the conduction band (CB), shown in **Figure 1.10**. At 0 K, the VB is typically a fully occupied band and the CB is unoccupied. To visualise the difference between conductors (metals), insulators and semiconductors, **Figure 1.10** is a schematic of energies for the electrons in the materials. The main distinguishing factor between these materials is the energy gap, E_g, between the valence and the conduction band.

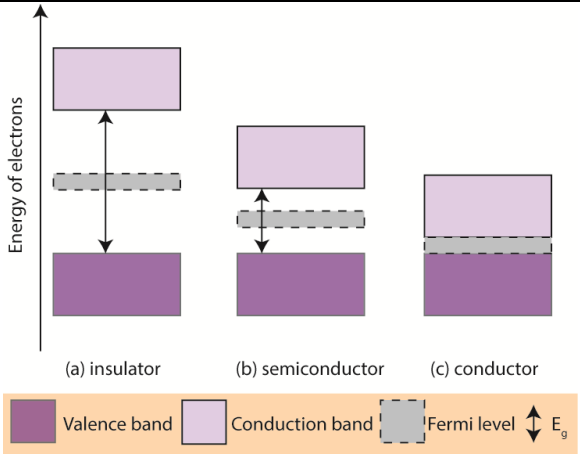

Figure 1.10 Schematic of the energy levels of (a) insulators, (b) semiconductors and (c) conductors

In insulators, the E_g is large, typically > 4 eV and at room temperature (r.t) electrons cannot gain sufficient energy to reach the conduction band. Conducting materials (such as metals) have no gap between the VB and CB (as shown previously) and their valence electrons are essentially free. This is indicated as an overlap region in the schematic (**Figure 1.10c**). Semiconductors are more interesting and fall in between these two extremes, with an E_g ~ 1 – 4 eV allowing for electrons to potentially reach the conduction band with an appropriate input of energy. An important term used to help classify these materials is the Fermi level and is used to describe the occupation of electron energy levels at absolute zero, and is also known as the electron chemical potential. The probability of an electron existing at a particular energy (E) is given by the Fermi-Dirac distribution shown in **Equation 1.1**

$$f(E) = \frac{1}{e^{\frac{E-E_f}{KT}}+1} \qquad \textbf{Equation 1. 1}$$

Where K is Boltzmann's constant, E_f is the Fermi level energy (theoretically the energy level where the population probability of an electron is 50 %) and T is the temperature. This indicates that at absolute zero all of the levels up to the E_f are filled and no electrons have enough energy to exist above the E_f (**Figure 1.11a**).

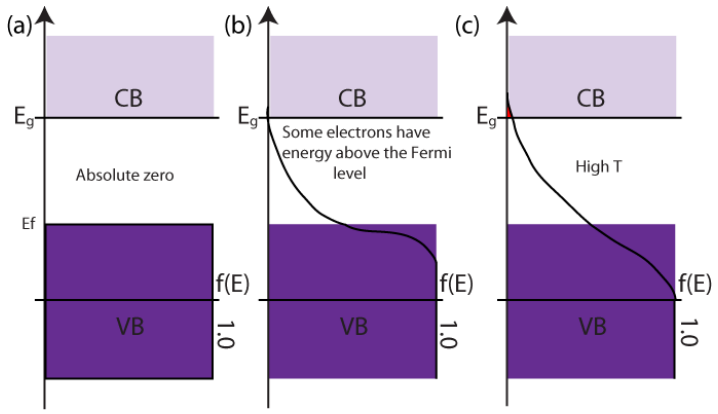

Figure 1.11 Band theory of solids showing the change in occupation of electrons with temperature

As T increases there is a greater probability of an electron existing at an energy above the E_f. At higher temperatures there is a larger probability that the electrons can spill into the gap and be promoted to the conduction band (**Figure 1.11c**) The Fermi level in intrinsic semiconductors (for e.g. pure silicon) is half way between the VB and CB and although at absolute zero there is no conduction, at room temperature electrons can occupy the CB and provide current. The position of the Fermi-level in semiconductors is extremely important as it determines whether there is an ohmic (low resistance junction) or a blocking contact at interfaces and describes whether the semiconductor favours holes in the VB (p- type) or electrons in the CB (n-type). **Figure 1.12** summarises the energy levels in both intrinsic and doped semiconductors.

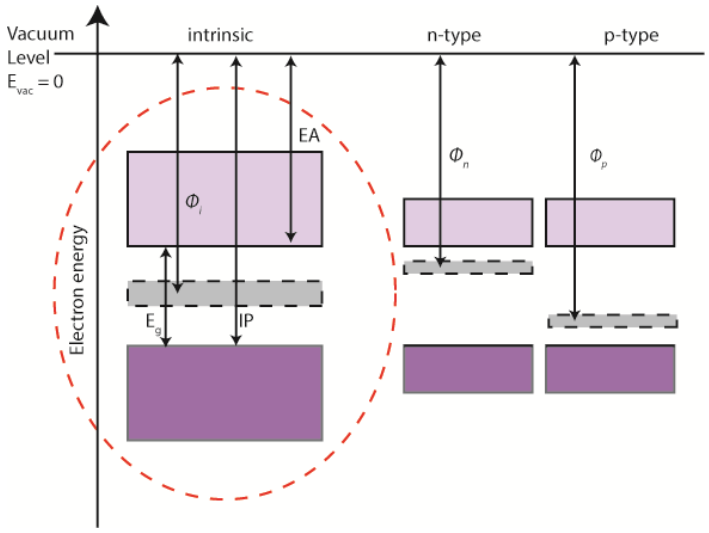

Figure 1.12 Schematic of semiconductor types with the electron affinity (EA), ionisation potential (IP), band gap (E_g) and work function (Φ) are labelled.

The electron affinity (EA) here is defined as the energy from the bottom of the CB to the vacuum level. The ionisation potential (IP) is defined as the energy from the top

of the VB to the vacuum level. The work function (Φ) is defined as the amount of energy it takes to remove an electron from the Fermi level to the vacuum level (V_l)

Doping in semiconductors is typically used to increase the number of free charges to be moved by an external applied voltage. Introducing "donor impurities" increases the number of electrons in the semiconductor and shifts the E_f closer to the VB. This results in a negative (n-) type semiconductor with electrons are considered the majority carrier. N - type impurities lose a valence electron when added to the semiconductor which increases the conductivity through the addition of an extra electron. The impurities contain five valence electrons (pentavalent) and will use four electrons to covalently bond to the host semiconductor leaving one free (see **Figure 1.13a** for Arsenic doping in Germanium). Through the addition of "acceptor impurities" which are trivalent, as shown in **Figure 1.13b**, they are short one electron to bond fully to the Ge (a tetravalent crystal structure). This creates a hole in the structure and increases the number holes present in the semiconductor. Holes are now considered the majority carrier and are known as positive (p) - type semiconductors with an E_f shifted closer to the CB.

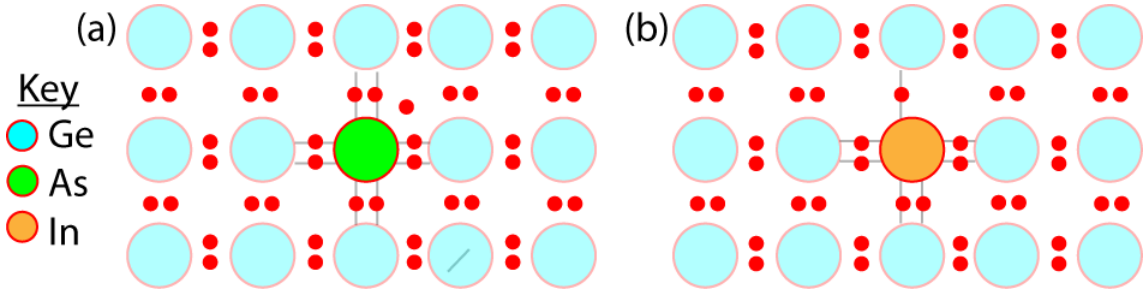

Figure 1.13 (a) Germanium crystal doped with Arsenic or **(b)** doped with Indium

1.2.2. Principles of device operation

A simple schematic of a planar bilayer OPV cell is shown in **Figure 1.14.**[38, 39]

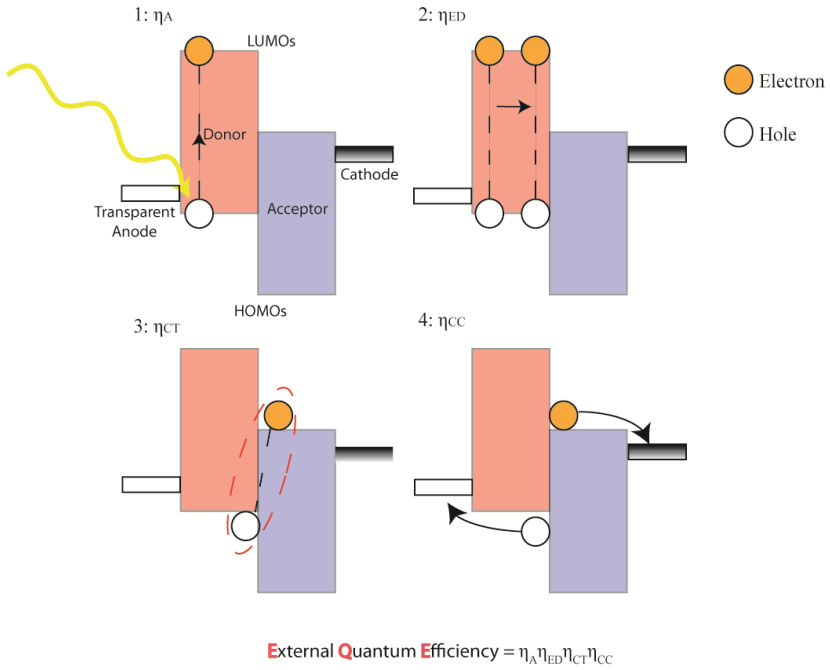

Figure 1.14 Schematic of the principles of organic photovoltaic device operation at open circuit.

The initial step is the absorption of light to form an exciton (which occurs with quantum efficiency, η_A), followed by the random diffusion of the exciton through the layer to a heterojunction or dissociation site, (η_{ED}). The exciton dissociates into free carriers (η_{CT}) and lastly, the free carriers are transported to their respective electrodes and collected, (η_{CC}). These quantum efficiencies (η_A, η_{ED}, η_{CT}, η_{CC}) relate to the external quantum efficiency (EQE), which is the number of collected charges per incident photon:[40]

$$\mathbf{EQE} = \boldsymbol{\eta_A \eta_{ED} \eta_{CT} \eta_{CC}} \qquad \textbf{Equation 1. 2}$$

Each quantum efficiency will be discussed in more detail below and it is prudent to state that in all four stages the charges can relax to the unexcited ground state (S_o)

through various mechanisms such as internal conversion and relaxation as well as geminate pair and bimolecular recombination.[41]

1. Light absorption to form Frenkel excitons, η_A

One of the reasons for using small molecule semiconductors is their ability to absorb light from the visible range of the spectrum and they predominately have a sharp, narrow absorption band. Once the light has been absorbed by the semiconductor material, an electron is excited from the highest occupied molecular orbital (HOMO) to the lowest unoccupied molecular orbital (LUMO) of the material, leaving behind a positive vacancy (or hole). This excited state relaxes into a coulombically bound electron – hole pair, known as an exciton. Excitons can be divided into three distinctive groups based on their electron – hole delocalisation known as either a (a) Wannier, (b) Charge-Transfer or (c) Frenkel exciton (**Figure 1.15**).[42]

Beginning with Wannier excitons, the electron and hole exist over several crystal units and therefore possess a large degree of delocalisation. These are most common in conventional inorganic semiconductors and have a low binding energy, due to their dielectric constant, $\varepsilon > 10$, and therefore can be separated by thermal dissociation at room temperature (~ 26meV).[43] Therefore as the dielectric constant decreases the binding energy increases, as seen from **Equation 1.3**, where ε is the dielectric constant, ε_o is the permittivity, e is the electron charge and r is the distance between the electron and hole pair.

$$\boldsymbol{B.E} = \frac{\mathbf{1}}{\mathbf{4\pi\varepsilon\varepsilon_o}}\frac{\boldsymbol{e^2}}{\boldsymbol{r}} \qquad \textbf{Equation 1.3}$$

If however, the electron and hole are localised on a single molecule (c) they are known as a Frenkel exciton. This is typical in organic semiconductors and

generally, due to ε ~ 3 - 4, carries a much larger binding energy of between 0.3 - 1 eV.[44,45]

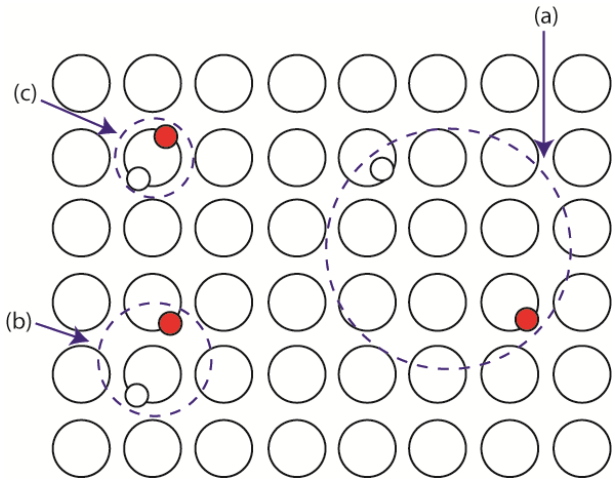

Figure 1.15 Schematic showing the three different types of exciton (a) Wannier, (b) charge – transfer and (c) Frenkel excitons

In some cases, electrons and holes can be separated by a small distance, perhaps a neighbour in overlapping conjugated systems, and this is known as a Charge-Transfer exciton (b).

Unfortunately in most organic cells only a small portion of the incident light is absorbed. This is for various reasons such as;

- The band gaps of the materials are generally too high. In silicon cells the optimum band gap of 1.1 eV is used to absorb ~ 77% of the photons in the solar spectrum, whereas in organic semiconductors band gaps can be as high as 2 – 3 eV and with their narrow absorption this limits the absorption to around 30 %.
- Due to the low charge carrier mobility and exciton diffusion lengths of the semicondcutors, the thickness of the layers is limited. This will reduce

the number of charge carriers that can be created and hence J_{sc}. This can be modified through using a reflective back electrode, optical field modelling and optical spacers to take full advantage of the light that is absorbed.

2. Exciton diffusion to a dissociation site (heterojunction), η_{ED}

As excitons are an electrostatically neutral species, the diffusion process is particularly random and not influenced by electric fields. Typically the generation rates of excitons are low and therefore the process is unlikely to be driven by a concentration gradient. It is accepted that the excitons diffuse via a random hopping process between molecules and domains.

Excitons can transfer from one molecule (emitter, E_m) to a neighbouring molecule (receiver, R_e) which leaves the emitter in the ground state (GS) and receiver in an excited state (ES). There are typically two mechanisms by which an exciton can be transferred 1) Förster or 2) Dexter energy transfer. Förster energy transfer relies on dipole – dipole electromagnetic interaction and requires an overlap between the emission spectra of the donor and absorption spectra of the acceptor. It is commonly referred to as Förster resonant energy transfer (FRET) which decreases dramatically with increasing distance, r, between the emitter / receiver as r^{-6}. Significant FRET occurs when the E_m/ R_e separation is between 2 - 5 nm. Usually, only singlets can be transferred, however triplet excitons located on a phosphorescent donor can also undergo FRET.[46]

Dexter energy transfer is the actual exchange of an electron between the E_m/ R_e when they are < 1 nm apart and therefore have significant electronic wave function

overlap.

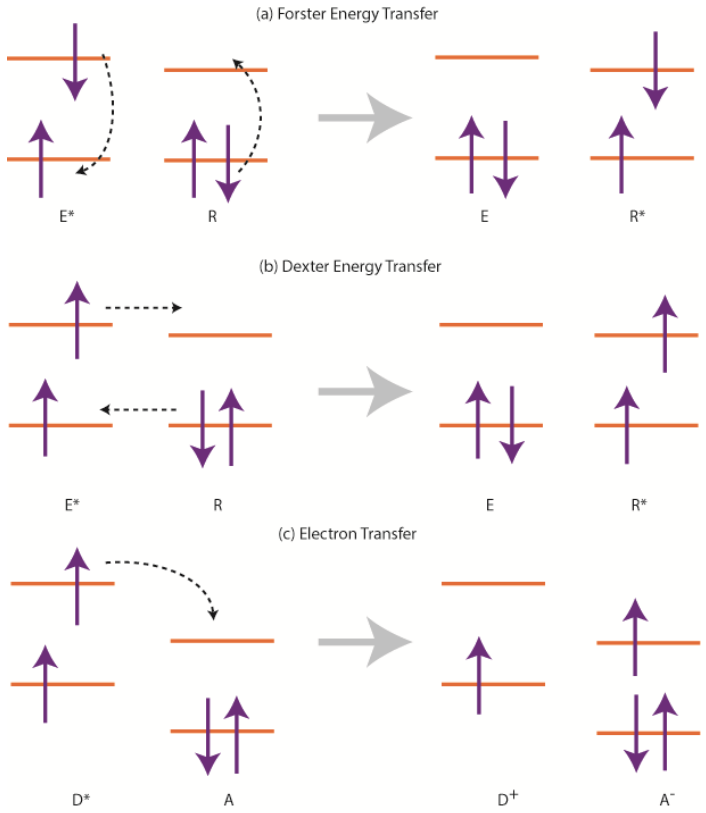

Figure 1.16 Schematic of (a) Förster energy transfer, **(b)** Dexter energy transfer. and **(c)** Electron transfer. The horizontal lines are the HOMO and LUMO energy levels of the emitter (E_m) and receiver (R_e) molecules; the asterisk denotes excited state (D – donor, A – acceptor when discussing electron transfer). The dashed arrows represent simultaneous rearrangement.

The probability of this occurring decreases exponentially with increased separation and is closer to hopping transport. Although FRET outperforms Dexter transfer for singlets, unlike Förster, both singlets and triplets can be transferred using this mechanism. It also does not require the same emission / absorption overlap, however the exciton energy of the acceptor should be lower than that of the donor for efficient transfer.[47]

The final mechanism in **Figure 1.16** is electron transfer (generally between two different materials i.e. in a heterojunction). This occurs when the LUMO of the acceptor is sufficiently low to overcome the binding energy and plays a large role in the function of OPVs. Typically in small molecule OPVs the thickness of layers is

between 5 – 40 nm, neither mechanism of transfer is likely to contribute 100 % to the transfer process and therefore it is thought of as a multi – step mechanism.

Ideally, all of the excitons will reach a dissociation site or heterojunction and whether this occurs is extremely dependant on the materials exciton diffusion length (L_D) as shown in **Equation 1.4**

$$L_D = \sqrt{D\tau} \qquad \textbf{Equation 1.4}$$

Here D is the diffusion coefficient and τ is the exciton lifetime. Low diffusion lengths in organic semiconductors mean that bilayer thicknesses are generally small (smaller than the diffusion length to ensure all excitons reach the heterojunction). Typical diffusion lengths for phthalocyanines are ~ 10 – 30 nm,[48, 49] with subphthalocyanines predicted to have an L_D of less than 10 nm.[50] Typical lifetimes are on the nanosecond timescale.[51] Single crystal acenes have been shown to have an L_D as large as 60 – 70 nm[52] and some pigments like perylene are believed to have diffusion lengths of > 100 nm.[53] To overcome the small diffusion lengths in organic semiconductors, the OPV community moved towards bulk heterojunction (BHJ) devices (device structures shown in **Figure 1.17**) Either blends of donor polymers / soluble small molecules with soluble fullerene derivatives, such as PCBM (phenyl-C61-butyric acid methyl ester), or small molecules co-deposited in vacuum to form mixed active layers allow for the majority of the excitons to reach a dissociation site.[54, 55] The disadvantage to BHJs is the reduction in charge mobility due to a lack of continuous transport pathways to the electrodes which increases the charge carrier recombination.[56] Nano-structured devices (c) are thought to be the ideal structure, allowing for both a short distance to the dissociation site and

continuous pathways to the electrodes to allow for optimum dissociation and charge collection.[57]

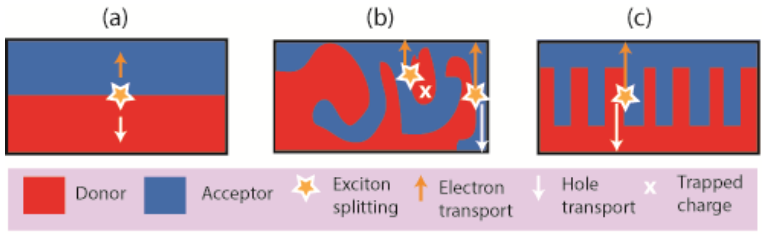

Figure 1.17 Different device structures (a) bilayer, (b) blend / codeposited, (c) nanostructured.

3. Exciton dissociation into free carriers, η_{CT}

One of the key differences between inorganic and organic PV is the ability to create free carriers. Due to the large stabilisation energy in bound Frenkel excitons they are unable to split via thermal excitation (~ 26 meV) and therefore require an energy level step provided at the D / A interface. This offset needs to be at least as large as the binding energy (E_B) of the exciton, (which can differ for organic semiconductors), at both the LUMO levels and the HOMO levels of the materials.[58] The amount of energy used to dissociate the excitons directly impacts the V_{oc} of the device, with the maximum achievable V_{oc} governed by the interface gap, I_g (difference in the energy between the $HOMO_{donor}$ and $LUMO_{acceptor}$).[59] If the energy offset is not large enough to separate the exciton, the exciton will recombine and not contribute to the photocurrent, if too big however the V_{oc} in devices can be extremely limited. In contrast to the notion of bound Frenkel excitons, recently Troisi has proposed that they form relatively delocalised charge transfer (CT) states with energy closer to that of free charges. Through modelling the donor – acceptor

interface he found that the most kinetically accessible CT state formed after donor excitation is closer to that of free charges.[60]

4. Free carrier transport and collection, η_{CC}

Once the excitons have separated into free carriers they are transported through their respective layers (holes – donor; electrons – acceptor) and are collected and extracted to the external circuit to generate current flow. The efficiency of this step is extremely dependant on the charge carrier mobility and the energy levels of the electrodes. Poor electrode choices can lead to large barriers at the semiconductor / electrode interface, which in turn lead to increased charge build-up, recombination and distortion of the built-in electric field.[61] Ideal contacts would be ohmic (a low resistance junction) in nature at both the anode and cathode to optimise extraction. Generally, although there is interest in replacing ITO, as of yet nothing is as versatile and suitable and therefore modifying this electrode work function is more apt than a direct replacement. This has previously been demonstrated via various methods such as using surface treatments,[62] the addition of self-assembled monolayers (SAMs)[62] and the deposition of thin metal oxides (TMOs) such as MoO_3 to improve the anode surface.[64,65] The cathode generally used is Al as materials with lower work functions tend to have greater instability, though a number of other metals have been used.[66] Exciton blocking layers at the active layer / cathode interface can also cause problems with charge collection and it is important to keep this layer thin to keep these problems to a minimum.[67]

Unfortunately, recombination pathways are intrinsic within PVs and to improve solar cells further a greater understanding of how to reduce recombination is essential. **Figure 1.18** summarises the processes and the loss mechanisms in OPVs.

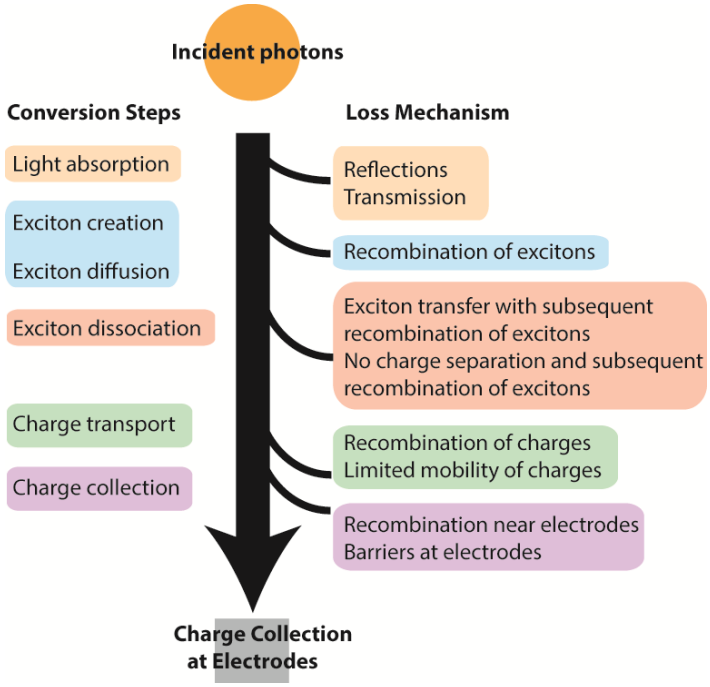

Figure 1.18 Summary of the conversion steps of light to electricity and the loss mechanisms in an OPV cell.

There are typically six possible recombination mechanisms in PVs, which are listed below:

- *Radiative recombination,* creating light with a wavelength depending on the energy of the exciton,
- *Non-radiative recombination of a singlet exciton*, where an exciton releases the energy as vibrations (=heat),
- *Intersystem crossing* to create a Triplet exciton (T),
- *Quenching* at e.g. a metal interface (this is not equal to dissociation, all the energy of the exciton will be quenched, while after dissociation you end up with carriers),
- *Free carrier (charge) recombination*
- *Exciton-exciton quenching,* where one exciton releases its energy to another exciton, hereby annihilating one of the two (both S –S -, S –T- and T–T- quenching processes are possible),

- *Exciton-polaron quenching*, annihilating the exciton and giving the polaron a higher energy.

In OPVs, the last two recombination processes are unlikely due to the need for high concentrations of two particles and the assumption that at low to normal light intensities they do not reach this threshold.

1.3. Open circuit voltage, V_{oc}.

Although all device parameters are important in a PV device, the open circuit voltage and the processes influencing it are not necessarily as straightforward to understand as the photocurrent.

The V_{oc} in SHJ OPV bilayers has been found to range anywhere from 0.2 to 1.4 V with the chosen active materials as the fundamental influence.[68-71] In the literature various models based on equivalent circuit (EC) modelling, semi-analytical approaches and experimental work determine the maximum achievable V_{oc} is limited to the difference between the $HOMO_D$ and the $LUMO_A$, i.e. interface gap (I_g).[72-74]

A basic overview of the open circuit voltage begins with the EC model and is the most simplistic way of describing this parameter:

$$V_{oc} = \frac{nkT}{J_o} \ln \left(\frac{J_{ph}}{J_o} + 1 - \frac{V_{oc}}{J_o R_p} \right) \qquad \textbf{Equation 1.5}$$

Here, because the generated light current is proportional to the light intensity (P_o), V_{oc} α $\ln(P_o)$ if $J_oR_p >> P_o$.[72] J_o and R_p are dark current and the parallel resistance respectively and the parameters T, K and n are temperature, the Boltzmann constant and an ideality factor respectively. This equation describes inorganic PVs accurately but unfortunately doesn't necessarily work for OPVs. In OPVs, J_o, R_p and n may be influenced by P_o and therefore this would alter the V_{oc} away from the proportionality

at different light intensities. It is also unclear how to relate this model to physical processes as the working principle of an OPV are inherently different to that of an inorganic cell.

In 2001, Brabec *et al.* implied there must be more complexity to V_{oc} than simply the difference in work function of the electrodes, and began to investigate the V_{oc} in polymer blends.[75] They assumed that V_{oc} underestimated the built-in field at room temperature and that it converges to it at low temperatures. Their study showed large changes in the V_{oc} occurred when the active materials were changed and that there was only a minimal effect on the V_{oc} when the cathodes were altered.[75] This contrasts other work that claims a cathodic dependence and a change in V_{oc} of up to 0.5 V. It is understood that if the contacts are ohmic the V_{oc} is work function independent.[76]

The maximum obtainable V_{oc} can be accurately described by using Marcus theory both for blends and bilayer devices.[76] There appears to be two regimes: the V_{oc} first increases then saturates with increasing light intensity and decreasing temperature. The ultimate limit in materials is the optical band gap minus the coloumbic binding energy. Cheyns *et al.* developed a detailed analytical model for the V_{oc} as shown below in **Equation 1.6**:[77]

$$\boldsymbol{V_{oc} = |HOMO_D - LUMO_A| + BB_D + BB_A - \Delta\varphi_D - \Delta\varphi_A} \quad \textbf{Equation 1.6}$$

where $BB_{D(A)}$ is the band bending at the donor interface D (or acceptor A) and $\Delta\varphi_{D(A)}$ describes the energy losses at the contacts. Cheyns found good agreement between the experimental results with CuPc / Perylene cells and the model and extended the model to include resistance effects around V_{oc}.[77]

Durrant *et al.* more recently investigated the bimolecular recombination in P3HT / PCBM blend and the ultimate effect it has on V_{oc}. The I_g in this cell is 1.1 eV but the subsequent V_{oc} achieved is only 0.6 V. When modelling the bimolecular recombination rate in this system, if the rate constant was decreased by a factor of 10 the V_{oc} was found to increase by 0.1 V implying that recombination effects indeed do also affect V_{oc}.[78]

1.4. Material properties

Choice of organic semiconductors within organic electronics is extremely important in achieving highly efficient devices. Absorption, energy levels, charge mobility, diffusion length, morphology and molecular packing are some, amongst other parameters, that govern cell performance and therefore it becomes imperative that the materials are fully understood and characterised. In this section all organic semiconductors used within this thesis will be discussed.

1.4.1. Acenes

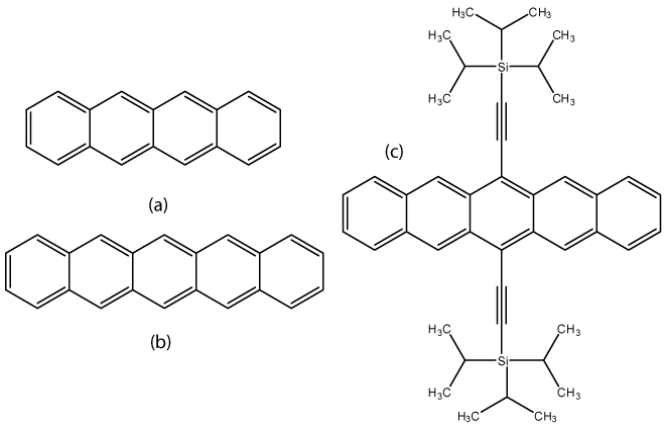

Figure 1.19 Molecular structures of the parent acenes used in OPVs (a) Tetracene (b) Pentacene (c) TIPSE-Pentacene

Oligoacenes have been shown to be attractive small molecule materials for OPVs as donor – type semiconductors due to their planar fused ring systems and crystalline structures which allow for high charge carrier mobilities (> 1 cm^2 V^{-1} s^{-1}),[79] and relatively long exciton diffusion lengths.[52] The structures of the acenes used within this study are shown in **Figure 1.19.**

Shown in **Figure 1.20** are the absorption spectra for the three oligoacenes deposited onto quartz substrates. The main absorption peaks are extremely distintive in the acenes, decreasing in intensity at higher energies which correspond to transitions to different vibrational levels. Pentacene (Pent) has the broadest absorption spectrum which is extremely attractive for use in solar cells. For both tetracene and pentacene, Davydov splitting of the main transition is apparent which suggests some order of crystallisation of the films.[80] Davydov splitting is the result of dimer formation. In the simplest instance two molecules can form physical dimers and arrange themselves either (a) parallel to each other or (b) tilted by an angle, θ, from the stacking axis. Coupling of electronic states can occur as the molecules move closer to each other and this results in altered optical properties more representative of the dimer. The excited state energy of the dimer is reduced in comparison to the monomer due to coulombic interactions and will also split due to resonance interactions – therefore seen as a split peak in the absorption spectra. This is absent in the 6,13-bis(triisopropylsilylethynyl)pentacene (TIPSEpent) spectra which implies a more amorphous film by comparison.

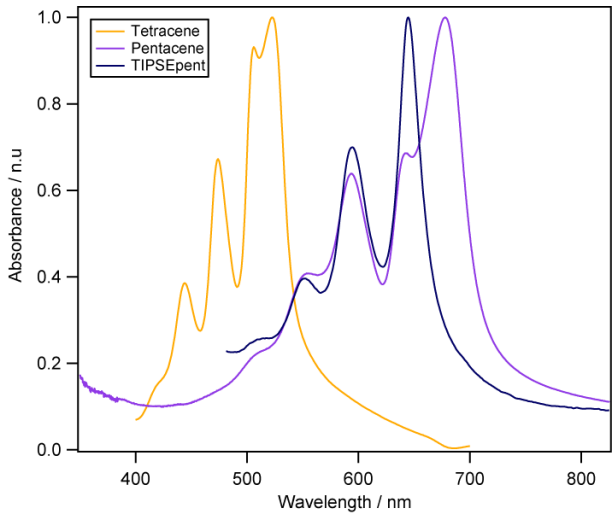

Figure 1.20 Normalized UV-vis electronic absorption spectra of 40 nm thin films of the parent acene

Both tetracene (Tc) and Pent are planar polycyclic hydrocarbons (4 benzene rings in tetracene and 5 in pentacene) with a triclinic single crystal orientation ($a \neq b \neq c$, $\alpha \neq \beta \neq \gamma$) with two molecules per unit cell.[80, 81] It is well established that both Tc and Pent form herringbone structures and many studies into polymorphs have been reported.[82] TIPSEpent was first synthesised by Anthony *et al*. in 2001 via a one – pot reaction from 6, 13 – pentacenequinone.[83] The goal was to impart solubility onto pentacene to allow for cheaper, quicker processing methods, and the hope of increasing the ability to self-assemble allowing for greater diffusion perpendicular to the substrate (compared to non-derivatised pentacene which has a high carrier mobility planar to the substrate).[83] Unlike pentacene, TIPSEpent does not adopt the herringbone structure and stacks in a 2-D columnar (brick like) array with increased overlap between the pentacene rings in adjacent molecules (face to face rather than face to edge). The interplanar spacing of the aromatic rings in TIPSEpent is also half the distance in comparison to un-substituted pentacene (3.47Å vs 6.27Å).[84] Sublimed TIPSEpent has been shown to have relatively high crystallinity with 001, 002, 003

and 005 peaks present in the X–ray diffraction (XRD) pattern shown by Nicolas *et al.*[85]

Pentacene has been the most extensively studied acene in OPVs resulting in a relatively high η_p of ~ 2.0 % when used in a SHJ cell in combination with C_{60} as the acceptor.[22, 52, 84] Although pentacene achieves a relatively high photocurrent in comparison to other small molecule donors, the restriction on the maximum achievable η_p is the relatively IP of 4.9 eV.[86] In contrast, Tc has received very little attention with regards to OPV applications despite having the potential, when used with C_{60}, to achieve a much greater I_g and therefore V_{oc} due to its larger IP of 5.4 eV.[87] Evaporated films of Tc can exhibit high molecular ordering with field effect transistors (FETs) revealing a high hole mobility (μ_h) of 1.32 $cm^2\ V^{-1}\ s^{-1}$.[88] The exciton diffusion length of Tc is also expected to be similar to other oligoacenes such as pentacene, allowing for thicker films to be utilised in OPV devices. Chu *et al.* incorporated Tc as the donor material in conjunction with C_{60} in SHJ devices and achieved a η_p of 2.2 %.[87] The devices were further improved using heat treatments which led to improved crystallinity, increased hole mobility and a higher device performance.[89] An efficiency of 0.5 % was reported by Lloyd for a TIPSEpent / C_{60} HJ in 2006 and due to minimal contribution from the TIPSEpent there is little literature on using it in OPVs[90] and this will be discussed in further detail in **Chapter 4**.

1.4.2. Phthalocyanines, Pcs.

Phthalocyanines were discovered in 1935 by Linstead and were typically used as dyes due to their intense coloured appearance.[91] They consist of an cylic conjugated 18 π e^-– system and can form stable metal free complexes (H_2Pc) as well as hold various different ions within the central cavity to form metal Pcs (MPcs).

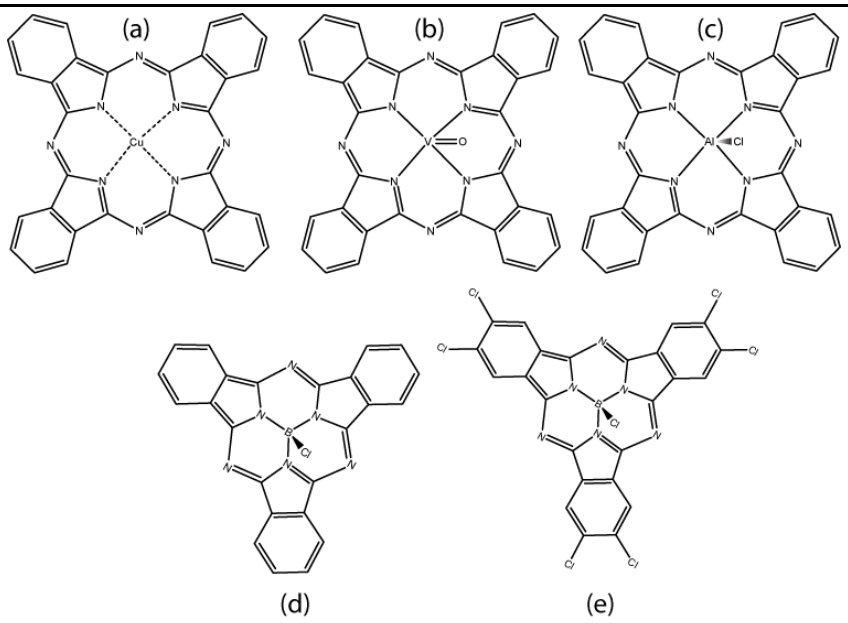

Figure 1.21 Molecular structures of the phthalocyanines used in OPVs (a) CuPc (b) VOPc (c) ClAlPc (d) SubPc (e) Cl_6-SubPc

Subphthalocyanines are related to the standard phthalocyanines, containing only three diiminoisoindole rings around a boron core and containing 14 electrons in the π – conjugated system. Due to the size of the cavity, boron – SubPc (SubPc) is the only known subphthalocyanine, larger cations result in the formation of regular Pcs and smaller cations lead to poor closure of the ring and unsuccessful formation of a SubPc. The structures of the phthalocyanines used within this study are shown in **Figure 1.21** including two boron - subphthalocyanines.

Figure 1.22 shows the normalised absorption spectra of the (Sub)Pcs used within this study. Compared to acenes they have fewer absorption peaks but still display quite broad absorption profiles, particularly in the CuPc and chloroaluminium phthalocyanines (ClAlPc) films. The degree of conjugation affects the absorption properties of Pcs; for example SubPc absorbs at lower wavelengths due to the decrease in π- conjugation from having 1 less diiminoisoindole unit.

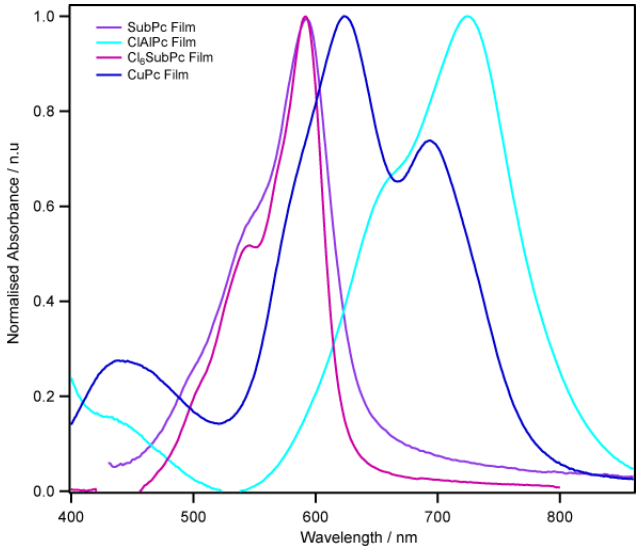

Figure 1.22 Normalized UV-vis electronic absorption spectra of 40 nm thin films of the phthalocyanines used within this study.

The red-shift in the ClAlPc spectra in comparison to the CuPc is due to the non-planar character of ClAlPc. All Pcs, including the SubPcs here show both a Q-band and a Soret B band as common to macrocylic compounds and due to it's symmetry has an extremely large molar extinction coefficient.[92]

Due to their central cavity holding various ions, Pcs can exist as planar (such as CuPc) and non-planar (such as ClAlPc) molecules due to the Cl ion jutting out from the central Al. SubPc exists as a cone (umbrella or bowl) - shaped molecule. The boron atom in SubPc has a protruding bond from the convex side of the "bowl" (axial bond) which is typically a halogen (in this work only the chloride SubPc will be discussed). Typically planar Pcs, such as CuPc, exhibit cofacial intermolecular stacking, due to the π-π overlap of nearby molecules, resulting in a herringbone type structure (shown in **Figure 1.23** a).[93]

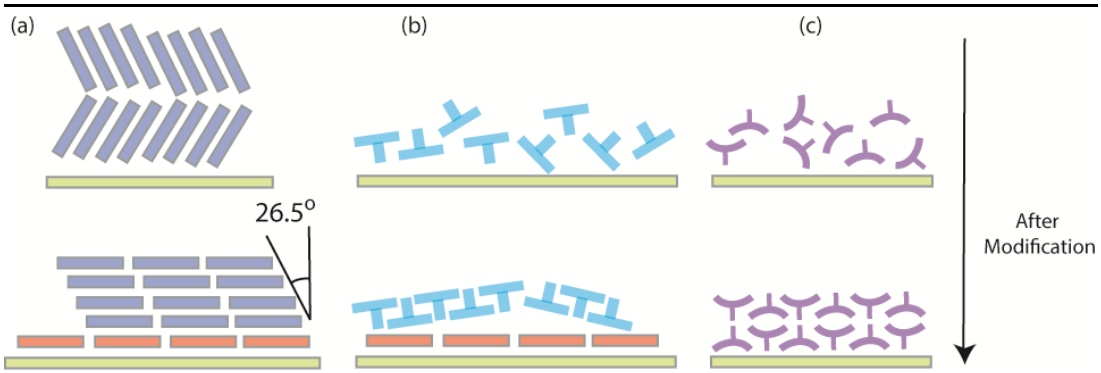

Figure 1.23 Summary of alignments of (a) CuPc, (b) ClAlPc, and (c) SubPc before and after modification – either templating in the case of (a) / (b) or annealing in (c).

The molecular planes of CuPc align parallel to each other tilted ~65° to the stacking axis. ClAlPc on the other hand, due to it's non planar structure, exhibits largely amorphous films.[23, 94] It has a hypothesized slipped disk structure[95] but generally exhibits no diffraction peaks when investigated by Mutolo *et al.*[95] More distinctively shaped molecules, such as SubPc, tend to form amorphous films, without any significant crystallisation.[95] Halogenated analogues of SubPc also exhibit amorphous character when vacuum deposited.

The thin film structures of organic semiconductors can be easily tuned and modified via various means such as: thermal methods - either during or post growth, by using different substrates, adding substituents to the periphery of the semiconductor and through the use of templating layers. A simple schematic of the CuPc, ClAlPc and SubPc thin film structures before and after treatment is shown in **Figure 1.23.** CuPc, normally exhibiting a herringbone structure, can be templated by inserting a thin layer of perylene-3,4,9,10-tetracarboxylic dianhydride (PTCDA).[93] Via this simple modification, the CuPc shifts into lying flat along the substrate with 26.5° angled stacks. This increases the charge transport through the CuPc

perpendicular to the substrate, rather than parallel, which in turn improves device performance.[93] This was also shown with ClAlPc. Although not typically ordered, through using a thin layer of PTCDA, the ClAlPc was found to increase in crystallinity with a d(014) peak emerging in the XRD at $2\theta = 26.8^{o}$.[96] Even SubPc has been shown to develop some crystallinity after heat treatment as demonstrated by Mattheus *et al.* where after annealing of the SubPc thin film, peaks at $2\theta = 17.09^{o}$ and 34.38^{o} were seen.[97] They attributed this to an alignment of the SubPc crystals and the B – Cl axis with the 001 plane perpendicular to the substrate to give an ordered SubPc layer as shown in **Figure 1.23c.**

CuPc is probably the most studied Pc and was first integrated into Tang's ground-breaking cell as a donor material achieving 1 % efficiency.[19] Studied in SHJs, co-deposited BHJs and the more complicated gradient BHJ, it has improved from 1 % to 4.5%.[25] With CuPc, most of the improvements came from improving the J_{sc} in the devices whereas when ClAlPc and SubPc were investigated, both changed the SHJ performance through increasing the V_{oc}. Through having larger IPs, (5.4 and 5.6 eV respectively) the V_{oc} increased from 0.4 V in CuPc / C_{60} devices to 0.7 V and 1.1 V for ClAlPc and SubPc optimised planar devices.[98] Further improvements through co-deposition also improved ClAlPc and SubPc devices as shown by Li *et al.* and Holmes *et al*. respectively.[99, 26]

Although SubPc is typically used as a donor material, the Cl_6-SubPc derivative is used as an acceptor material.[70] From the addition of 6 chlorine atoms to the periphery of the SubPc the IP was increased to 5.8 eV with minimal changes to the band gap, and could be used as an acceptor with SubPc as a donor material. This allowed for an extremely large increase in V_{oc} to 1.31V, one of the largest V_{oc} values for a SHJ cell and one of the first displays of an acceptor that could potentially

compete with C_{60}, due to obtaining a similar PCE to the reference cell. (2.7 % vs 3.2% (C_{60}))[70]

1.4.3. Fullerenes , C_{60}

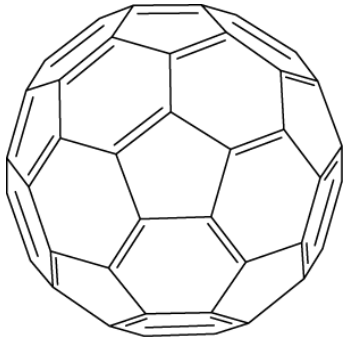

Figure 1.24 Molecular structure of C_{60}

Discovered in 1985 by Kroto,[20] C_{60} revolutionised the world of OPVs as it can accept between 6 and 12 electrons, and is therefore still the dominant acceptor in OPVs to date. It consists of 60 sp^2 hybridised carbon atoms, forming 12 pentagons and 20 hexagons in a spherical structure. Although, typically sp^2 carbons would structurally be trigonal planer, due to the ring strain, they are closer to tetragonal carbons (or sp^3). Unfortunately, this renders C_{60} quite reactive to any potential reactions that could release the strain and hybridise the carbons to sp^3 as this would result in a more stable product.

C_{60} contains a 5 fold degenerate HOMO level, h_{u1}, and a triply degenerate LUMO level (t_{1u}) as shown in **Figure 1.25**. The triply degenerate LUMO can accept 6 electrons and although the $h_u \rightarrow t_{1u}$ transition is forbidden, the $h_u \rightarrow t_{1g}$ and $h_g \rightarrow t_{1u}$ transitions result in absorption bands at 190 and 410 nm.[100]

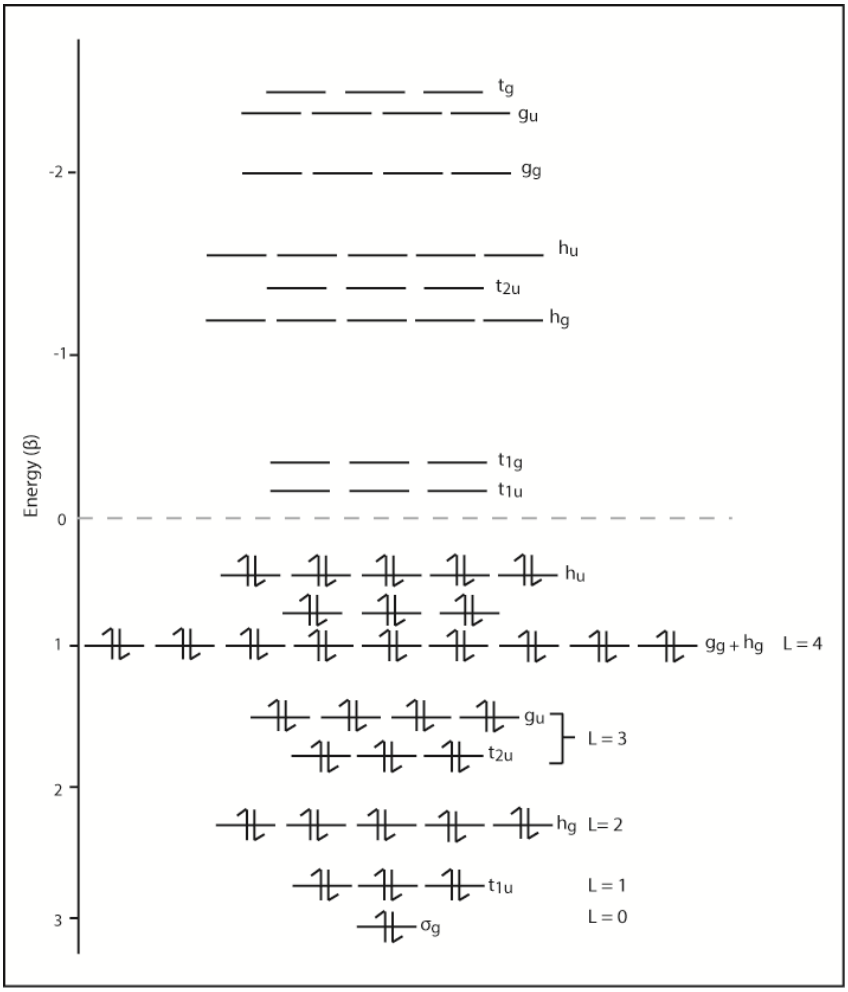

Figure 1.25 The Hückel Molecular Orbitals of C_{60}[100]

Figure 1.26 is the normalised absorption spectrum of a C_{60} film. and shows absorption both in the UV and the visible parts of the spectrum with an absorption between 300 – 420 nm extending out to 700 nm as it tails off. The absorption spectrum of C_{70} is shown as a comparison and clearly shows improved absorption between 400 – 700 nm as the previously forbidden transition is now accessible.

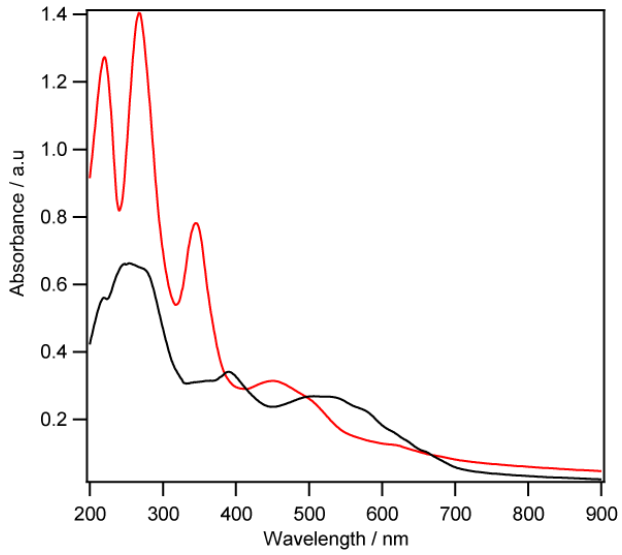

Figure 1.26 UV-vis electronic absorption spectra of 40 nm thin film of C_{60} (red) with C_{70} (black) shown as a comparison.

Non-directional intermolecular interactions between the spherical molecules result in predominately amorphous thin films with few crystalline domains and although this normally would suggest a problem with charge transport and low charge mobility, C_{60} has one of the highest electron mobilities for an organic thin film measured at $1x10^{-2}$ V cm^2 s^{-1}.[101] This is possibly due to the numerous LUMO / LUMO + 1 states where charges can be accepted and transported easily.

Although fullerenes are extremely good acceptors they still have their limitations. Successful donor / acceptor (D / A) HJs depend on well-chosen $HOMO_D$ – $LUMO_A$ energies, allowing for a large open circuit voltage. Shown in **Figure 1.27** are combinations of various donor materials with C_{60}. The table displays the I_g created with the various donor materials, the Δ_{LUMO} and the resulting V_{oc} of the cell. As expected, as the I_g is increased from Pentacene (0.7) to SubPc (1.4) the V_{oc} indeed increases. Unfortunately, due to the deep LUMO of C_{60}, potential V_{oc} is lost as the

Δ_{LUMO} ranges from 0.6 to 1.5 eV. As it is thought that a separation of only 0.3 eV is necessary at the heterojunction, there is room for improvement here![102] Loss in the V_{oc} inherently lowers the overall PCE, and with commercial products needing high voltages, other materials are needed to improve this parameter.

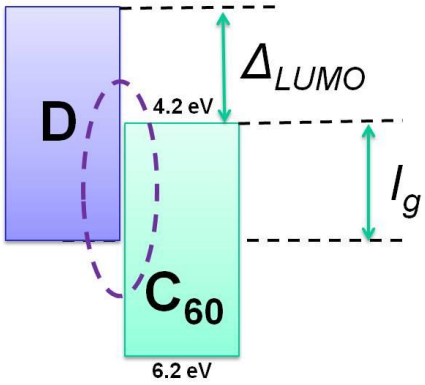

Donor	I_g	V_{oc}	Δ_{LUMO}
Pentacene	0.7	0.45	1.2
CuPc	0.9	0.50	0.7
ClAlPc	1.2	0.70	0.6
Tetracene	1.2	0.76	1.5
SubPc	1.4	1.1	0.7

Figure 1.27 Summary of the I_g, V_{oc} and Δ_{LUMOs} of different donors with C_{60} as the acceptor

Another important aspect of PV is the long term stability of the cell. C_{60} is known to photo-oxidise due to the tendency of the sp^2 carbons to saturate to become sp^3 hybridised. The O_2 incorporation into the C_{60} decreases the conductivity and defects (oxygen traps) induce recombination.[103] Cell stability and the effect on cell stability when replacing C_{60} in OPVs will be discussed in greater detail in the introduction to the results **Chapters 5** and **6**.

1.4.4. Blocking layers and electrodes.

1.4.4.1. Exciton blocking layer, BCP

2,9 – dimethyl -4, 7 –diphenyl- 1,10-phenanthroline, or more commonly known as bathocuproine, (BCP) is used as an exciton blocking layer in the devices presented here. Thin films (8-10nm) of BCP are relatively transparent and are deposited in

between the acceptor layer and the Al contact in these SHJs. Due to its large band gap, it prevents excitons reaching the electrode to reduce losses in efficiency from quenching at the interface.[104] As the band gap is large, transport of the charges through this material is thought to occur via defect states introduced by the initial stages in the metal deposition.[105] It also acts as a sacrificial layer which protects the active layers from damage from the deposition of electrodes.

1.4.4.2. Electrodes and modifications.

Indium tin oxide (ITO) is a solid comprising 90 % In_2O_3 and 10 % SnO_2. Due to its good electrical properties and optical transparency it is used as the anode in many different optoelectronic devices including organic light emitting diodes (OLEDs), transparent OTFTs and OPVs as well as in more commercial applications such as touch screen technology.[106-108] It is one of the most common transparent conducting oxides (TCOs) but it has its limitations, one of which is the relatively low work function compared to the HOMO energies of most donor organic materials used. This prevents the ohmic contact necessary for good charge extraction and the inhomogeneity across the ITO surface also affects the chance of extraction.[65]

The work function of ITO is extremely sensitive to the state of the surface and therefore different cleaning methods can vary the measured work function between 4.1 - 5.5 eV.[62, 109] Many methods have been used, such as the insertion of SAMs in between the ITO and organic layer, to improve the work function and increase efficiency.[63, 110-112] As shown in **Figure 1.28** through the use of para-chlorobenzoic acid addition to the ITO surface a ClAlPc / C_{60} device can be greatly improved, both in terms of short circuit current and open circuit voltage, resulting in a dramatic

increase in the PCE from 1.3 % to 3.3 %.[63]

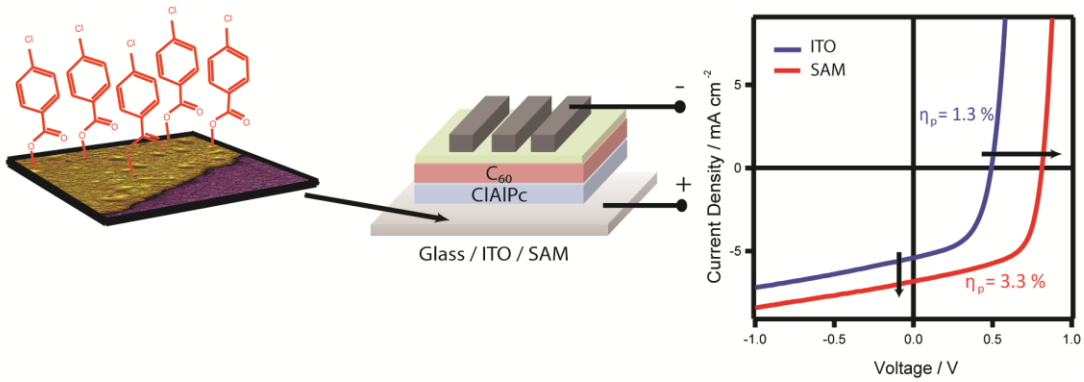

Figure 1.28 Summary of improving the work function of ITO using SAMs in ClAlPc / C_{60} devices.[63]

Another way of modifying the work function and surface of the ITO is through the addition of a conductive polymer. PEDOT:PSS is a polymer mixture of ionomers and comprises of sodium polystyrene sulphonate (PSS) which carries a negative charge and poly-3, 4-ethylenedioxythiophene (PEDOT) which carries a positive charge (structure shown in **Figure 1.29**). The PEDOT:PSS forms a dispersion of "gel-like" particles in water (typically 1.6 wt % in H_20).[113] Although typically commercially bought PEDOT:PSS only has a conductivity ~ 1 Scm^{-1}, through the use of additives the conductivity can be increased by many orders of magnitude and recently 3000 Scm^{-1} has been achieved through the addition of sulphuric acid.[114] At these high conductivities this conductive polymer can be used as an electrode to replace the more commonly used ITO and will lend itself to roll to roll processing more easily than brittle transition metal oxides (TMOs).

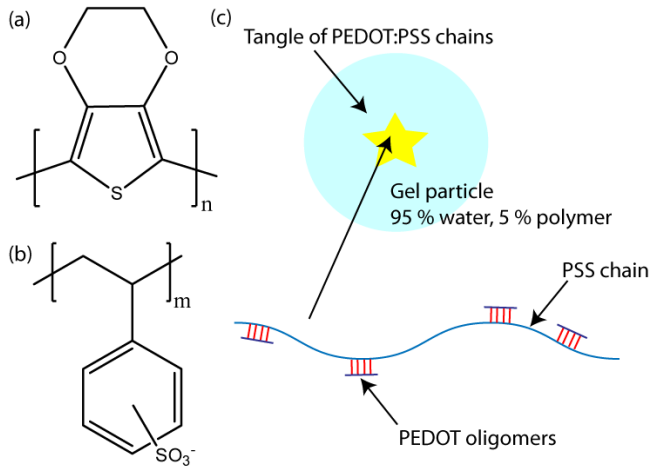

Figure 1.29 Chemical structure of (a) PEDOT (b) PSS anion and (c) a simple schematic of the proposed composite of PEDOT:PSS[113]

PEDOT:PSS has high conductivity, high transparency and is used in many applications from photographic film coatings as an antistatic agent, as well as a transparent electrode in touch screens. PEDOT:PSS has been widely used in bulk heterojunction devices as well as bilayer planar devices to ensure ohmic contact, to enhance hole collection, to increase cell open-circuit voltage (V_{oc}) and to enhance electrical uniformity.[115] Unfortunately, many problems are associated with the acidic nature of PEDOT:PSS such as indium etching, and it still only has a work function of ~ 5.1 eV (which is still low in comparison to some donor HOMO levels).

More recently, introducing metal oxides as hole – extracting layers at the anode has also been shown to increase the work function and in turn cell performance through an increase in the V_{oc}.[65, 116] A thin layer (~5nm) of MoO_x has be.0en shown to increase cell performance due to its lower work function and increased compatibility with donor materials. Through using a thin layer of MoO_x, ohmic contact is created at the anode / donor interface through the MoO_x gap states, allowing for the V_{oc} to only be dependent on the interface gap of the active materials.

Thicker layers of MoO_x have a detrimental effect on device performance due to the increased resistance caused by the addition of the thick, insulating oxide.[65] One of the major benefits to using MoO_x over SAMs or PEDOT:PSS is its stability. Utilising oxide layers as a barrier between the ITO and the active layer improves the device stability in air with minimal degradation in a nitrogen atmosphere.[117] Other oxides such as tungsten oxide, WO_x, and vanadium oxide, V_2O_x, have also been shown to improve the contacts between ITO and more recently, efforts to solution process these oxides have shown promising results.[118,119] This could lend more stable extracting layers to large scale printing methods for future technologies.

Aluminium (Al) is typically used as the back electrode for these device architectures due the low work function of ~ 4.2 eV, is easily evaporated, of low cost and abundant. Other available metals with low work functions generally have high chemical reactivity such as Mg and Ca or are more expensive e.g. Ag.

1.5. The drive to find new materials

One of the limiting factors in achieving high efficiencies in OPVs is the lack of optimised organic semiconductors, especially with regards to acceptor materials. Progress has been made in new donor materials for both bulk heterojunction and small molecule planar heterojunction devices. Functionalisation of existing donor materials has quite recently been show to tune the stability, energy levels as well as device performance and the hopes of achieving high efficiencies can be realised with these "ideal" materials being produced. Donor materials have primarily been at the forefront of design, and Pcs, being chemically and thermally stable, have become even more of an interest due to the wide range of possibilities that are open for electronic and physical modification. Dyes such as Pcs, SubPcs, merocyanines

(MC), squaraines (SQ), diketopyrrolopyrroles (DPP), borondipyrromethane (BODIPY), perylene diimides (PPI), dicyanovinyl (DCV)-substituted oligothiphenes and many more have recently been functionalized to improve performance, and several groups have demonstrated that this is a promising method for material design. A few material sets will be discussed here.

In 2006, when SubPc / C_{60} cells were reported by Forrest *et al.* the V_{oc} of 0.94 V (resulting in a PCE of 2.1 %) was a promising achievement, further improved by Gommans *et al.* through an improvement in J_{sc} and a higher PCE of 3 %.[25,120] A few years later in 2009, subnaphthalocyanine (SubNPc) was reported to be a promising donor material due to having a strong absorption, high solubility and low tendency to aggregate.[121] This material formed amorphous films but exhibited high charge transport and could be easily processed via spin casting. Solution processed into a bilayer device (with an evaporated C_{60} layer) efficiencies of 1.5 % could be achieved. Through changing the method of deposition to a vacuum processed layer of SubNPc the efficiency was further improved to 2.5%, with large increases in both J_{sc}, and V_{oc}.[122]

MC dyes offer high absorption coefficients of ~10^5 $M^{-1}cm^{-1}$ as well as large variability in the position of the HOMO and LUMO levels.[123] In 2006, Meerholtz showed their potential in BHJ devices with PCBM resulting in efficiencies of 1.74%. To improve the efficiencies further, the MC dye was vacuum co-deposited with C_{60}, resulting in an extremely large improvement to 6.1 % and a V_{oc} of 1 V.[124] Wurthner *et al.* used thermal evaporated planar MC / C_{60} devices to study charge dissociation with respect to dye orientation. As – deposited MC / C_{60} devices displayed distinct s – shaped kinks in their *J-V* curves indicative of a charge transport problem within the layers, greatly affecting the FF of the devices and hence efficiency.[125] Through

deposition of the MC onto a heated substrate, surprisingly, this s – shaped kink disappeared. Fourier transform infra-red ellipsometry showed a distinct change in dye orientation once the layers had been heated past their glass transition temperature (~77^{o}C). Before this temperature, no real change in the *J-V* curves, FF or orientation is apparent. To further understand this improvement QM / MM methods were used to calculate the influence the orientation has on the CT state and it was found that with the heat treated films, charge dissociation was greatly increased in comparison to as – deposited films.[125] To further demonstrate the capabilities of this family of dyes, a MC dye was also incorporated into a tandem cell configuration where two of the same codeposited MC / C_{60} cells were sandwiched together via a MoO_x / Al recombination layer, reaching a V_{oc} of > 2 V and an efficiency of close to 5 %.[126]

Marks and co-workers in 2008 showed that SQ dyes had some promise in OPVs by manufacturing BHJ cells in air with PCBM and achieving PCEs of 1.8%.[127] Unfortunately, although the red shift in SQs (compared to other materials) seemed initially promising, it has an extremely low L_D ~ 1.6 nm keeping bilayers very thin. The easy functionalization of SQs means that a wide range can be produced with various absorption, energetic and morphological properties and through tweaking the molecular structure and using hexenyl groups (replacing the 2-ethynyl side chains) the performance was improved to > 2 %.[127] SQ dyes also offer high absorption coefficients and can offer lots of variations in molecular energy levels as shown by Thompson and Forrest through various tweaks in the structure.[128] SQs are also extremely versatile with regards to processing conditions and can be both vacuum deposited; demonstrated by Thompson, Forrest and co. by creating a bilayer SQ / C_{60} cell, fully evaporated, achieving an efficiency of 3.2 %; and by

solution processing for e.g. solution processing the SQ dye and evaporating C_{60} to achieve an efficiency of 4.1 %.[128,129]

Dicyano (DCV)-substituted oligothiophenes, DCVnT (where n = 1-6) were introduced as a donor by Fitzner *et al.*[130] The novel series was synthesised and structural analysis determined almost ideal π-π stacking as a prerequisite for good charge transport for materials with n > 4. These longer oligomers were implemented into vacuum processed devices achieving an impressive efficiency of 2.8 % for planar structures. The optimisation of co-deposited cells for DCV5T and C_{60} (2:1 ratio) resulted in an efficiency of 5.2 %, one of the highest efficiencies for a vacuum deposited single heterojunction device.[130] These materials were then used in their 6 % tandem cells in 2011[32] and may possibly be used in Heliateks 12 % tandems.[17]

Tuning the electronic and structural properties of acenes has also shown some promise in designing optimal semiconductors. Fused acenes such as pentacene and tetracene have been extensively studied in OFETs and typically studied as p-type semiconductors. Anthony *et al.* functionalised pentacene with two solubilising groups (triisopropylsilylethynyl) to impart solubility to these materials and enable fast, easily processed BHJs as mentioned previously.[83] Functionalisation of the donor material TIPSEpent will be discussed in results **Chapter 4**.

Although many variations of donors have been investigated with varied amounts of success, new acceptors still remain a mystery to the OPV community, and the most commonly used acceptors are fullerene based molecules such as C_{60}, C_{70} and their soluble derivatives, PCBM and $PC_{70}BM$. Although C_{60} is extremely efficient as an acceptor its limitations have been previously discussed. Prior to fullerenes, perylenes were used as the common acceptor material in OPVs but had

lower V_{oc}s and FF.[131] In the past few years finding new non – fullerene based acceptors has become of great interest with many variations of molecules being tested.

One method of increasing the n-type character of molecules is to introduce electron withdrawing units, such as fluorine and cyano, to the periphery of the aromatic rings. Peisert *et al.* synthesised a fluorinated Copper Phthalocyanine (F_{16}CuPc) which normally without fluorination exhibits p – type behaviour. Subsequent fluorinations increased the molecule's IP whilst keeping the band gap relatively similar.[132] Recently, Yang *et al.* incorporated the n – type F_{16}CuPc into an OPV device with SubPc as the donor material, reaching a power conversion efficiency of 0.56%, unfortunately much lower than a C_{60} cell would normally achieve (3.2%).[133] Perfluorinated SubPc (F_{13}SubPc) has also been trialled as an acceptor material in combination with acenes and other MPcs by Torres and co-workers (**Figure 1.30a**).[134] Although there is a marginal improvement in V_{oc} in some cases, there is a large decrease in both J_{sc} and FF in comparison to using C_{60}.[134] The highest PCE achieved was 0.96% for the SubPc / F_{13}SubPc device, much lower than the C_{60} control cell.

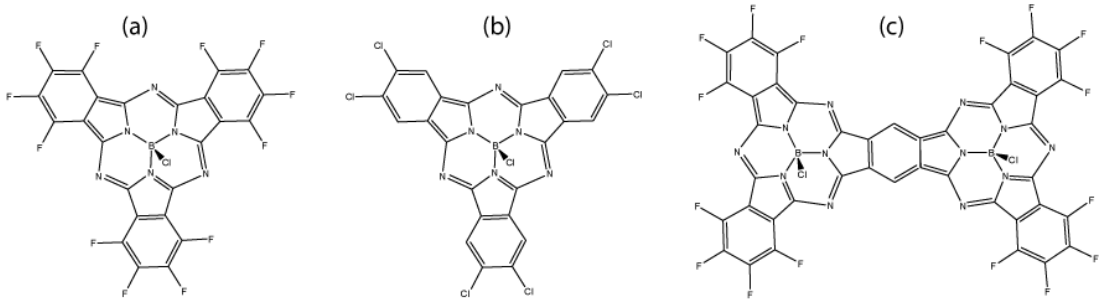

Figure 1.30 New molecular acceptors

In 2011 Sullivan *et al.* displayed one of the first competitive replacements for C_{60}.[70] Through using 6 Cl atoms on the periphery of the SubPc, Cl_6SubPc showed promising performance. Selective halogenation to tune the energy levels of SubPc provided sufficient offset at the HJ when using SubPc as the donor material to maximise the interface gap while still efficiently dissociating the exciton, leading to PCEs of 2.7 % and a high V_{oc}.[70]

Recently, Verreet *et al.* reported the use of fused F-SubPcs dimers in planar SHJ cells. (**Fig. 1.30c**).[135] Due to the extended conjugation the absorption spectra of this dimer is red-shifted compared to the parent SubPc and therefore is extremely complementary. The SubPc / F-SubPc dimer cells achieve 1.2 % PCE and 2.5 % when used in an inverse architecture. Lower fill factors of 0.24 and 0.48 respectively keep the efficiencies limited, and only when adding C_{60} in a triple layer architecture does the fill factor recover to 0.54. This leads to an efficiency of 4% due to an increase in J_{sc} of 2 mA cm^{-2} to 7.8 mA cm^{-2}.[135]

Although new acceptor materials are beginning to be researched, as of yet, not many materials have come close to being used as a direct replacement for fullerene derivatives. This will be further discussed in **Chapters 5** and **6**.

Besides the discovery of new materials, the development of organic semiconductors requires achieving a much better understanding of the nature of electronic structure and charge transport properties, as well as light and charge interactions, if we are to find improved materials. Even though 12 % is less than the standard efficiency of silicon cells (~18 %), with recent progress organic photovoltaics are beginning to become competitive and are showing good potential to enter the market with a viable product.

1.6. Thesis outline

The focus of this thesis is predominantly on the use of new organic semiconductors in organic photovoltaics, understanding their optical and physical properties and how these link to device performance. The work here surrounds the use of planar "bilayer" OPVs, with heavy interest in the energetics of the systems, specifically at the D / A interface. This interface is the dominant factor in determining the V_{oc} of a device and an attempt is made here to discover how to achieve the maximum voltages and hence improve efficiencies. The inherent limitations and challenges that exist when trying to improve this parameter are also discussed throughout.

Chapters 2 and **3** cover all the experimental and analysis techniques used throughout this work from thin film formation and film characterisation to OPV device fabrication and analysis.

The quest for improving an existing donor semiconductor is the focus of **Chapter 4**, investigating the use of chlorination to modify frontier molecular orbitals for the improvement of TIPSE-pentacene to increase $J_{sc,}$ V_{oc} and stability.

Phthalocyanines, although typically used as donor materials, display ambipolar characteristics and to gain an understanding of their use as acceptor materials, bilayer devices were grown in both **Chapters 5** and **6**. **Chapter 5** initially discusses the use of an underused acene, tetracene, and the optimisation of both the vacuum deposited thin films and devices. The use of SubPc as a direct replacement for C_{60} is then discussed and a detailed analysis of the energetics of these systems is given with data from soft x – ray spectroscopy. The optimised devices are then discussed using the original Tc / C_{60} devices as a reference.

Chapter 6 employs Pentacene as the donor material and discusses again the use of SubPc and ClAlPc as direct replacements for C_{60} in the hope of improving the V_{oc} and stability of the devices. Here some unusual results are discovered and discussed with interest in the photophysics of the cells due to the formation of triplets in the Pentacene semiconductor.

Chapter 7 brings together some concluding remarks with possible further future directions discussed.

1.7. References

1. *http://www.ipcc.ch/index.htm*.
2. World key energy statistics. **2012**. *www.iea.org*
3. World Energy Outlook **2010**.
4. A. E. Bequerel *Comptes Rendus* **1839**, *9* 561.
5. W. Smith. *Soc. Teleg. Eng*., **1873**, *2*, 31.
6. D. M. Chapin, C. S. Fuller, and G. L. Pearson, *J. Appl. Phys*., **1954**, *25*, 676.
7. http://code8100.nrl.navy.mil/about/heritage/vanguard.htm
8. M. A. Green, K. Emery, Y. Hishikawa, W. Warta, *Progress in Photovoltaics: Research and Applications*, **2010**, *18*, 346.
9. S. Benagli, D. Borrello, E. Vallat-Sauvain, J. Meier, U. Kroll U, J. Hotzel. *24th European Photovoltaic Solar Energy Conference*, Hamburg, September **2009**.
10. http://www.nrel.gov/solar/
11. G. J. Bauhuis, P. Mulder, E. J, HaverKamp, J. C. C. M. Huijben, and J. Schermer. *J.Sol.Energy Mater. Sol. Cells* **2009,** *931488*, 1491
12. C. J. Keavney, V. E. Haven, S. M. Vernon. *Conference Record, 21st IEEE Photovoltaic Specialists Conference* ,Kissimimee, May **1990**, 141.
13. I. Repins, M. Contreras, Y. Romero, Y. Yan, W. Metzger, J. Li, S. Johnston., B. Egaas, C. DeHart, J. Scharf, B. E. McCandless and R. Noufi *33th IEEE Photovoltaics Specialists Conference Record*, **2008.**
14. X. Wu, J. C. Keane, R. G. Dhere, C. DeHart, T. A. Duda T. A. Gessert, S. Asher D. H. Levi P. Sheldon P*roceedings of 17th European Photovoltaic SolarEnergy ConferenceMunich*, October **2001**, 995.
15. P. L. Ong, I. A. Levitsky, *Energies***, 2010**, *3*, 313.
16. M. Ohmori, T. Takamoto, E. Ikeda, H. Kurita *Techical Digest, International PVSEC-9*, Miyasaki, Japan, November **1996**, 525.
17. *Press release* http://www.heliatek.com/newscenter/latest_news/ *January* **2013**.
18. J. S. Bonham. *J. Chern.* **1976**, *29*, 2123.
19. C. W. Tang, *Applied Physics Letters*, **1986**, *48*, 183.
20. H. W. Kroto, J. R. Heath, S. C. Obrien, R. F. Curl and R. E. Smalley, *Nature*, 1985, **318**, 162.
21. P. Peumans and S. R. Forrest, *Applied Physics Letters*, 2001, **79**, 126.
22. P. Sullivan, T. S. Jones, *Org. Electron.* **2008**, *9*, 656.

23. R. F. Bailey-Salzman, B. P. Rand and S. R. Forrest, *Applied Physics Letters*, 2007, **91**, 013508.
24. V. Steinmann, N. M. Kronenberg, M. R. Lenze, S. M. Graf, D. Hertel, K. Meerholz, H. Buerckstuemmer, E. V. Tulyakova and F. Wuerthner, *Advanced Energy Materials*, 2011, **1**, 888.
25. S. Uchida, J. G. Xue, B. P. Rand and S. R. Forrest, *Applied Physics Letters*, 2004, **84**, 4218.
26. R. Pandey and R. J. Holmes. *Appl. Phys. Lett.* **2012**, *100*, 083303.
27. A. W. Hains, Z. Liang, M. A. Woodhouse and B. A. Gregg, *Chemical Reviews*, **2010**, *110*, 6689.
28. G. Yu, J. Gao, J. C. Hummelen, F. Wudl, A. J. Heeger, Science, **1995**, 270, 1789.
29. J. Gilot, M. M. Wienk, R. A. J. Janssen, *Appl. Phys. Lett.* **2007,** *90*, 143512.
30. N. S. Sariciftci, L. Smilowitz, A. J. Heeger, F. Wudl, *Science*, **1992**, *258*, 1474.
31. D. Cheyns, B. P. Rand, P. Heremans, *Appl.Phys.Lett.***2010**, *97*, 033301.
32. M. Riede, C. Ulrich, J. Widmer, R. Timmreck, D. Wynands, G. Schwartz, W-M. Cnehr, D. Hildebrandt, A. Weiss, J. Hwang, S. Sundarraj, P. Erk, M. Pfeiffer and K. Leo, *Adv. Funct. Mater.* **2011**, *21*, 3019.
33. http://optics.org/indepth/2/9/1 September, **2011**.
34. Y. Sato, R. Niinomi, Y. Abe, Y. Matsuo, E. Nakamura, *Proc. of SPIE* **2008**, *7052*, 70520J.
35. http://www.mitsubishichem-hd.co.jp/english/group/strategy/major_project/solar_cell.html
36. J. Nelson, The Physics of Solar Cells, Imperial College Press, London, **2003**.
37. P. Wuerfel, U. Wuerfel, Physics of Solar Cells: From Basic Principles to Advanced Concepts, Wiley-VCH Verlag GmbH & Co KGgA, Weinheim, **2009**.
38. P. Peumans, A. Yakimov, S. R. Forrest, *Journal of Applied Physics*, **2003**, *93*, 3693.
39. P. Heremans, D. Cheyns, B. P. Rand, *Accounts of Chemical Research*, **2009**, *42*, 1740.
40. B. P. Rand, D. P. Burk, S. R. Forrest, *Physical Review B*, **2007**, *75*, 115327.
41. J. L. Bredas, J. E. Norton, J. Cornil, V. Coropceanu, *Accounts of Chemical research*, **2009**, *42*, 1691.
42. S. E. Gledhill, B. Scott, B. A. Gregg, *Journal of Materials Research***, 2005**, *20*, 3167.
43. M. A. Green *Silicon Solar Cells. Advanced Principles and Practice.* University of New South Wales, Sydney, **1995**.
44. I. G. Hill, A. Kahn, Z. G. Soos, R. A. Pascal, *Chemical Physics Letters*, **2000**, *327*, 181.
45. M. Knupfer, *Appl. Phys. a-Mater. Sci. & Proc.* **2003**, *77*, 623.
46. K. Feron, W. J. Belcher, C. J. Fell and P. C. Dastoor. *Int. J. Mol. Sci*. **2012**, *13*, 17019.
47. S. Jang, Y. Jung, R. Silbey, *J. Chem. Phys.* **2002**, *275*, 319.
48. P. W. M. Blom, V. D. Mihailetchi, L. J. A. Koster, D. E. Markov, *Adv. Mater.* **2007**, *19*, 1551.
49. T. Stubinger, W. Brutting, *J. Appl. Phys.* **2001**, *90*, 3632.
50. (a) W. A. Luhman, R. J. Holmes, *Adv. Funct. Mater,* **2011**, *21*, 764. (b) H. Gommans, S. Schols, A. Kadashchuk, P. Heremans, S. C. J. Meskers, *J. Phys. Chem. C*, **2009**, *113*, 2974.
51. B. Kippelen, J. L. Bredas, *Ener. Environ. Sci.* **2009**, *2*, 251.

52. S. Yoo, W. J. Potscavage, B. Domercq, S-H. Han, D. Levi and B. Kippelem. MRS Proceedings. **2006,** *965*, 1100.
53. T. Yago, Y. Tamaki, A. Furube and R. Katoh. *Phys.Chem.Chem.Phys.,* **2008**, *1*, 4435.
54. K. Y. Law *Chem.Rev.* **1993**, *93*, 449.
55. (a) G. Yu and A. J. Heeger, *J. Appl. Phys* **1995,** *78*, 4510. (b) J. J. M. Halls, C. A. Walsh, N. C. Greenham, M. E. A., R. H. Friend, S. C. Moratti, and A. B. Holmes, *Nature*, **1995**, *376*, 498.
56. (a) P. Peumans, S. Uchida, and S. R. Forrest, *Nature*. **2003**, *425*, 158. (b) D. Gebeyehu, M. Pfei_er, B. Maennig, J. Drechsel, A.Werner, and K. Leo, *Thin Solid Films*, **2004**, *451*, 29.
57. (a) X. Yang, J. Loos, *Macromolecules,* **2007**, *40,* 1353. (b) S. Günes, H. Neugebauer, N. S. Sariciftci, *Chemical Reviews*, **2007**, *107*, 1324.
58. B. P. Rand, J. Genoe, P. Heremans, J. Poortmans, *Progress in Photovoltaics,* **2007**, *15*, 659.
59. M. C. Scharber, D. Wuhlbacher, M. Koppe, *Adv. Mater.*, **2006**. *18*(6), 789.
60. A.Troisi. *Faraday Discuss.*, **2013**, *163*, 377.
61. M. Riede, T. Mueller, W. Tress, R. Schueppel, K. Leo, *Nanotechnology*, **2008**, *19*, 424001.
62. F. Nuesch, K. Kamaris, L. Zuppiroli, *Chem. Phys. Lett.* **1998,** *283*, 194. (b) F. Nuesch, L. J. Rothberg, E. W. Forsythe, T. E. Le, Y. Gao. *Appl. Phys. Lett***. 1999,** *74*, 880. (c) F. Nuesch, E. W. Forsythe, T. E. Le, Y. Gao, L. Rothberg, *J. Appl. Phys.* **2000**, *87*, 7973.
63. N. Beaumont, I. Hancox, P. Sullivan, R.A. Hatton, T. S. Jones. *Energy Environ. Sci.* **2011**, *4*, 1708.
64. C. Tao, S. Ruan, G. Xie, X. Kong, L. Shen, F. Meng, C. Liu, X. Zhang, W. Dong, W. Cheng, *Appl. Phys. Lett.* **2009,** *94*, 043311.
65. I. Hancox, K. V. Chauhan, P. Sullivan, R. A. Hatton, A. Moshar, C. P. A. Mulcahy, T. S. Jones, *Energ. Environ. Sci.* **2010**, *3*, 107.
66. M. Kaltenbrunner, M. S. White, E. D. Glowacki, T. Someya, N. S. Sariciftci and S. Bauer. *Nature Commun.* **2013**, *3*, 770.
67. M. Ichikawa, J. Amagai, Y. Horiba, T. Koyama, Y. Taniguchi, *J. Appl. Phys.* **2003**, *94*, 7796.
68. P. Peumans and S. R. Forrest, *Appl. Phys. Lett*., **2001,** *79*, 126.
69. S. Schumann, R. A. Hatton and T. S. Jones, *J. Phys. Chem. C*, **2011**, *115*, 4916.
70. P. Sullivan, A. Duraud, l. Hancox, N. Beaumont, G. Mirri, J. H. R. Tucker, R. A. Hatton, M. Shipman, T. S. Jones, *Adv. Energ. Mater.* **2011**, *1*, 352.
71. D. Cheyns, H. Gommans, M. Odijk, J. Poortmans, and P. Heremans, *Sol. Energy Mater. Sol. Cells,* **2007,** 91, 399.
72. J. G. Xue, S. Uchida, B. P. Rand. *Appl. Phys. Lett.*, **2004**. *84(16),* 3013.
73. R. A. Marsh, C. Groves, and N. C. Greenham,. *J. Appl. Phys.* **2007,** *101(8*), 083509.
74. P. K. Watkins, A. B. Walker, and G. L. B. Verschoor, ,*Nano Lett.*,**2005** *5(9),* 1814.
75. C. J. .Brabec *Adv. Funct. Mater,* **2001**. *11(5*), 374.
76. B. P. Rand, D. P. Burk, and S. R. Forrest, *Phys. Rev. B,* **2007,** *75*, 115327.
77. D. Cheyns, J. Poortmans, P. Heremans, *Phys. Rev. B.*, **2008**. *77*(16), 165332.
78. C. G. Shuttle, B. O'Regan, A. M. Ballantyne, J. Nelson, D. D. C. Bradley and J. R. Durrant. *Phys. Rev. B.*, **2008**. *78*(11), 113201.

79. C. Goldmann, S. Haas, C. Krellner, K. P. Pernstich, D. J. Gundlach and B. Batlogg, *J. Appl. Phys.* **2004**, *94*, 2080.
80. A. F. Prikhotko, A.F. Skorobogat'ko, and L. I. Cikora, *Optika I Spektroskopiya*, **1969**, *26*, 214.
81. J. M. Robertson, V. C. Sinclair and J. Trotter. *Acta. Cryst.* **1961**, *14*, 697.
82. C. Ambrosch-Draxl, D. Nabok, P. Puschnig and C. Meisenbichler. *New. J. Phys*. **2009**, *11*, 125010.
83. J. E. Anthony, J. S. Brooks, D. L. Eaton, S. R. Parkin.*J. Am. Chem. Soc.* **2001**, *123*, 9482.
84. S. Yoo, B. Domercq, and B. Kippelen *Appl. Phys. Lett.* **2004**, *85*, 5427.
85. Y. Nicolas, F.Castet, M. Devynck, P. Tardy, L. Hirsch, C. Labrugère, H. Allouchi, and T. Toupance *Org. Elec.* **2012**, *13*, 1392.
86. B. Kippelen, W. J. Potscavage, A. Sharma. *Acc. Chem. Res.* **2009**, *42*, 1758.
87. C. W. Chu, Y. Shao, V. Shrotriya, Y. Yang, *Appl. Phys. Lett.* **2005**, *86*, 243506.
88. R. J. Tseng, R. Chan, V. C. Tung and Y. Yang *Adv. Mater.* **2008,** *20*, 435.
89. Y. Shao, S. Sista, C. W. Chu, D. Sievers, Y. Yang, *Appl. Phys. Lett.* **2007**, *90* 103501.
90. M. T. Lloyd, A. C. Mayer, A. S. Tayi, A. M. Bowen, T. G. Kasen, D. J. Herman, D. A. Mourey, J. E. Anthony, G. G. Malliaras *Org. Elec.* **2006**, *7*, 243.
91. P. Gregory. *J. Porphyrins and Phthalocyanines*, **2000**. *4(4*), 432.
92. C. G. Classens, U. Hahn and T. Torres. *The. Chem Record.* **2008**, *8*, 75.
93. P. Sullivan, S. Heutz, S. M. Schultes and T. S. Jones, *Appl. Phys. Lett.* **2004**, *84*, 1210.
94. J. B. Whitlock, P. Panayotatos, G. Sharma, M. D. Cox, R. R. Sauers and G. R. Bird, *Optical Engineering*, **1993**, *32(8)*, 1921.
95. K. L. Mutolo, E. I. Mayo, B. P. Rand, S. R. Forrest and M. E. Thompson. *JACS* **2006,** *128*, 8108.
96. K. V. Chauhan, P. Sullivan, J. L. Yang and T. S. Jones. *J. Phys. Chem. C*. **2012**, *114*, 3304.
97. C. C. Mattheus, W. Michaelis, C. Kelting, W. S. Durfee, D. Wohrle and D. Schlettwein, *Synth. Metals*. **2004**,*146*, 335.
98. K. V. Chauhan, R. Hatton, P. Sullivan T. S. Jones, S.W Cho, L. Piper, A. deMasi, and K. E. Smith *J. Mater. Chem.*, **2010**, *6***,** 1173.
99. N. Li and S. R. Forrest. Appl. Phys. Lett. **2009,** 95, 123309.
100. R. C. Haddon, L. E. Brus andn K. Raghavachari, *Chem. Phys. Lett.* **1986**, *125*, 459.
101. B. P. Rand, J. Xue, S. Uchida and S. R. Forrest *J. Appl. Phys*. **2005**, *98*, 124902.
102. S. W. Cho, L. F. J. Piper, A. DeMasi, A. R. H. Preston, K. E. Smith, K. V. Chauhan, R. A. Hatton, and T. S. Jones, *J. Phys. Chem. C* **2010,** *114*, 18252.
103. T. Asakawa, M. Sasaki, T. Shiraishi and H. Koinuma, Jpn. *J. Appl. Phys.* **1995**, *34*, 1958.
104. J. Xue, B.P. Rand, S. Uchida, S.R. Forrest, *Adv. Mater*. 2**005,** *17*, 66.
105. H. Hommsnd, B. Verreet, B.Rand, R.Muller, J.Poortmans *Adv. Func. Mater.* **2008,** *18***,** 3686.
106. R. Po, C. Carbonera, A. Bernardi and N. Camaioni, *Energy & Environmental Science*, **2011**, *4*, 285.
107. https://spie.org/x18008.xml?highlight=x2402
108. S. Schaefer, A. Petersen, T. A. Wagner, R. Kniprath, D. Lingenfelser, A. Zen, T. Kirchartz, B. Zimmermann, U. Wuerfel, X. Feng and T. Mayer, *Physical Review B*, **2011**, *83*, 165311.

109. S. Khodabakhsh, B. M. Sanderson, J. Nelson and T. S. Jones, *Adv. Funct. Mater.* **2006**, *16*, 95.
110. A. Sharma, A. Haldi, W. J. Potscavage, Jr., P. J. Hotchkiss, S. R. Marder and B. Kippelen, *J. Mater. Chem.* **2009**, *19*, 5298.
111. K. Sarangerel, C. Ganzorig, M. Fujihira, M. Sakomura and K. Ueda, *Chemistry Letters*, **2008**, *37*, 778.
112. R. M. Cook, L-J. Pegg, S. L. Kinnear, O. S. Hutter, R. J. H. Morris and R. A. Hatton. *Adv. Ener. Mater.* **2011**, *21*, 1709.
113. L. S. Roman, W. Mammo, L. A. A. Petersson, M. R. Andersson and O. Inganas, *Adv. Mater.*, **1998**, *10*, 774.
114. L. S. Roman, M. Berggren and O. Inganas. Appl. Phys. Lett. **1999**, 75, 3557.
115. Y. Xia, K. S. J. Ouyang, *Adv. Mater.* **2012**, *24*, 2436.
116. V. Shrotriya, G. Li, Y. Yao, C. W. Chu and Y. Yang, *Applied Physics Letters*, **2006**, *88*, 073508.
117. I. Hancox, P. Sullivan, K. V. Chauhan, N. Beaumont, L. A. Rochford, R. A. Hatton, T. S. Jones, *Org. Electron.* **2010**, *11*, 2019.
118. I. Hancox, L. A. Rochford, D. Clare, M. Walker, J. J. Mudd, P. Sullivan, S. Schumann, C. F. McConville and T. S. Jones, J. Phys. Chem. C**. 2013**, *117*, 49.
119. K. Zilberberg, S. Trost, J. Meyer, A. Kahn, A. Behrendt, D. Luetzenkirchen-Hecht, R. Frahm and T. Riedl, *Advanced Functional Materials*, **2011**, ***21***, 4776.
120. H. Hommans, B. Vereet, B. P. Rand, R. Muler, J. Poortmans, P. Heremens and J. Genoe. Adv. Func. Mater. **2008**, *18*, 3686.
121. B. Ma, C. H. Woo, Y. Miyamoto and J. M. J. Frechet. *Chem Mater* **2009,** *21*, 1413.
122. F.Wurthner, R. Wortmann and K. Meerholz, *Chem. Phys. Chem*, **2002**, *3*, 17.
123. V. Steinmann, N. M. Kronenberg, M. R. Lenze, S. M. Graf, D. Hertel, K. Meerholz, H. Burckstummer, E. V. Tulyakova and F. Wurthner. *Adv. Energy Mater*, **2011**, *1*, 888.
124. A. Ojala, A. Petersen, A. Fucs, R. Lovrincic, C. Polking, J. Trollmann, J. Hwang, C. Lennartz, H. Reichelt, H. W. Hofken, A. Pucci, P. Erk, T. Kirchartz and F. Wurthner. *Adv. Funct. Mater.* **2012**, *22*, 86.
125. V. Steinmann, N. M. Kronenberg, M. R. Lenze, S. M. Graf,D. Hertel, H. Burckstuemmer, F. Wurthner and K. Meerholz. *Appl. Phys. Lett*, **2011**,*99*, 193306.
126. F. Silvestri, M. D. Irwin, L. Beverina, A. Facchetti, G. A. Pagani and T. J. Marks. *J. Am. Chem. Soc.* **2008**, *30*, 17640.
127. D. Bagins, L. BEverina, H. Huang, F. Silvestri, Y. Yao, H. Yan, G. A. Pagani, T. J. Marks and A. Facchettti, *J. Am. Chem. Soc*. **2010**, *132*, 4074.
128. S. Wang, E. I. Mayo, M. D. Perez, L. Griffe, G. Wei, P. I. Djurovich, S. R. Forrest and M. E. Thompson. *Appl. Phys. Lett.* **2009**, *94*, 233304.
129. G. Wei, S. Wang, K. Renshaw, M. E Thompson and S. R. Forrest. *Adv. Energy. Mater*. **2011**, 1, 184.
130. R. Fitzner, E. Reinold, E. Mishra, E. Mena-Osteritz, H. Ziehlke, C. Körner, K. Leo, M. Riede, M. Weil, O. Tsaryova, A. Weiss, C. Uhrich, M. Pfeiffer and P. Bauerle. *Adv. Funct. Mater.* **2011**, *21*, 897.
131. X. Y. Guo, L. J. Bu, Y. Zhao, Z. Y. Xie, Y. H. Geng and L. X. Wang. *Thin solid films.* **2009**, *517*, 4654.
132. H. Peisert, M. Knupfer, T. Schwieger, G. G. Fuentes, D. Olligs, J. Fink and Th. Schmidt, *J. Appl. Phys.* **2003**, *93*, 9863.

133. J. L. Yang, P. Sullivan, S. Schumann, I. Hancox and T. S. Jones *Appl. Phys. Lett.* **2012**, *100*, 023307.
134. H. Gommans, T. Aernouts, B. Verreet, P. Heremans, A. Medina, C. G. Claessens, T. Torres, *Adv. Funct. Mater.* **2009**, *19*, 3435.
135. B. Verreet, B. P. Rand, D. Cheyns, A. Hadipour, T. Aernouts, P. Heremens, A. Medina, C. G. Claessens and T. Torres. *Adv. Ener. Mater.* **2011**, *1*, 565

Chapter 2

Experimental, characterisation and analysis

This chapter discusses the various sample preparation methods and a general description of the principle experimental procedures. Solution and thin film analysis is discussed as well as device characterisation and analysis techniques. More detailed experimental information is given in the results chapters since they provide better context alongside the data.

2.1. Thin film and device fabrication

2.1.1. Material purification

Having high material purity is extremely important in the preparation of organic photovoltaics and therefore impurities were removed from the materials via thermal gradient sublimation.[1,2]

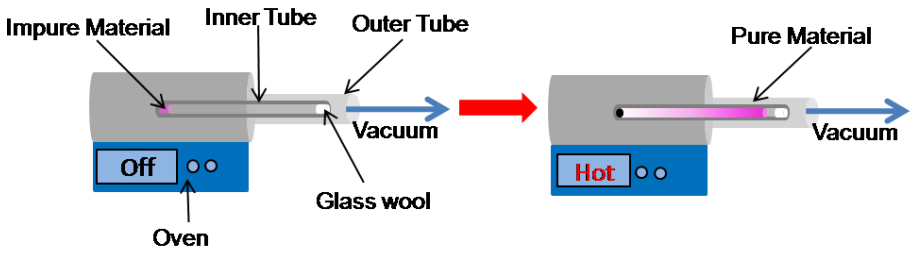

Figure 2. 1 Schematic of the thermal gradient sublimation system.

Through purifying the organic materials there is reduced batch to batch variance and greater device consistency. The method places the powdered organic semiconductor at the end of a disposable quartz tube which is then placed into a larger quartz tube. A small amount of glass wool is placed in the end of the inner quartz tube to stop any small traces of organic material being drawn into the vacuum pump. The large tube is placed into the furnace and connected to the vacuum system and taken to ~ 10^{-5} mbar with both a backing (~10^{-1} mbar) and turbo pump (~ 10^{-5} mbar). Once under vacuum the temperature is ramped to the sublimation temperature at a rate of 0.1-1 ^{o}C min^{-1} (dependent on material) and then held at the temperature for 10 - 15 hours. Having a slow ramp to sublimation temperature allows for any impurities with lower sublimation points to evaporate first and travel furthest down the tube and into the glass wool. Once cool, the fraction of interest is then collected and stored under inert atmosphere.

Substrate cleaning

All layers were grown onto commercially available ITO coated glass (R_s < 15 Ωsq^{-1}) or quartz. Each substrate before use was thoroughly cleaned using the following process:

- ✓ Rinse with acetone
- ✓ Sonicate in acetone for 15 minutes
- ✓ Rinse with acetone
- ✓ Rinse with water
- ✓ Sonicate in Water:Decon mix (70:30) for 15 minutes
- ✓ Rinse with water
- ✓ Sonicate in water for 15 minutes
- ✓ Rinse with water

- ✓ Rinse with IPA
- ✓ Sonicate in IPA for 15 minutes.
- ✓ Dry with a jet of nitrogen

Substrates were then treated with ozone using a Novascan PSD-UVT temperature controlled UV- surface decontamination system which removes any residue organic matter from the surface.

2.1.2. Solution processed thin films

Spin coating is a solution processing method for depositing thin films very quickly at room temperature and pressure.[3] A substrate is held in place with a vacuum, and accelerated to a desired rotational speed. Drops of solution are added to the substrate, spread evenly across the surface due to the centrifugal force of the rotation and the solvent evaporates to leave a thin film on the surface (**Figure 2.2**). The thickness of the film is controlled by the concentration of the solution and the rotation speed – higher concentrations and slower speeds give thicker films.

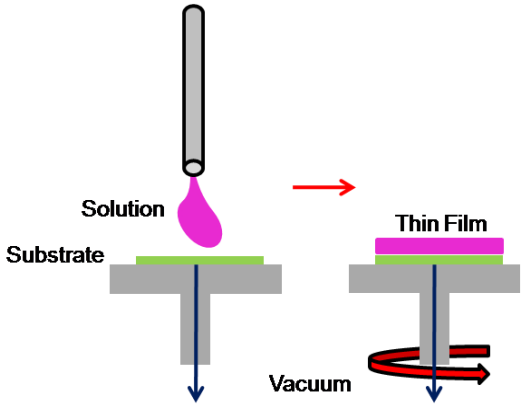

Figure 2. 2 Schematic of spin coating technique for thin film deposition.

This method, although fast and under ambient conditions, produces films with less accurate thicknesses and homogeneities compared to organic molecular beam deposition (OMBD). All solution processed layers were made using a Laurell technologies spin coater. (see results **Chapter 4** for more detail).

2.1.3. Vacuum deposited thin films

Organic molecular beam deposition (OMBD) is the growth of thin films of small molecular weight semiconductors via sublimation and a schematic of the system is shown in **Figure 2.3**.

The growth is carried out in a high vacuum environment (~10^{-7} mbar) to ensure a clean environment, lack of impurities, ease of multilayer growth and formation of discrete interfaces, and to aid high reproducibility and consistency. Typically the chamber is pumped by a cryogenic pump (1 x 10^{-8}) after roughing by a scroll pump. A resistively heated boron nitride crucible is filled and ramped up to the sublimation point of the material (50 - 500^{o} C).[4]

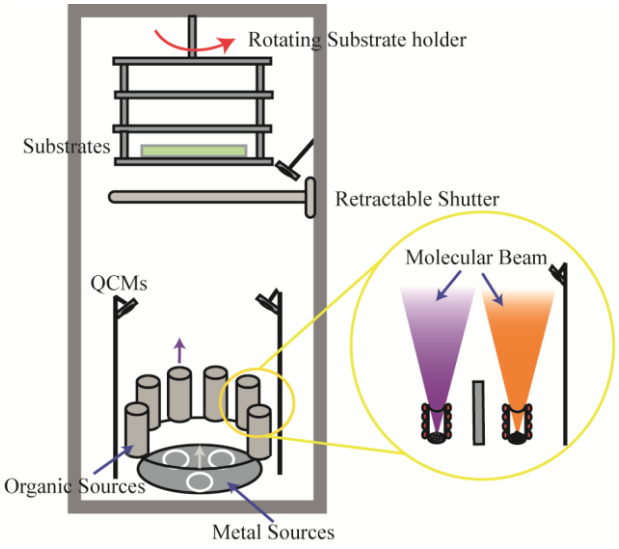

Figure 2.3 Schematic of the OMBD Kurt J. Lesker Spectros system

The resultant vapour pressure escapes through the crucible aperture as a molecular beam and deposits onto the substrate. A quartz crystal microbalance (QCM) is used to monitor the rate and thickness *in situ* of the semiconductor layers to ensure high accuracy and control over the growth parameters.[4] The monitored thicknesses are calibrated using *ex situ* analysis of step edges of the grown films using AFM (as discussed later). A Kurt J. Lesker Spectros system was used for the growth of all thin films and devices unless otherwise stated. With all the growth systems the substrates can be moved via a manipulator, which allows for the placement of the substrates on to shadow masks. This allows for multiple device structures to be grown in a single growth (without venting the vacuum chamber) including electrode deposition via a shadow mask to allow for accurate, precise pixels on a substrate.

A schematic of the final grown devices is shown in **Figure 2.4**. Device structures in this thesis are represented schematically as follows:

ITO / interlayer (IL) (nm) / Donor (nm) / Acceptor (nm) | BCP (nm) / Al (100 nm)

where the "/" symbol is used to denote an interface.

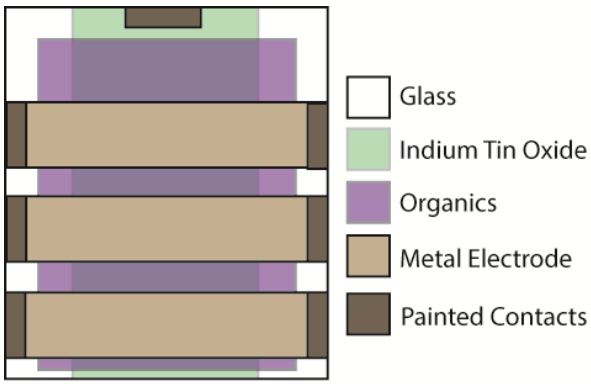

Figure 2.4 Device schematic

See results sections for extra experimental details such as information on growth temperatures, rates and thicknesses (*in situ* and *ex situ*) for the materials used.

In-situ and ex-situ thickness measurments.

In-situ thickness measurements of the layers and deposition rates were measured using a series of gold coated QCM crystals (Kurt J.Lesker). As the material is evaporated, the resonant frequency of the QCM changes as mass is deposited and this change is monitored.[5] Each QCM thickness is calibrated *ex-situ* to allow for accurate measurements during growth.

Ex-situ measurements are carried out with step edge analysis using tapping mode atomic force microscopy (TM- AFM, a detailed explanation is provided about TM-AFM in section 2.2.6).[6] 30 – 50 nm layers (QCM measured) of the material of interest were grown onto ITO substrates. The films were carefully scored horizontally and vertically using a sharp needle to generate a void / step from the film to the substrate. A normal TM-AFM scan is then used across the step edge and the height difference between the film surface and the substrate is the actual film thickness. To ensure complete accuracy, the step edge is measured at a few locations on the substrate and a statistical height distribution analysis is used to average over the whole scanned area (rather than taking a single height point).

2.2. Solution and thin film analysis

2.2.1. UV/Vis absorption spectroscopy

Absorption spectroscopy is a technique that measures the absorption intensity of photons through a sample at a particular wavelength. The amount of light, *I*, transmitted through a sample can be related to its concentration by Beer-Lambert's law:

$$A = log\frac{I_0}{I} = \varepsilon lc \qquad \textbf{Equation 2. 1}$$

Where A = absorbance, I_o is the incident light intensity, I is the attenuated light leaving the sample, ε is the molar extinction coefficient for a given wavelength, l is the path length and c is the concentration. In solids, the concentration is related to the molecular mass and density. For thin films, the molar extinction coefficient and concentration are defined by the absorptivity of the material, α and the path length is now the film thickness (**Equation 2.2**).

$$A = log\frac{I_0}{I} = \alpha l \qquad \textbf{Equation 2. 2}$$

Different materials absorb in different areas of the UV – Vis spectrum and it is extremely important in OPVs to understand the position and extent of absorption to determine which combinations of materials will give the optimum spectral coverage.

All UV-Vis absorption spectra were taken on a Perkin-Elmer Lambda 25 Spectrometer.

2.2.2. Photoluminescence spectroscopy (PL)

Photoluminescence spectroscopy, PL, measures the emission that occurs after a sample has been photo - excited to a higher energetic state (S_n) from the ground state (S_o). The Jablonski diagram, shown in **Figure 2.5**, illustrates the various mechanisms for an excited molecule to decay back down to the ground state (S_o or GS).

All emitted photons come from the ν = 0 vibrational level of the singlet excited state as stated by Kasha's rule due to rapid vibrational relaxation after electronic excitation. After vibrational relaxation, non-radiative processes such as internal conversion (IC) or intersystem crossing (ISC), or radiative processes such as fluorescence from a singlet state or phosphorescence from a triplet state, can occur to relax the excited species to the ground state.

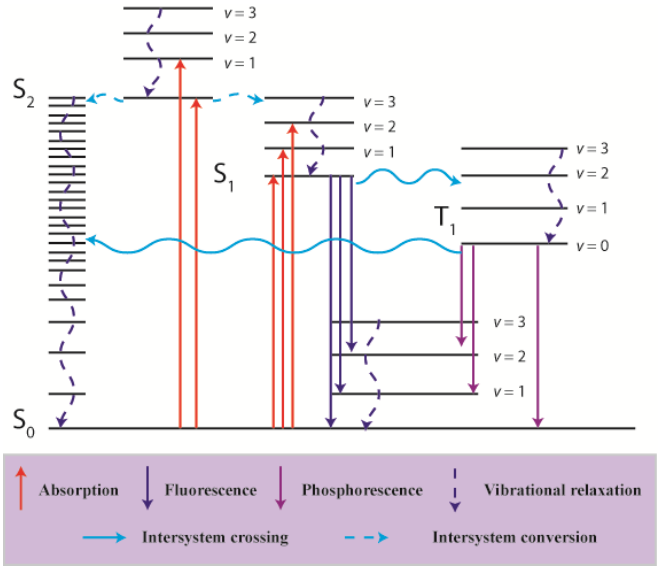

Figure 2.5 Jablonski diagram illustrating the electronics states of a molecule and the transitions between them.

Generally, there is an energetic difference between the absorbed wavelength (from the ground state (S_0) to the excited state (S_1)) and the emission from S_1 back to S_0 as shown in **Figure 2.6**.

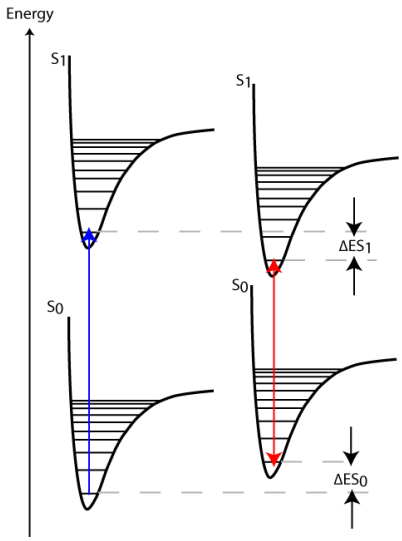

Figure 2.6 Schematic diagram illustrating the origin of the Stoke's shift between the absorption and emission energy.

This difference can give an indication between the ground state and the excited state interactions of a solution or film and is known as the Stoke's shift. There can be considerable differences in Stoke's shift depending on whether the surrounding environment will stabilise the excited state for e.g. a molecule in a strongly interacting solvent.

Shown in **Figure 2.7** is a simple schematic of a PL spectroscopy set up. Light is directed onto a sample, where it can be absorbed and excites a molecule to an excited state.

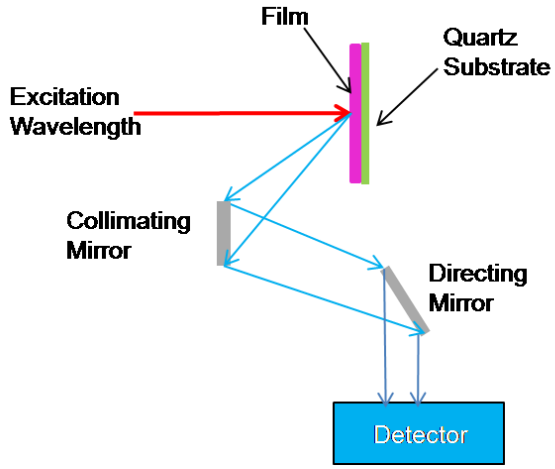

Figure 2.7 Schematic of the photoluminescence set up.

This excess energy can be dissipated through the emission of light. The energy of the emitted light relates to the difference in energy levels between the two electronic states involved in the transition. The intensity and spectral content of this photoluminescence can determine the purity, whether defects and impurities are present in the films, the band gaps of materials, and can relate to various recombination mechanisms (or transfer mechanisms when looking at more than one

material).All PL measurements were taken on a Horiba Jobin Yvon PL system and FluorEssence™ software 2.1.

2.2.3. Cyclic Voltammetry (CV)

Cyclic voltammetry is a measurement usually used to study electrochemical properties of an analyte in solution. It differs from linear voltammetry as the voltage is swept from an initial voltage, V_1, to a final voltage, V_2, and then back again (example shown in **Figure 2.8a**)

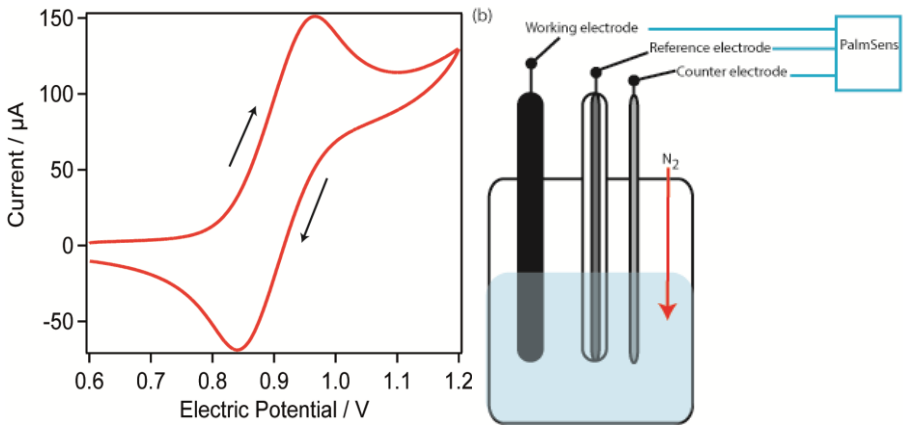

Figure 2.8(a) An example of a Ferrocene voltammogram and **(b)** a schematic of the electrochemical set up.

Typically, a three electrode set up is used as seen in **Figure 2.8b** consisting of a working, reference and counter electrode. The working electrode will be platinum, glassy carbon or gold, the reference electrode Ag / AgCl and the counter electrode is typically a metal wire such as platinum that conducts electricity well but will not interfere with the solution.

In the context of this thesis cyclic voltammetry was carried out to obtain the HOMO of the organic donor materials using a method developed by D' Andrade *et al.*[6] This method showed a linear relationship between the HOMO and the oxidation potential of the organic semiconductors as shown below in **Equation 2.3**:

$$E_{HOMO} = -(1.4 \pm 0.1)x\,(qV_{cv}) - (4.6 \pm 0.08)\,eV \qquad \textbf{Equation 2.3}$$

Where q is the charge and V_{cv} is the difference between the semiconductor oxidation potential and the reference (in this case ferrocene) oxidation potential as labelled in **Figure 2.9.** The donor materials were dissolved in acetronitrile with tetra-n-butylammonium fluoride phosphate (TBAPF) as an electrolyte with respect to a Ferrocene / Ferrocene^{+} (Fc/ Fc^{+}) reference. CV measurements were taken using PalmSens portable potentiostat and analysed using PSTrace software.

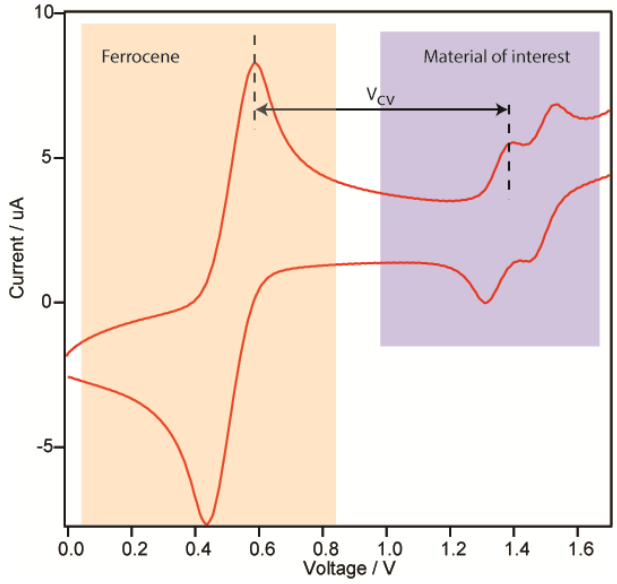

Figure 2.9 Example of CV of ferrocene and an organic semiconductor of interest. V_{cv} is highlighted.

2.2.4. Kelvin Probe (KP)

Kelvin probe (KP) is a non contact, non destructive, vibrating capacitor device that measures the work function (ϕ) of a surface and generally consists of a two conductive materials sandwiching a dielectric (insulator) (**Figure 2.10a**). As separate plates they will have common vacuum levels. The work functions of the conductors are fixed and are given by:

$$\boldsymbol{\varphi_i = -e\,x\,VL_i - (E_f)_i} \qquad \textbf{Equation 2.4}$$

Where VL is the vacuum level near the surface, E_f is the Fermi level of the conductor and the *i* denotes either the sample (s) or the reference (r). When the two conducting materials are connected, electrons in the material with lower work function flow into the material with the higher work function and this creates equal and opposite charges within the capacitor (**Figure 2.10b**).

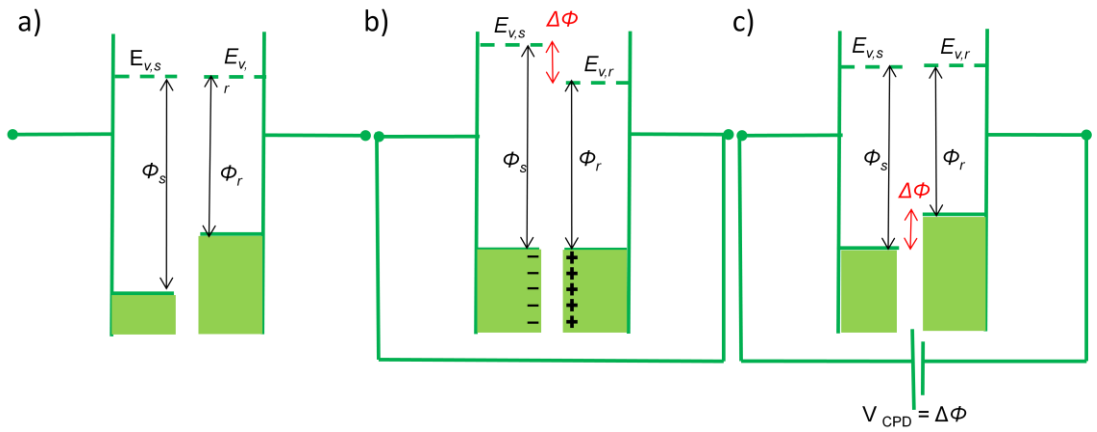

Figure 2.10 Schematic energy level diagrams for the Kelvin probe (parallel plate capacitor) with (a) isolated plates, (b) at short circuit and (c) with a DC voltage equal to the built in potential (V_{CPD})

This resulting flow of charge induces a potential gradient which is termed the contact potential difference (CPD) and is equal the difference in the work functions, $\Delta\varphi = \varphi_s - \varphi_r$. At this point the Fermi levels of the conductors align thus changing the vacuum level. Simply to measure this difference, an external voltage is applied (V_{CPD}) so that there is no charge flow between the plates. Through oscillating the probe and therefore altering the distance between the probe and the sample we can vary the capacitance and the result of this is an AC current flows in the circuit. To make the current zero, the capacitor needs to be discharged and this can be achieved through applying a DC voltage to the circuit (V_{CPD}) and biasing one electrode with respect to the other resulting in a null output signal. This potential offset is the relative work function of the sample.

As this is a relative measurement rather than absolute it is calibrated against a reference. In this case the values are compared to a freshly cleaved graphite reference, which has a work function of 4.48 eV.

The Kelvin probe used here was a Besocke Delta Phi

2.2.5. Photoelectron spectroscopy (PES)

2.2.5.1. The Basic principles.

The basic principles of photoelectron spectroscopy are shown in **Figure 2.11**. An incoming photon of energy *hv* enters through the surface and is absorbed by an electron with a binding energy E_B, which then emerges from the solid with a kinetic energy (KE) of $hv - E_B$. The energy distribution of the subsequent emitted electrons should represent the energy distribution of the electronic states in the solid shifted by *hv*.[9] Conservation of energy states that:

$$E_B = h\nu - \Phi - KE \qquad \textbf{Equation 2.5}$$

Where E_B is the binding energy of the emitted electron and Φ is the work function of the solid. This equation assumes that the binding energy of the electron is unchanged after ionisation, implying that the initial and final state of the remaining electrons is the same. This is known as Koopman's theorem[10] and in reality is not actually the case.

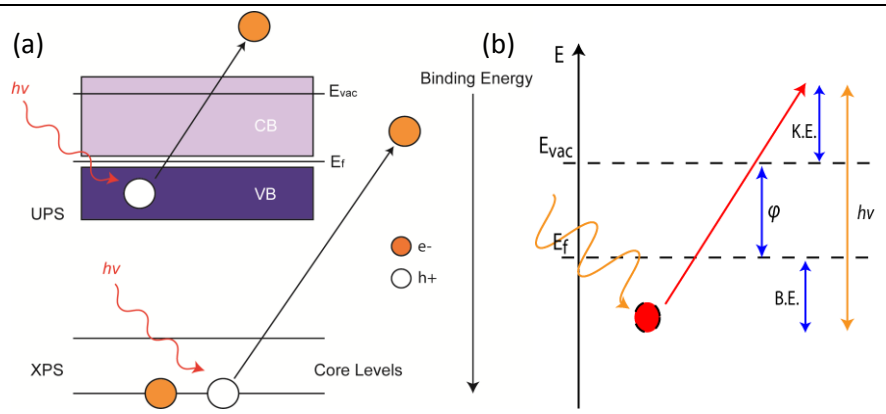

Figure 2.11 (a) Basic Schematic of Photoelectron Spectroscopy and (b) some important parameters labelled.

Due to the remaining electrons relaxing to different energies after photoemission and the core hole influencing the final state, these final states can be extremely significant when investigating the valence states of molecular materials.[9]

The E_B increases with increasing atomic number and increases with decreasing orbital quantum number ($E_{B1s} > E_{B2s}$ and Helium E_{B1s} < Carbon E_{B1s}). The schematic shown in **Figure 2.12** shows the two main relaxation processes after photoionization of the sample. After initial photoemission (**Figure 2.12a**) and subsequent relaxation of a valence electron into the core hole (b) either Auger electron emission or x – ray fluorescence can occur (c). Auger electron emission occurs after a valence electron

has relaxed into the core hole another electron is immediately emitted carrying off the excess energy. The process of x – ray decay sees the excess energy emitted as x – ray fluorescence photons. For K – shell (1s) ionisations Auger decay is the more favourable process.

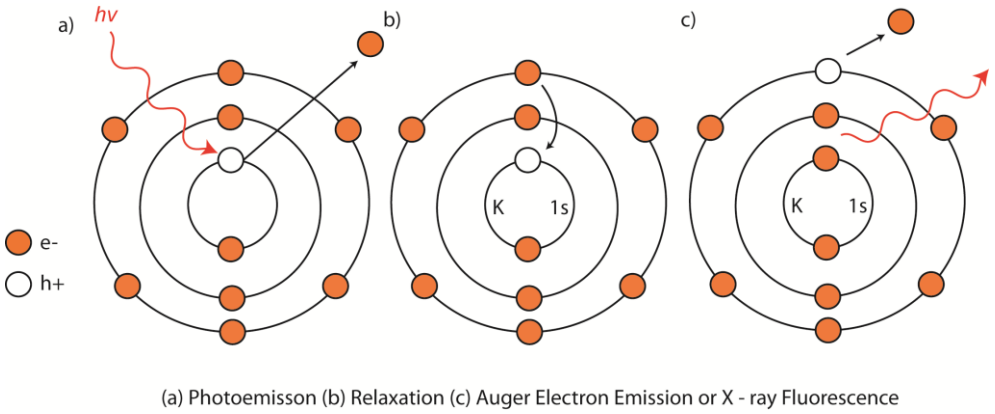

Figure 2.12 The fate of a core hole.

Any photon energy greater than the work function ($h\nu > \Phi$) of the solid can be used for PES. There are two main sources of lab photon energies: Light from gas discharge sources (He and other inert gases) and Al and Mg K_α x – ray emissions.

Firstly, with a He source the two main lines of energy are 21.2 and 40.8 eV (other inert gases have lower energies). These energies are not capable of emitting electrons from the core levels of elements and provide the means to investigate valence band electrons as UPS. Secondly, the Al and Mg K_α X – ray emissions are generally restricted to 1486.6 eV and 1253.6 eV respectively. These soft x – rays form the basis of XPS experiments and the large energy gap between the two sources forms a clear gap between the two techniques UPS and XPS.

Another energy source for PES is synchrotron radiation which is increasing in its use. This has led to a weakening between the two techniques as it allows for a range of photons to be used from soft UV to hard x – rays ($h\nu$ > 10keV). Using suitable monochromators PES can be performed at any energy within this range.

2.2.5.2. Synchrotron Source

There are many advantages to using a synchrotron light source, mainly the invariably useful range of accessible energies from soft UV to hard X – rays. To achieve the energies needed for spectroscopy the synchrotron radiation follows classical electrodynamics. Electrons accelerated in a circular motion emit radiation in a dipole pattern, but electrons travelling in a synchrotron are travelling at relativistic velocities. The pattern of radiation is therefore modified in comparison to the reference motion and it actually emits radiation in a narrow cone in the forward direction of the electrons motion (**Figure 2.13**).

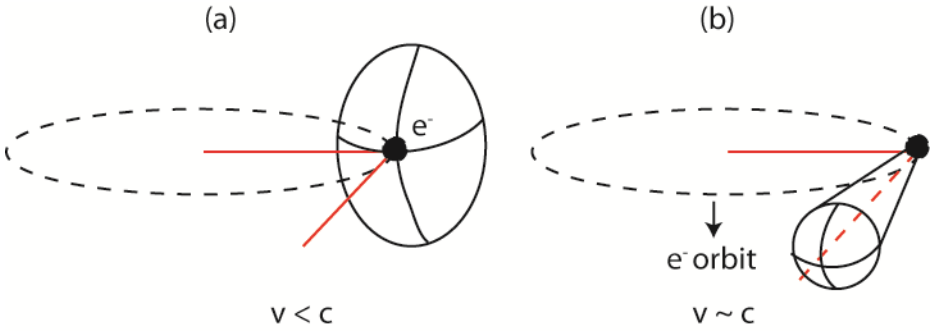

Figure 2.13 Radiation pattern emitted by an electron when (a) v < c and (b) v ~ c

As shown in **Figure 2.14** synchrotrons consist of several components. The linear accelerator accelerates the electrons to medium energies and stores them in the booster ring. Once enough have accumulated and are circling the booster ring they

are accelerated further and injected into the synchrotron (main storage) ring. Once the electrons have reached sufficient numbers they are accelerated to their final energy and the energies are maintained against radiation losses by acceleration states positioned around the ring. The trajectory of the electrons is modified using magnetic fields and this is performed using bending magnets, wigglers and undulators. Bending magnets are positioned on the synchrotron ring and work by accelerating the electrons using a constant magnetic field. This generates a fan of radiation in the horizontal direction which is normally guided to the work station using mirrors.

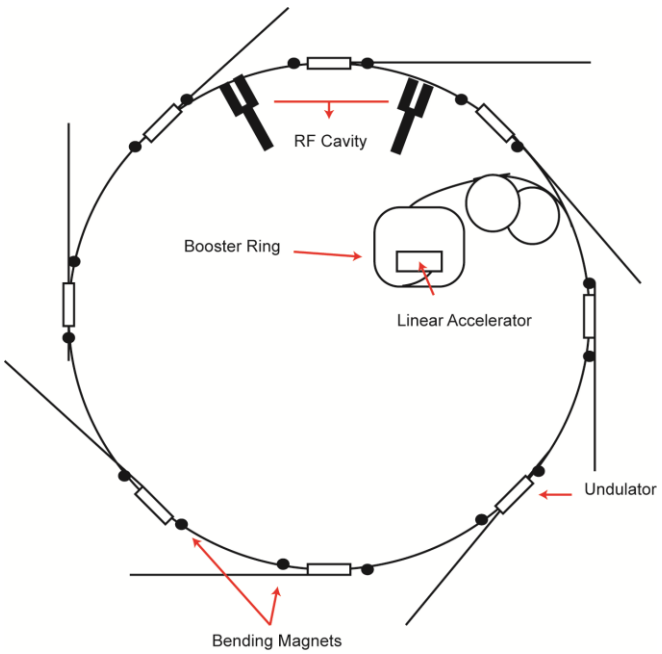

Figure 2.14 Synchrotron schematic - not to scale – of the Australian Synchrotron.

Undulators and wigglers are referred to as insertion devices and are positioned in between the bending magnets on the synchrotron ring. They use alternating magnetic structures that force the orbiting electrons to move in the horizontal plane. The

difference between the two devices is the strengths of the magnetic fields and the period of the magnetic structures used.

The beamline X1B at the National Synchrotron Light Source (NSLS) at Brookhaven National Laboratory (BNL) is off an undulator insertion device and **Figure 2.15** is a simple schematic of the custom built chamber at the beamline.

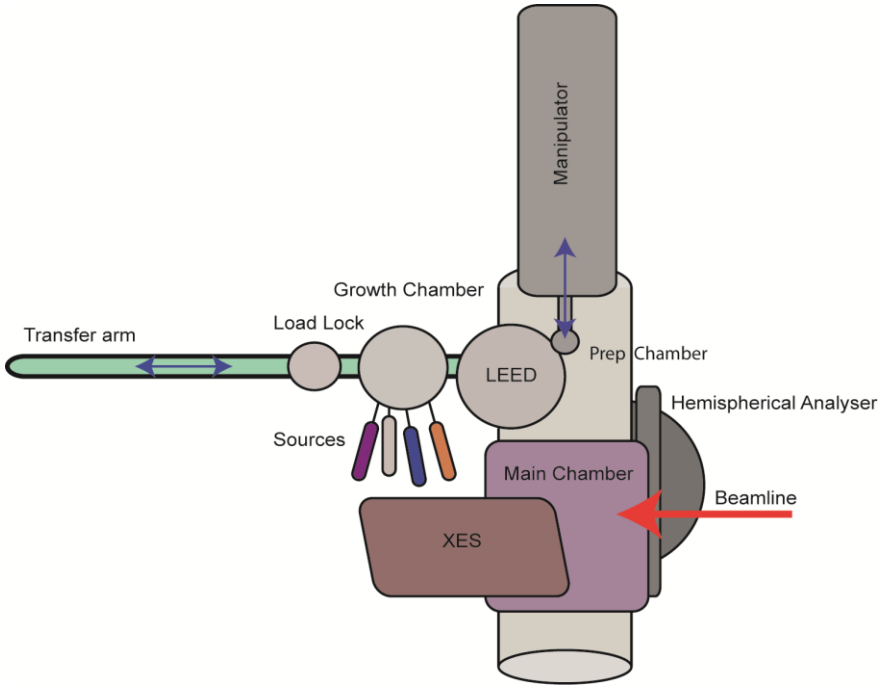

Figure 2.15 Simple Schematic of the custom built chamber at beamline X1B

Data analysis

HOMO energies are typically determined from UPS and **Figure 2.16** demonstrates how to retrieve this information from the secondary electron cut off and $HOMO_{onset}$ spectra.[11] Secondary electrons are inelastically scattered electrons which still have enough energy to escape into vacuum. Using **Equation 2.4**, as the *hv* is known the KE is measured in order to determine the binding energy with reference to E_f. The workfunction is measured by monitoring the position of the secondary electron cut

off (SEC_{cutoff}) which occurs at the low KE edge and has a sharp decrease in intensity known as the "tail" relating to a large majority of slow electrons. The lowest possible energy of the escaping electrons is the workfunction. The $HOMO_{onset}$ is the low binding energy onset relative to the E_f and is used due to the lack of distinct bands in an organic semiconductor, which actually contains a manifold of states.

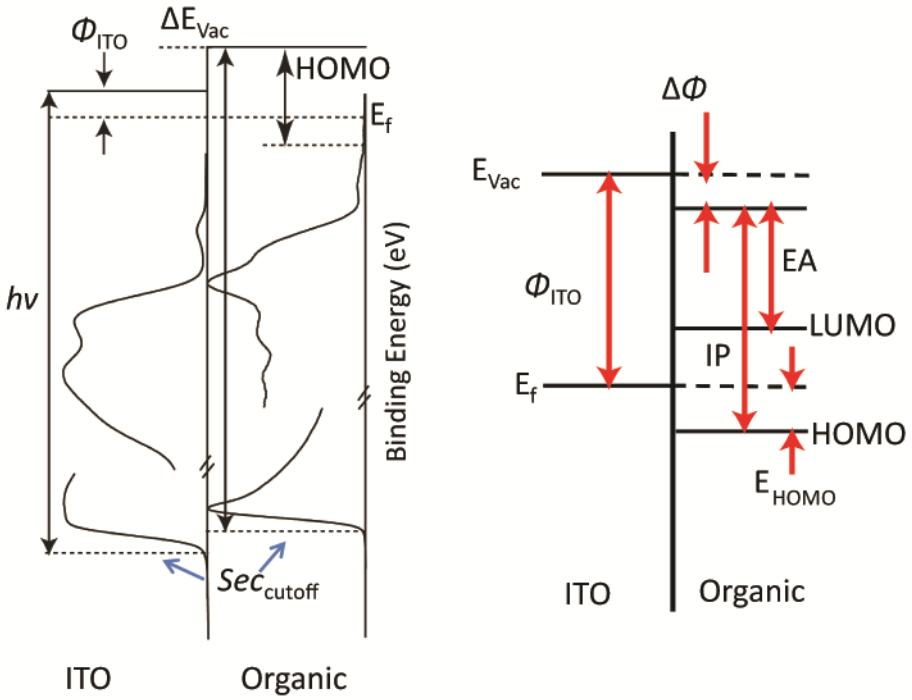

Figure 2.16 (a) Schematic of the important parameters derived from PES. (b) Energy level diagram for a generic junction formed at an ITO / organic interface.

The IP is calculated through the addition of the $HOMO_{onset}$ and the workfunction. The LUMO has been estimated by the absorption onset of the organic material, although this is not necessarily the most accurate technique.

The energy used for investigating core levels was 750 eV, for valence levels 250 eV and when measuring the work function of the sample a -9 V bias was applied. The bias is applied generally when taking the SEC_{cutoff} measurements to help accelerate

the lowest kinetic energy electrons into the spectrometer and also overcome the potential difference of the detector.

2.2.6. Atomic Force microscopy (AFM)

Atomic force microscopy (AFM) provides an accurate description of surface topography, typically by monitoring the Van der Waals (VdWs) interaction between a sharp tip and a sample. Other forces such as chemical bonding, electrostatic and magnetic forces can also be encountered by the tip and used to image a surface. A schematic of the AFM setup is shown in **Figure 2.17.**

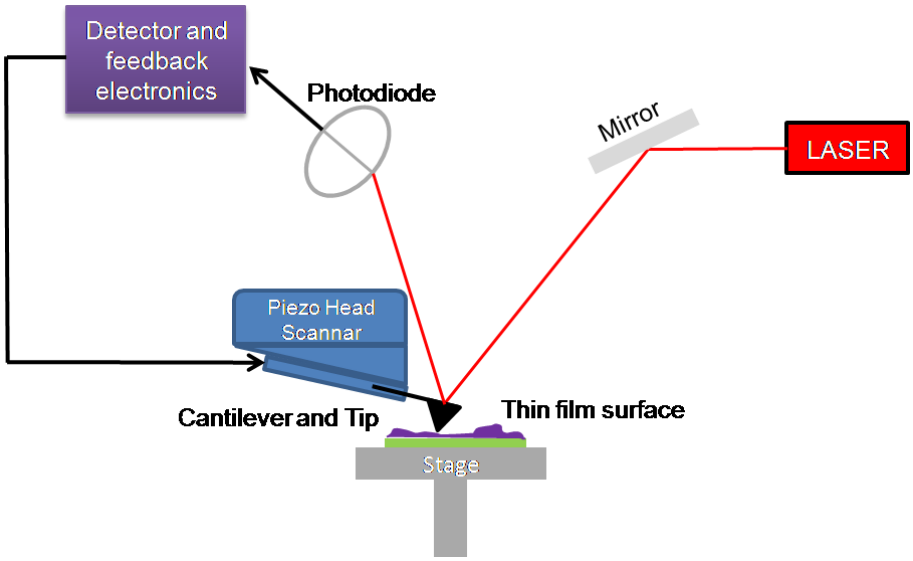

Figure 2.17 Schematic of the AFM.

The tip is located at the free end of a cantilever that is 100 to 200 um long. Forces between the tip and the sample surface cause the cantilever to bend or deflect. While scanning the tip over the sample, the cantilever deflection will be detected by a position sensitive photodetector. This is done by focusing a laser beam onto the mirror and onto the back of the cantilever. Typically there are two main modes that

the AFM will operate in either contact mode or intermittent contact mode (tapping mode, TM).

In contact mode, the force between the tip and the sample is repulsive. In this configuration, the AFM tip makes soft "physical contact" with the sample. The repulsive force bends the cantilever, inducing a change in the position of the reflected laser. The force interactions are strongly dependent on the distance which allows a very high spatial resolution. Unfortunately, when imaging soft samples such as small molecule organic films or polymers, the nature of the contact can damage or distort the surface and therefore tapping mode is generally the chosen imaging mode for the materials shown here.

In tapping-mode (TM) AFM the tip of a stiff cantilever vibrates near its resonant frequency and the amplitude is dampened when the tip encounters the surface. The oscillating tip is moved towards the surface until it begins to detect the repulsive force from the surface. Changes in the topography affect the amplitude of the oscillation which is corrected by the feedback system in order to keep the amplitude constant (set point). All AFM images within this thesis were taken using an Asylum Research MFP-3D in tapping mode. MFP-3D software (based on Igor Pro) was used to reconstruct and analyse the images.

2.2.7. Scanning Electron Microscopy (SEM)

Scanning electron microscopy is an extremely important technique for imaging through the use of electrons. A simple schematic of an SEM is shown in **Figure 2.18.** Electrons are fired down a column using an electron gun, (in this case a field emission gun), through a condenser lens, scan coils and an objective lens onto the sample. When an electron beam hits the sample a range of interactions occur which

can produce a variety of signals such as; back scattered electrons, secondary electrons, auger electrons, specimen current, x – rays and cathodoluminescence.

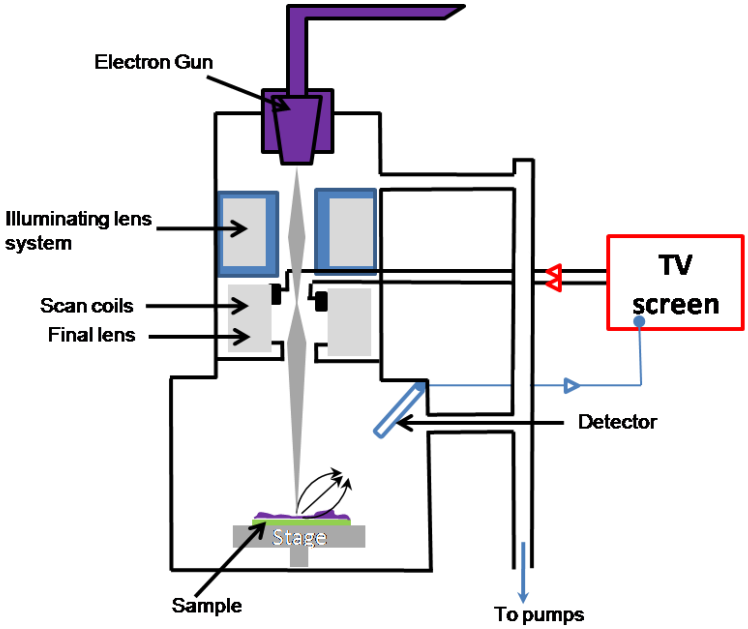

Figure 2.18 Schematic of a FE-SEM.

Images are typically taken using secondary electrons (SEs) which originate from the surface and give good spatial resolution. High resolution SEMs, have inbuilt InLens detectors which detect both SEs and back scattered electrons (BSEs).

Charging is a particular problem when imagining samples, particularly insulators or low conductivity materials. To avoid charging effects in the samples, they were coated with a thin conductive layer of sputtered carbon, Pt, Pd or Au. In this case, secondary electron (low energy) signals were detected using a positive electric field. For high resolution the In Lens detector was used. All SEM images were taken using a FEG – SEM Zeiss 55VP SEM. The samples were pre-coated with a thin film of carbon or platinum using a sputterer before being placed into the SEM to reduce charging of the samples.

2.2.8. X – Ray diffraction (XRD)

X – ray diffraction is thought to have been developed in 1922 after much interest in crystal structures and the study of X – rays and photons. XRD is an extremely useful and non-destructive method to investigate the orientations of single crystals or grains, atom and row spacings and structural properties.

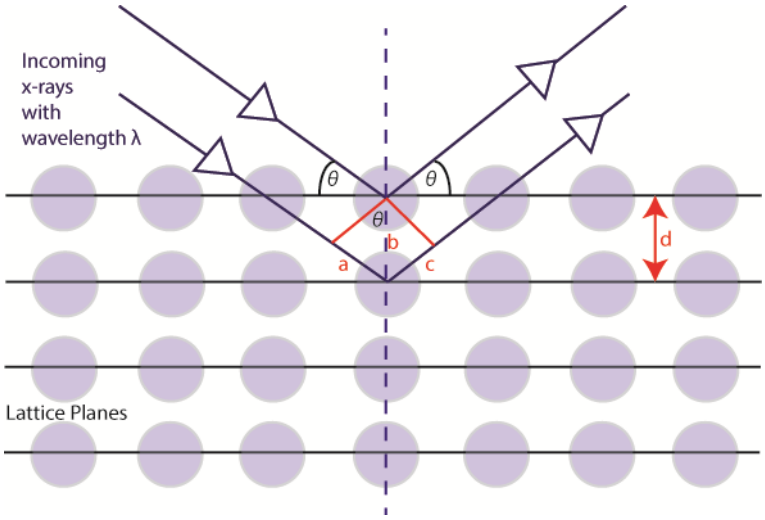

Figure 2.194 Schematic of X – Ray diffraction

Crystals consist of a periodic arrangement of unit cells into a lattice; where the unit cell contains fixed atoms or molecules at specific points. Regular arrays of artefacts (atoms or molecules) are separated by a distance d, but can be resolved into atomic (molecular) planes due to their different d – spacings. Diffraction is observed with the path length difference, ab + bc, of two parallel waves reflecting from identical planes is equal to an integer multiple of the wavelength of the incident. This is when Bragg's law is satisfied for constructive interference from planes with separation d (shown in **Figure 2.19**).

Bragg's Law: $\mathbf{n\lambda = 2d \sin \theta}$ **Equation 2.6**

From the changes in the angle of the x-rays after exiting the crystal, and knowing the incident wavelength, the d spacing can be calculated and the crystal structure can be determined. Shown in **Figure 2.20a** are the lattice parameters; lengths a, b, c and angles α, β, γ. The points at which planes intercept the unit cell axes are defined by the Miller indices (hkl) or Miller Planes. The indices are given as three integers 1/ h, 1/k, 1/l. As shown in **Figure 2.20b** the highlighted Miller plane is a (010).[12]

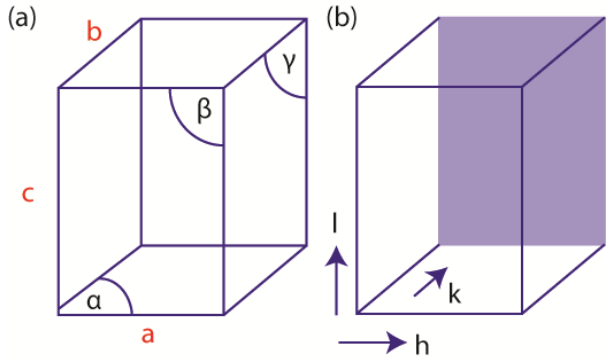

Figure 2.20 (a) are the lattice parameters; lengths a, b, c and angles α, β, γ (b) the highlighted Miller plane is a (010).

XRD traces were taken on a Philips PANalytical x'pert PRO MPD diffractometer using Cu Kα radiation and a Ni filter.

2.3. References

1. B. P. Rand, J. Genoe, P. Heremans and J. Poortmans, *Progress in Photovoltaics*, **2007**, *15*, 659.
2. R. F. Salzman, J. G. Xue, B. P. Rand, A. Alexander, M. E. Thompson and S. R. Forrest, *Organic Electronics*, **2005**, *6*, 242.
3. L.-J. Pegg, S. Schumann and R. A. Hatton, *Acs Nano*, **2010**, *4*, 5671-S. R. Forrest, *Chemical Reviews*, **1997**, *97*, 1793.
4. R. Gutzler, W. M. Heckl and M. Lackinger, *Review of Scientific Instruments*, **2010**, *81*, 015108.
5. M. Campione, M. Cartotti, E. Pinotti, A. Sassella and A. Borghesi, *Journal of Vacuum Science & Technology A*, **2004**, *22*, 482.
6. B. W. D'Andrade, S. Datta, S. R. Forrest, P. Djurovich, E. Polikarpov, M. E. Thompson. *Org. Electron.* **2005**, *6*, 11.
7. L. Kronik and Y. Shapira, *Surface and Interface Analysis*, **2001**, *31*, 954.

8. H. Ishii, K. Sugiyama, E. Ito and K. Seki, *Advanced Materials*, **1999**, *11*, 605.
9. D. P. Woodruff, and T. A. Delchar. *Modern Techniques of Surface Science*. **1990**: Cambridge University Press.
10. R. Schlaf, B. A. Parkinson, P. A. Lee, K. W. Nebesny, N. R. Armstrong, *J. Phys. Chem. B.* **1999**, *103*, 2984.
11. P. Atkins and J. de Paula, *Atkins' Physical Chemistry Seventh Ed.*, Oxford University Press, **2002**.

Chapter 3

Device characterisation and analysis

3.1. Solar spectrum

Although the ultimate goal is to use solar cells outdoors, for reproducible, reliable and comparative performance lab solar simulators are used for testing where the illumination conditions are specifically tuned to match a standardised solar spectrum. The sun is a typical black body emitter: i.e. it absorbs all radiation incident at it's surface and emits radiation dependant on the temperature as shown below:

$$F(\lambda) = \frac{2\pi hc^2}{\lambda^5\left(exp\left(\frac{hc}{k\lambda T}\right)-1\right)} \qquad \textbf{Equation 3.1}$$

In **Equation 3.1,** F(λ) is the spectral emissive power, λ is the wavelength, h is Planck's constant, k is Boltzmann's constant, c is the speed of light and T the blackbody temperature. The Air mass (AM) defines the light spectrum depending on the path taken through the Earth's atmosphere as a function of angle. As shown in **Figure 3.1** extra-terrestrial light, i.e. that which has not entered the atmosphere, is known as AM 0. As the light travels through the atmosphere the light intensity is altered due to scattering by particles and/or absorption by atmospheric gases, such as ozone, O_3, CO_2 and water vapour, H_2O. The angle at which the light hits the earth affects the spectrum and light intensity.

AM1.0 is the zenith point, the lowest pathway to the earth which is directly overhead at 0^o. AM 1.5 is 48^o from the zenith point and AM 2.0 is 60^o.[1]

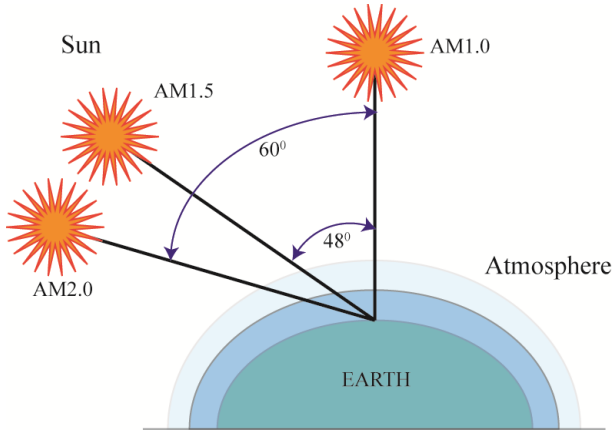

Figure 3.1 The path length of the solar radiation through the Earth's atmosphere.

The simulation of light when testing devices is typically created using a xenon lamp and filter combinations to give a standardised light source with the desired Air Mass and intensity. The sun is typically modelled around 6000K (see inset **Figure 3.2**) as this has the largest emission of light in the visible range.

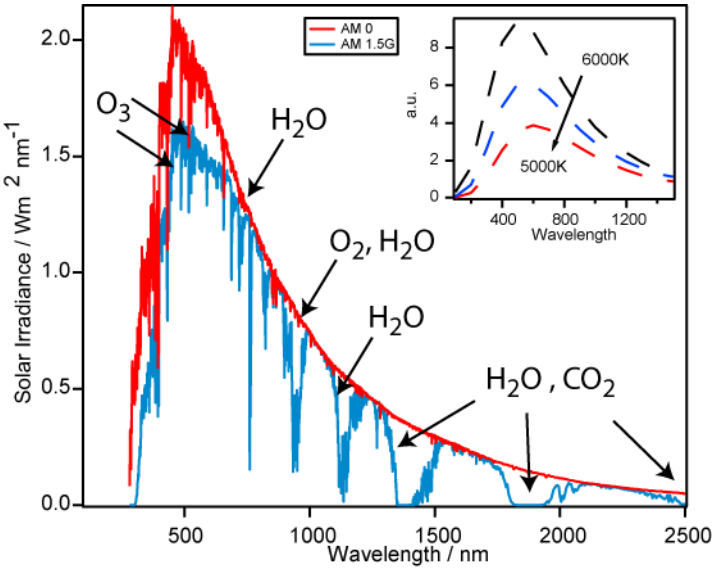

Figure 3.2 AM 0 and AM1.5G solar spectrum.[2] Inset: Black body emitters at T = 5000K, 5500K and 6000K.

In this thesis, simulated light of 100mWcm^{-2} of AM1.5G (G = global, combines both direct and diffuse light) is used as the accepted standard testing condition, shown in **Figure 3.2**. To simulate sunlight a Newport Oriel simulator with a xenon arc lamp was used in combination with a Fraunhofer calibrated PVM 482 photodiode with a KG-5 filter.

3.2. *J-V* characterisation for solar devices

Shown in **Figure 3.3** are the current density – voltage *(J-V)* characteristics of an example solar cell.

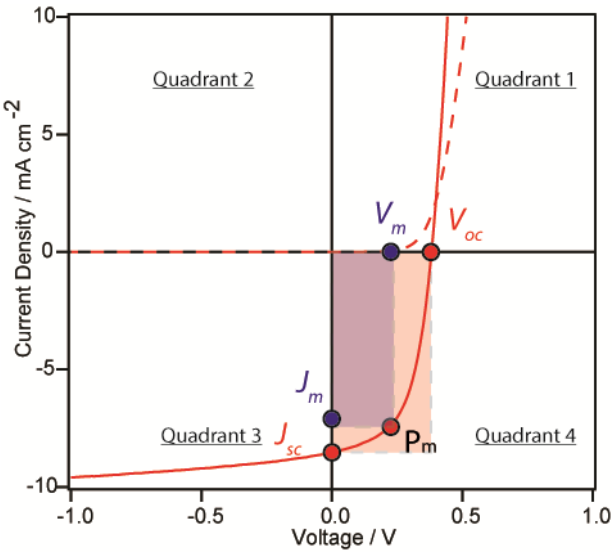

Figure 3.3 Current – voltage graph of a solar cell and the four quadrants and important parameters labelled. (Dark curves – dashed lines, Light curves – solid lines.

When a cell is not under illumination (dark) the *J-V* curve should resemble diode-like behaviour and shows essentially zero current at negative bias and an exponentially increasing current under positive bias (dashed line in **Figure 3.3**). Under illumination, the maximum power is the maximum product of J_m and V_m that is found in the fourth quadrant. The ratio of this area (highlighted in purple) to the

area defined by V_{oc} x J_{sc} (highlighted in orange) is a measure of the quality of the cell and is known as the fill factor, FF. The important parameters at the axes intercepts are the short circuit current density (J_{sc}) and the open circuit voltage (V_{oc}) respectively. **Equation 3.2** describes the power conversion efficiency (η_p, PCE) of a solar cell and relates the maximum power output (P_m) to the incident light (P_{inc}):

$$\eta_p = \frac{P_m}{P_{inc}} = \frac{V_m J_m}{P_{inc}} = \frac{V_{oc} J_{sc} FF}{P_{inc}} \qquad \textbf{Equation 3. 2}$$

Another way of looking at solar cells is through the use of an equivalent circuit diagram (ECD, **Figure 3.4**). It consists of the following ideal components: A current source, I_L, which generates the current upon illumination, a diode and shunt (R_{sh}) and series (R_s) resistors. Also shown are the load resistor R_L and its voltage drop and current. Arrows indicate current flow (equivalent to hole flow).

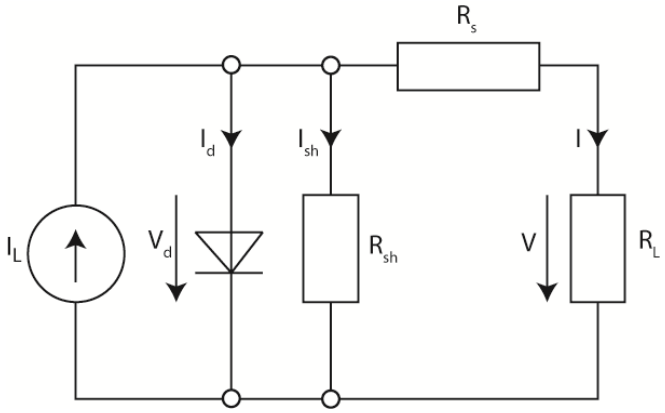

Figure 3.4 Equivalent circuit diagram of a solar cell.

The J_{sc} is at V = 0 and indicates the photocurrent generation under conditions where R_l is 0 Ω. V_{oc} occurs when R_l is infinite and the generated photocurrent is equal to the current flow in the opposite direction (no net current flow).[3,4]

The series resistance (R_s) is the resistance in series between the current source and the load. The series resistance is affected by the mobility of charge carriers in their respective mediums (conductivity) and therefore space charges, traps and other barriers can change the R_s. Thicker layers can also increase R_s due to the longer travelling distance. Ideally, the R_s should equal zero and an increase in R_s leads to a decreased slope in the *J-V* curve under positive bias (which results in a lower fill factor, **Figure 3.5a**). The shunt resistor, $R_{sh,}$ parallel to the load, is generally due to recombination of charge carriers near the dissociation site, or if R_s is a magnitude lower, recombination further from the dissociation site may be included in this resistance. Ideally, R_{sh} should be equal to infinity and a decrease leads to loss of current through the load resulting in a deviation from flat diode behaviour at negative bias. This can also result in a lower fill factor (**Figure 3.5b**).

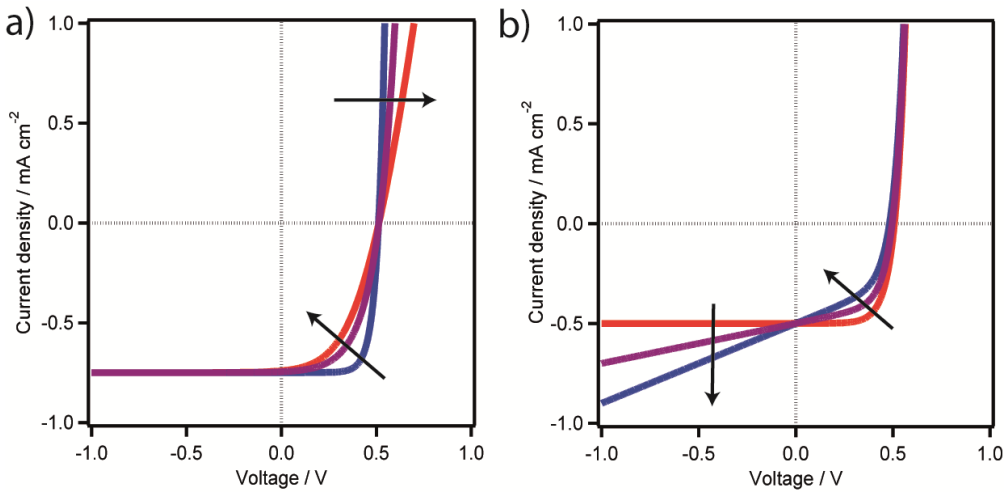

Figure 3.5 *J-V* curves indicating a change in (a) series and (b) shunt resistance.

3.3. Space Charge Limited Current (SCLC) theory.

Charge mobility has been proposed to be one of the most important physical properties in photovoltaics. To assess the dual donor/acceptor character in (sub) phthalocyanines both hole and electron charge mobilities of all materials were obtained via space charge limited current (SCLC) theory, though there are many other methods.

As mentioned previously charge transport and collection is one of the main processes in OPVs and critically depends on the efficiency with which charge carriers move within the layers. Mobility is strongly dependant on the structure, nature and purity of the material and conductivity is determined by the dominant charge carrier. There are many methods for measuring mobility such as electric field generated (FETs), doping generated (charge extraction by linearly increasing voltage (CELIV), conductivity), photo-generated (Time of Flight, (ToF)) and injection generated (SCLC and transient electroluminescence).

SCLC involves analysis of the *J-V* characteristics of the single carrier cell in the dark giving a description of the voltage dependence on the current in a semiconductor. It occurs when the charge carrier concentration is larger than the number of free carriers in the semiconductor. A thin film of thickness *d*, is sandwiched between ohmic contacts. At low voltages, generally the device follows ohmic behaviour and the *J-V* characteristics are linear. At higher applied voltages, the characteristics are said to become space – charge limited due to the injection of carriers from one electrode and the current is transport rather than injection limited (if the contacts are ohmic). This high charge carrier concentration affects the electric field distribution

which makes a feedback loop between the field and current described by Child's Law (**Equation 3.3**):

$$J = \frac{9}{8}\varepsilon\varepsilon_o\mu\frac{V^2}{d^3} \qquad \textbf{Equation 3.3}$$

Where ε is the relative dielectric constant of the organic film (typically ~ 3 for organic materials), ε_o is the vacuum dielectric constant, d is the film thickness, V is the applied voltage, J is the SCLC and μ is charge-carrier mobility.

In reality there will be some free carriers in the device before injection (as mentioned previously) and as a result at low voltages the injected carrier density is lower than the background charges (shown in region I in **Figure 3.6**). There will be a transition voltage, V_{tr}, where the injection charges = the background charges (**Equation 3.3**). This is valid for the trap free insulator but is unlikely for most semiconductors.

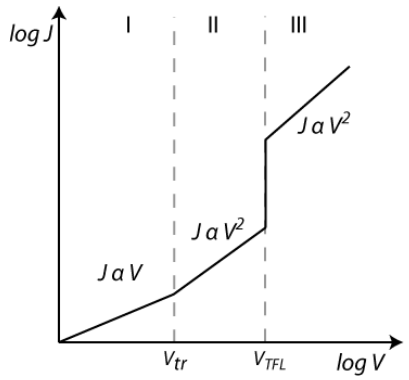

Figure 3.6 Schematic graph showing *J* vs *V* for an insulator with single energy traps (I) – ohmic region, (II) trap limited SCLC and (III) trap free SCLC.

Existing traps will capture charge, reducing the expected current and immobilizing the injected carriers. Finally, at a given voltage (V_{TFL}) all traps will be filled and the value of the current will rise to the trap – free value (schematically shown in **Figure 3.6** region III).

Another approach to determine mobility in amorphous organic materials is to assume that the transport is trap free but the mobility is not constant with electric field. The mobility tends to follow a Poole – Frenkel dependence shown in **Equation 3.4**:

$$\mu(E) = \mu_o \exp\left[\gamma E^{\frac{1}{2}}\right] \qquad \textbf{Equation 3.4}$$

μ_o is the field independent mobility (E = 0) and γ is the field activation parameter. With a field dependant mobility, **Equation 3.3** is no longer entirely valid however the two laws can be combined to approximate the SCLC by:

$$J = \frac{9}{8}\varepsilon\varepsilon_o\mu_o \exp\left[0.89\beta\sqrt{\frac{V}{d}}\right]\frac{V^2}{d^3} \qquad \textbf{Equation 3.5}$$

Although the mobility is dependent on the electric field E, the SCLC is a function of voltage. A non-uniform distribution of space charge inside the device results in an varied electric field across the device. The magnitude of E (V/d) is therefore only an average of the field and therefore it is presented as a function of the well defined voltage.

The *J-V* characteristics are then fitted to extract the carrier mobility. A simple Labview program was used to fit the *J-V* curves.

3.4. External quantum efficiency, EQE

EQE is the ratio of the number of charge carriers collected from the OPV cell to the number of incident photons of a given energy.

$$EQE(\lambda) = \frac{J_{sc}(\lambda)}{qN(\lambda)} \qquad \textbf{Equation 3.6}$$

Where q is the elementary charge and N(λ) is the monochromatic incident photon flux density. A Si photodiode with a known spectral response is used as a reference

and the EQE and J_{sc} of the diode is used to determine the EQE of the OPV device using **Equation 3.6**:

$$EQE_{OPV} = \frac{EQE_{ref}\, x\, J_{sc}(\lambda)_{OPV}}{J_{sc}(\lambda)_{ref}} \qquad \textbf{Equation 3.7}$$

A broad band light source is passed through a monochromator to allow for specific wavelengths to be selected. This monochromatic light is chopped at 510 Hz through a pin hole to allow for an accurate comparison between a reference diode and sample. EQE measurements were obtained using the Scientech solar simulator with a xenon arc lamp as a white light source and a PTI Monochromator. The monochromatic light intensity was calibrated with a Si photodiode (818nm Newport) and chopped at 510 Hz. Signal detection was performed with a current-voltage amplifier (Femto, DHPCA-100) and a lock-in amplifier (Stanford Research SR 830 DSP).

3.5. Degradation studies.

Degradation studies have been performed in this thesis where the cell is under constant AM 1.5G illumination and tested every minute for a period of time, up to 24 hours.

3.6. References

1. V. Shrotriya, G. Li, Y. Yao, T. Moriarty, K. Emery and Y. Yang, *Advanced Functional Materials*, **2006**, *16*, 2016
2. P. Peumans and S. R. Forrest, *Applied Physics Letters*, **2001**, *79*, 126.
3. B. P. Rand, D. P. Burk and S. R. Forrest, *Physical Review B*, **2007**, 75, 115327.
4. C. Uhrich, D. Wynands, S. Olthof, M. K. Riede, K. Leo, S. Sonntag, B. Maennig and M. Pfeiffer, *Journal of Applied Physics*, **2008**, *104*, 043107.

Donors

Chapter 4.

TIPSE-Pentacene derivatives

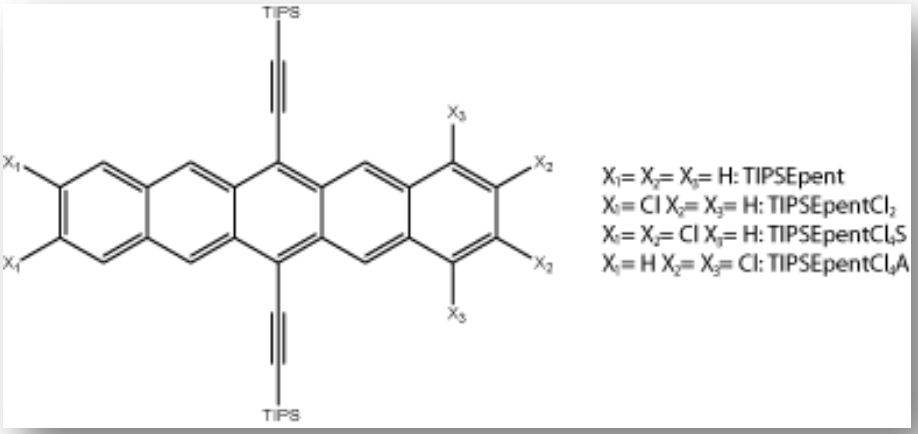

Figure 4.1 TIPSEpentacene and derivatives.

In this chapter the several synthesised chlorinated derivatives of the soluble molecular semiconductor 6,13-bis(triisopropylsilylethynyl)pentacene (TIPSEpent) **(Figure 4.1)** are used. With reference to the parent molecule, increasing the extent of chlorination can be correlated with changes in the molecular orbital (MO) energies, the stability towards reaction with C_{60}, and both the processability and performance as the electron donor in planar OPV devices. The derivatives were studied in detail using UV/Vis absorption spectroscopy and CV to build a picture of the frontier molecular orbital energies and through combining with *J-V* device analysis a deeper understanding of the relation between material characteristics, energy levels and the subsequent impact on OPV device behaviour is presented.

4.1. Introduction

Oligoacenes, such as pentacene, have been shown to exhibit promising properties as donor materials in OPVs not least because of the high charge carrier mobilities they exhibit (> 1 cm^2 V^{-1} s^{-1}).[1] Although Pent / C_{60} cells produce large short circuit current densities (~ 9 mA cm^{-2}), one drawback is that the V_{oc} achieved is rather low (0.40 V). This is due to the small interface gap i.e. the difference between the highest occupied molecular orbital of the donor and the lowest unoccupied molecular orbital of the acceptor ($HOMO_D$ – $LUMO_A$), which is known to play a fundamental role in controlling the V_{oc}.[2,3] In an attempt to increase the hole mobility, modify the IP, and impart solubility to pentacene, Anthony *et al.* synthesised a pentacene derivative having two bis(triisopropylsilyethynyl) (TIPSE) moeities tethered to the central ring.[4] Whilst the hole mobility and IP (4.9 - 5.0 eV) were not significantly altered, the solubility was dramatically increased enabling thin film preparation from solution which allows for significantly cheaper processing costs.

Organic semiconductors are amenable to large modifications of the electronic structure by substitution at the periphery of the fused ring system such that the properties of the parent molecule can be engineered continuously from p- to n-type character.[5] For OPV applications, the ability to manipulate the frontier orbital energies of the photoactive components offers a path to simultaneously increasing the power conversion efficiency (η_p) and stability of the material without adversely impacting the light harvesting capability. Through using strong electron withdrawing groups such as F,[6] CN,[7] alkanoyl,[8] perfluorobenzene[9] *etc.* the semiconductors can be modified into stronger electron accepting materials. Halogenation of small molecules has been shown previously

to be extremely promising as a route towards more n – type semiconductors with typical donor materials such as CuPc converted to F_{16}CuPc, but also with already low reduction potential materials such as fullerenes.[10]

Tang *et al.* compared fluorinated and chlorinated versions of acenes, Pcs and PDI based semiconductors and found chlorination to be as capable as fluorination. Selective chlorination has been shown to be a particularly effective means of improving the stability of acenes and phthalocyanines in air and converting them from archetypal hole-conductors to electron-transport materials suitable for use in n-type OFETs and acceptors in OPVs.[11,12] A smaller band gap was achieved when using Cl rather than F but generally the derivatives performed similarly. They did find however, that with partial fluorination, materials would adopt face to face stacking (through increased π-π interactions) compared to the typical herringbone type structure, and this could be extremely important for OPVs where perpendicular transport occurs giving improved charge transport and an increase in current.

Chlorinated molecular semiconductors are generally cheaper and easier to produce and provide an energetically more accessible LUMO for electron transport than their more commonly studied fluorinated analogues.[13] Hence, the synthesis and study of new types of selectively chlorinated organic semiconductors offers an attractive strategy to enhance the performance characteristics of OPV devices derived from these materials.

4.2. Results

4.2.1. Synthesis

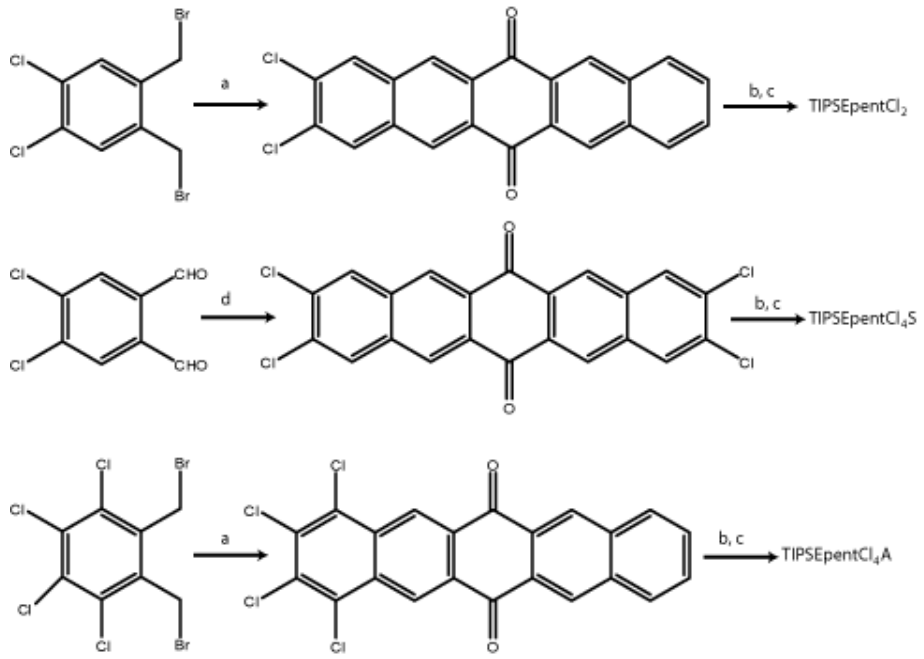

Scheme 4.1. *Reagents and conditions*: (a) 1,4-anthraquinone, KI, DMF, 120 °C, sealed tube, 2 d, 65% for $TIPSEpentCl_2$, 92% for $TIPSEpentCl_4A$; (b) TIPSC≡CMgCl, THF, 70 °C, 1 h; (c) $SnCl_2$, aq. HCl, 30 min, 70 °C, 32% for $TIPSEpentCl_2$, 40% for $TIPSEpentCl_4S$, 33% for $TIPSEpentCl_4A$; (d) 1,4-cyclohexanedione, KOH, EtOH, rt, overnight, 62%.

$TIPSEpentCl_2$ and $TIPSEpentCl_4A$[13] bearing substituents at one end of the pentacene core were made through application of the Cava reaction.[14] Thus, reaction of 1,2-bis(dibromomethyl)-4,5-dichlorobenzene and 1,2-bis(di-bromomethyl)-3,4,5,6-tetrachlorobenzene with 1,4-anthra-quinone provided the corresponding pentacene quinones which were further transformed into the TIPS pentacenes using an ethynylation/deoxygenation sequence (**Scheme 4.1**).[16-17] Symmetrical $TIPSEpentCl_4S$ was made by aldol condensation between 4,5-

dichlorophthaldehyde and 1,4-cyclohexanedione and further ethynylation/deoxygenation. TIPSEpentacene and derivatives were synthesised by Dr. A Duraud and Prof. M. Shipman in the University of Warwick Chemistry Department.

4.2.2. Solution and thin film studies.

Shown in **Figure 4.2** is the normalised absorption spectra of the TIPSEpent and Cl_2TIPSEpent in solution. TIPSEpent in solution has a similar absorption spectra to pentacene with strong absorption between 500 – 680 nm with peaks at 508, 551, 595, 644 nm, and a lower wavelength peak at 409 nm. The Cl_2TIPSEpent derivative contains sharp peaks at 653, 603, 557 nm and a shoulder at 517 nm with two distinctive lower wavelength peaks at 446 and 422 nm. As seen previously, after chlorination the derivative exhibits a red – shift in absorption of ~ 13 nm.[18, 19] Due to the addition of further chlorine atoms, the Cl_4 derivatives are inherently non soluble.

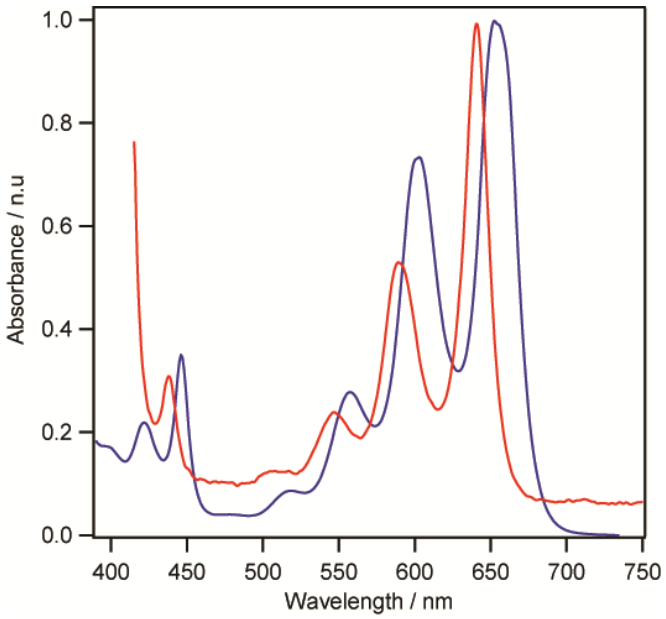

Fig 4.2. Normalised UV-Vis absorption spectroscopy of TIPSEpent (red) and Cl_2TIPSEpent (blue) in solution.

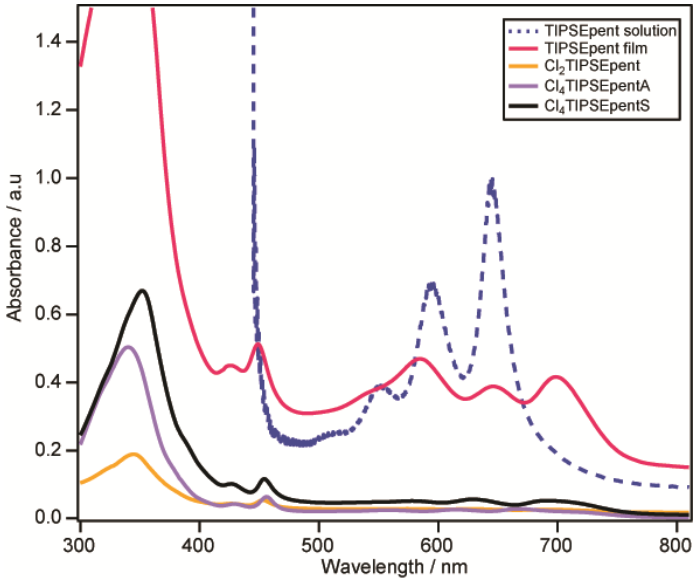

Figure 4.3 Thin film UV-Vis absorption spectroscopy of the TIPSE derivatives (40 nm films), with TIPSEpent solution UV-Vis as a reference.

The thin film absorbance of all derivatives is shown in **Figure 4.3.** There is a large red-shift between the TIPSEpent solution and the solution processed thin film of TIPSEpent of approximately 55 nm due to an increase in coloumbic interactions. The TIPSEpent film contains less defined peaks and displays a much broader absorption over the range which could potentially benefit the device. The Cl_2 and Cl_4TIPSEpent derivatives all display a similar red shift, but it is clear from the un-normalised UV-Vis spectra that for the same thickness of film, the absorption is clearly lower than the 40 nm TIPSEpent film. The reason for this at present is unknown but could potentially be due to a change in packing arrangement reducing the absorption coefficient with the addition of chlorines in the thin film. The peaks at ~ 422 and 446 nm are common to all TIPSEpent derivatives (and the parent molecule) and are due to a decrease in crystallinity in comparison to pentacene films (where these low wavelength peaks are not present). This has also been seen with 1, 3-dioxolane TIPSEpent derivatives.[20]

The relative oxidation potentials of TIPSEpent and the three chlorinated derivatives were measured in solution using cyclic voltammetry (CV) (**Figure 4.4**), from which the HOMO energy in the solid state was estimated using the method of D'Andrade *et al*.[21] (**Table 4.1**). Site-specific chlorination of the outermost rings of the pentacene core was chosen on the basis of the quantum-chemical calculations conducted by Medina *et al*,[9] which predict that the largest decrease in the HOMO energy of pentacene will result when the 2,3,9,10-positions are substituted. Consistent with the stabilising effect of electron-withdrawing substituents at peripheral sites around a conjugated core,[22, 23] the HOMO energy does become more negative with the extent of chlorination (roughly 150 meV per two chlorine atoms). The largest change in the HOMO energy (~ 0.3 eV) is achieved upon addition of four chlorines, although this does not depend on whether they are symmetrically (TIPSEpentCl_4S) or asymmetrically (TIPSEpentCl_4A) distributed. The optical band gap determined from the UV-Vis absorption spectra onset was fractionally reduced by chlorination with the largest change, -0.03 eV, occurring for the tetra-chlorinated derivatives.

TABLE 4.1. HOMO energies and optical band gaps of the materials studied, as determined by CV and UV-Vis measurements.

	HOMO Energy / eV[a]	Optical Bandgap / eV[b]
TIPSEpent	-5.02	1.93
TIPSEpentCl_2	-5.19	1.92
TIPSEpentCl_4A	-5.29	1.90
TIPSEpentCl_4S	-5.30	1.90

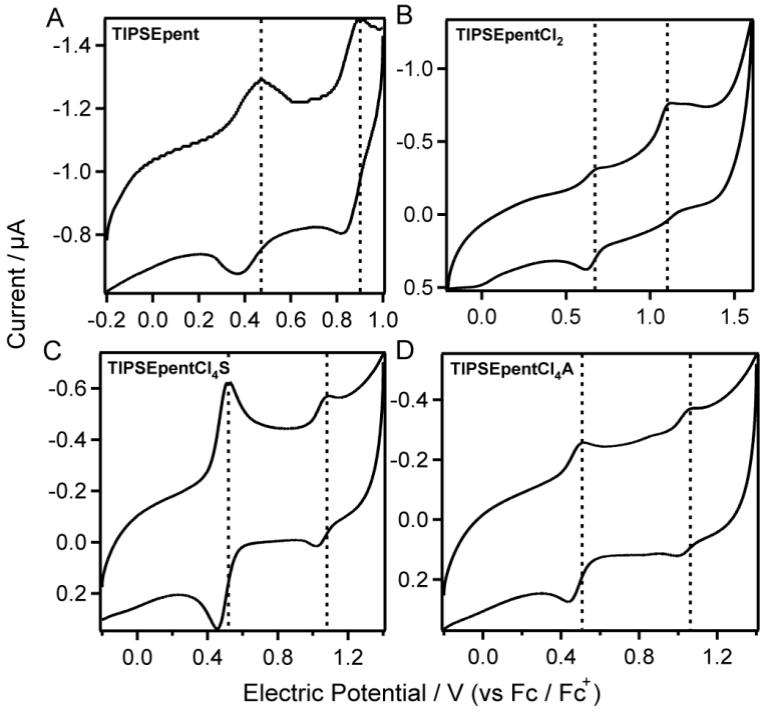

Figure 4.4 Cyclic voltammograms of TIPSEpent and its chlorinated derivatives in solution. The left-hand dashed lines in each plot represent the first oxidation potential of ferrocene (Fc).

This small modification of the optical band gap is consistent with an increase in the extent of conjugation resulting from the empty 3d orbitals in the Cl substituents accepting π-electrons from the fused ring system, hence increasing their delocalisation.[24] As the ionisation potential of the derivatives has been increased we would expect an increase in molecular stability with increasing chlorination.

Figure 4.5 shows a schematic of the corresponding energy levels in the OPV devices. The HOMO energies for C_{60}[25] and BCP[26] are taken from ultra-violet photoelectron spectroscopy (UPS) measurements in the literature, with the TIPSEpent and derivatives from the CV data shown above (LUMOs were established from optical band gaps). The schematic demonstrates the improved energy level alignment between the Fermi level of the PEDOT : PSS treated ITO and

the HOMO levels of the chlorinated derivatives. It also reveals the increase in I_g between the derivatives and the C_{60} which as discussed previously is an important factor in determining V_{oc}.[27-29]

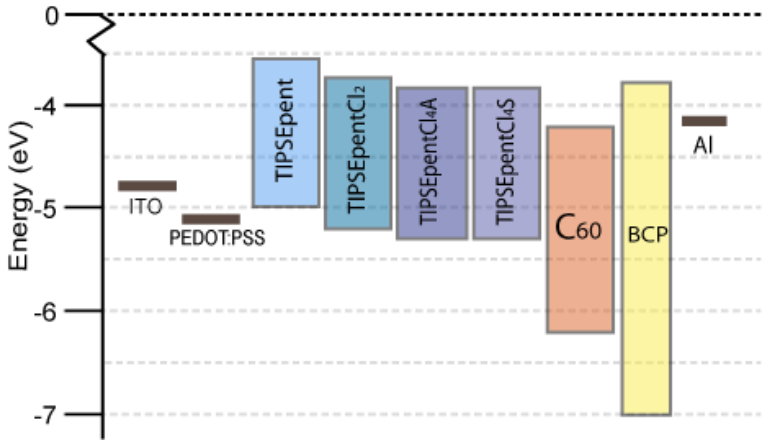

Figure 4. 5 Schematic energy level diagram depicting the HOMO-LUMO gap of the materials used in OPV devices.

Pentacene derivatives are prone to cycloaddition reactions with fullerenes,[21] and substitution of the central aromatic ring with bulky substituents is not sufficient to prevent these facile reactions.[30] Such degradation reactions of acenes are particularly problematic for OPV applications which invariably employ fullerenes as the electron acceptor. Since the $HOMO_{(diene)}$–$LUMO_{(dienophile)}$ gap controls the rate of normal Diels-Alder reactions it was anticipated that the larger ionisation potential in the chlorinated derivatives would slow this degradation pathway. To test this hypothesis changes in the strength of the most intense optical absorptions of TIPSEpent and the dichlorinated derivative ($TIPSEpentCl_2$) were recorded over 15 hours in toluene with and without C_{60} present at the same molarity, shown in **Figure 4.6**. Over 15 hours the total absorbance of the TIPSEpent degrades (A) and at an increased rate with the presence of C_{60} (C). It is clear from both B and D that the chlorinated derivative is

significantly more stable than TIPSEpent, particularly towards reaction with C_{60} with a percentage decrease of ~15 % in comparison to ~ 30 % over the 15 hours.

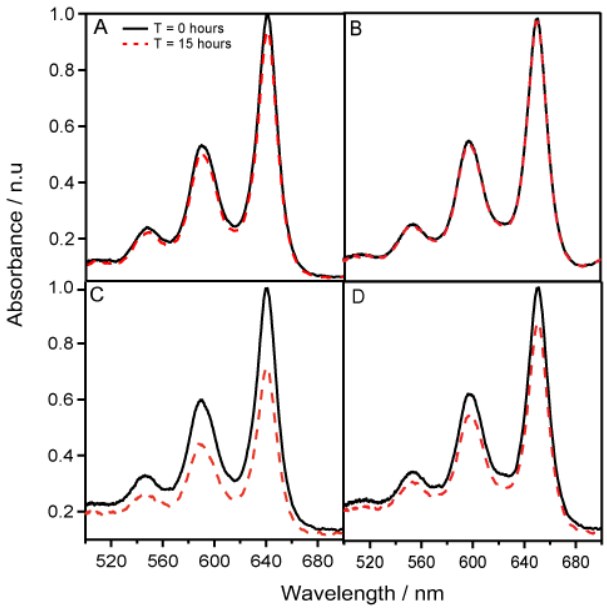

Figure 4.6 UV-Vis absorption spectra in solution measured at time intervals t = 0 (solid line) and t = 15 h (dotted red line) (A) TIPSEpent (B) $TIPSEpentCl_2$ (C) TIPSEpent and C_{60} (1:1 ratio) (D) $TIPSEpentCl_2$ and C_{60} (1:1 ratio) in toluene. The concentrations of the C_{60}, TIPSEpent and $TIPSEpentCl_2$ were 1 x 10^{-6}M

4.2.3. Morphology

The morphology of semiconductors is extremely important and the difference in crystallization of thin films that have been solution processed compared to vacuum deposited can be exceptionally large. The crystallinity of TIPSEpent has been shown to be extremely important in OTFTs as it can develop large and/or dendritic grains and this has been shown to have a large influence on the physical properties of the layer, particularly the mobility.[31] Shown in **Figure 4.7** are optical microscope images of 40 nm TIPSEpent films formed from (a) toluene and (b) 1, 2 dichlorobenzene. The films regardless of solvent appear to be relatively similar with large crystals

forming across the surface of the ITO.

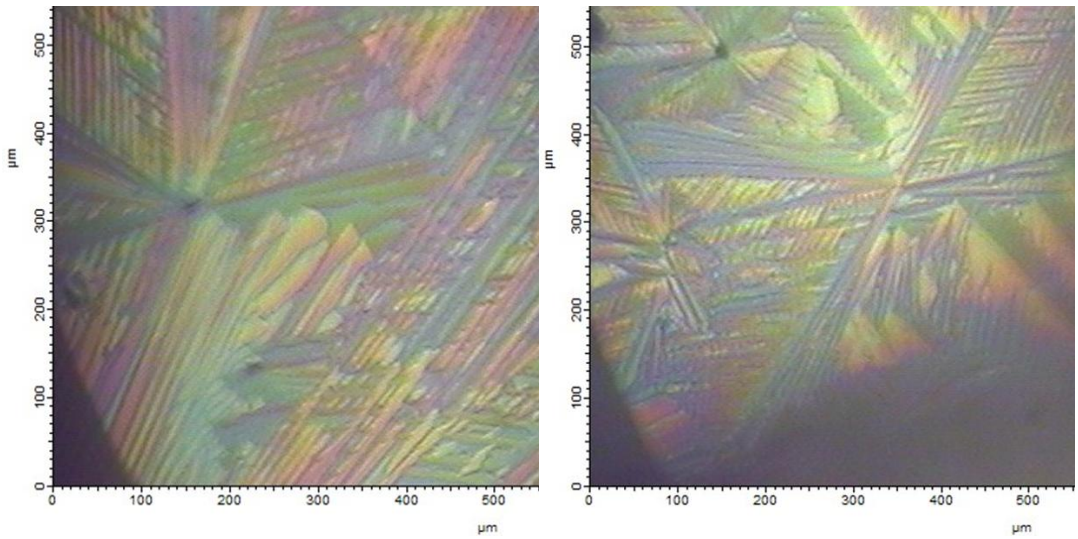

Figure 4.7. Optical microscope images of 40nm film of TIPSEpent in (a) toluene and (b) 1,2 – dichlorobenzene.

The dendritic crystals are similar to pentacene but are on a much larger scale. AFM was used to further image the spin coated TIPSEpent films (in contact mode) and similar to the optical microscopy, there are large dendritic like features present across the 40 µm scan shown in **Figure 4.8**

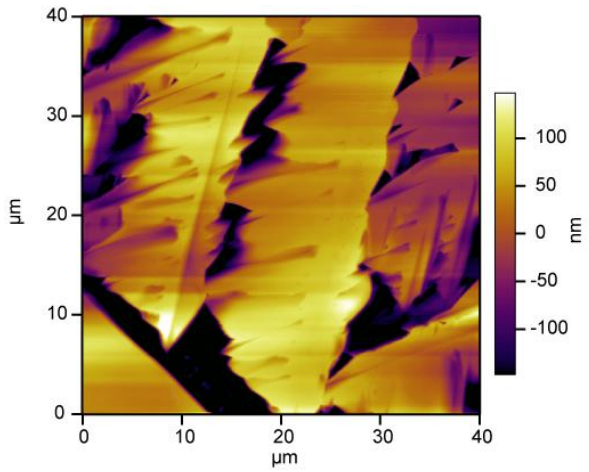

Figure 4.8 Contact mode AFM of the TIPSEpent (in toluene) solution processed film.

Such high crystallinity could be promising for high charge transport throughout the films in an OTFT but could potentially be detrimental in OPVs where consistent interfaces are required. Once the films are annealed, even at only 50^{o}C for 30mins the films begin to break apart, leaving large voids revealing the substrate underneath, therefore no annealing post spin coating was used in devices

The morphology of the evaporated TIPSEpent derivative TIPSEpentCl$_4$ is shown in **Figure 4.9.** Although this derivative contains the TIPSEpent moieties and four large Cl atoms on the periphery, the AFM is extremely similar to a vacuum deposited pentacene layer. It contains large crystals of ~ 500 nm in size (much smaller than the spin coated films) and parts of the film contain large dendritic grains, also seen previously in pentacene. Previous work on vacuum deposited TIPSEpent derivatives have shown amorphous films when evaporated onto an unheated substrate. Crystallinity only occurred when grown onto a heated substrate, though they admitted that some degree of crystallinity could not be ruled out.[32]

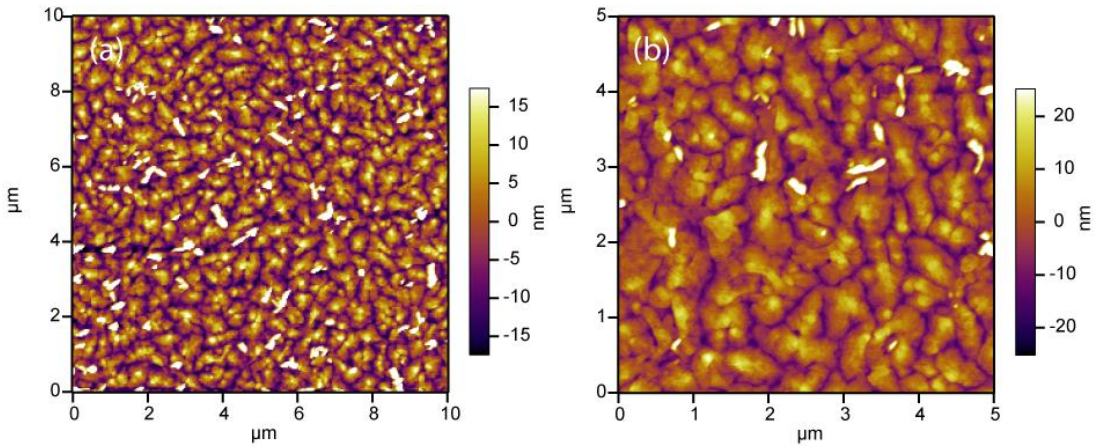

Figure 4.9 AFM morphology of vacuum deposited 40 nm thin films of Cl$_4$TIPSEpent.

The main difference between the two processing techniques is the size of the semiconductor crystalline regions with the films. The solution processed films are

allowed a longer period of time to aggregate and crystallize in comparison to the vacuum deposited films. This slower growth method results in larger crystals as seen in the morphology.

4.2.3. Devices

In addition to modification of the frontier orbital energies and optical band gap, any change in the processability as compared to the TIPSEpent molecule is also important for device applications. Anthony *et al.* [6-7] first functionalised pentacene with TIPSE to render it soluble in common solvents, thereby removing the requirement for vacuum deposition. However, whilst TIPSEpentCl_2 is also amenable to processing from solution, TIPSEpentCl_4S and TIPSEpentCl_4A are not. Consequently for device applications TIPSEpent and TIPSEpentCl_2 were spin cast from toluene and 1,2-dichloromethane respectively (25mg ml^{-1}) whilst TIPSEpentCl_4S and TIPSEpentCl_4A were deposited using vacuum evaporation at a rate of 0.1 nm s^{-1}. Although attempts were made to vacuum deposit TIPSEpent and Cl_2TIPSEpent they were unsuccesful and the material decomposed (as were the attempts to solution process the tetrachlorinated derivatives). TIPSEpent has previously been employed as the electron donor in OPVs in conjunction with C_{60} as the electron acceptor.[23] To test the suitability of the chlorinated TIPSEpent derivatives as electron donor materials they were incorporated into the bilayer OPV structure: ITO coated glass / PEDOT:PSS (40 nm) / TIPSEpentCl_x (40 nm) /C_{60} (40 nm) / BCP (8 nm) /Al (60 nm). Typical current-voltage characteristics in the dark and under 1 sun simulated solar illumination are shown in **Figure 4.10** and the average device characteristics are given in **Table 4.2**

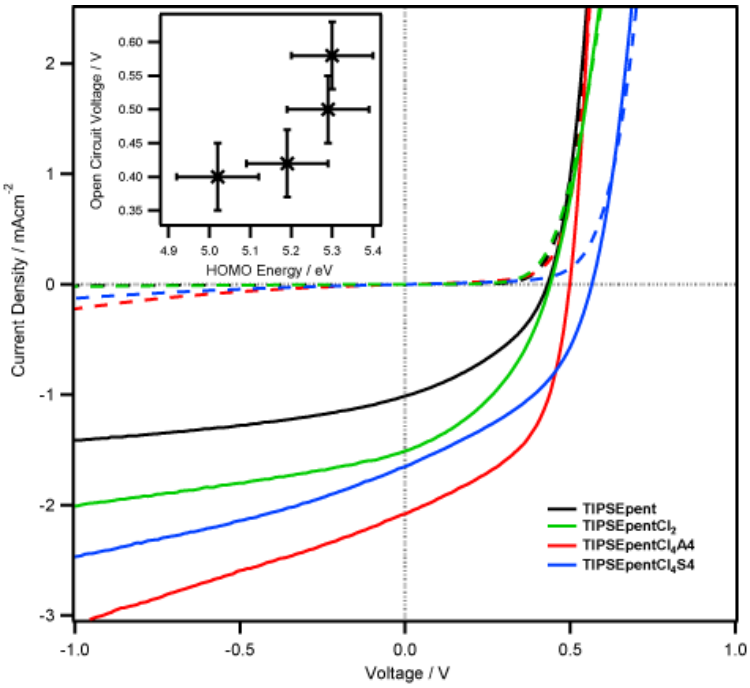

Figure 4.10 Typical light and dark device characteristics for the bilayer OPVs: ITO/ PEDOT:PSS / donor / C_{60} / BCP / Al. Inset: Open circuit voltage (V_{oc}) *vs* HOMO energy with respect to vacuum level.

TABLE 4.2. Summary of average device performance parameters.

Donor	J_{sc}/mA cm^{-2}	V_{oc}/V[a]	FF	ηp
TIPSEpent	0.90 ± 0.2	0.41	0.38 ± 0.03	0.14
TIPSEpentCl$_2$	1.51 ± 0.3	0.44	0.40 ± 0.05	0.26
TIPSEpentCl$_4$A	1.94 ± 0.3	0.50	0.44 ± 0.07	0.39
TIPSEpentCl$_4$S	1.65 ± 0.4	0.57	0.42 ± 0.09	0.40

[a] ±0.05

It is clear that chlorination at the ends of the pentacene core is an effective strategy for enhancing OPV performance. The η_p of devices employing TIPSEpentCl$_2$ is significantly improved as compared to those employing unsubstituted TIPSEpent. It is difficult to directly compare the performance of these devices with those using TIPSEpentCl$_4$A and TIPSEpentCl$_4$S as the

electron donor, since the latter are not amenable to solution processing and unsubstituted TIPSEpent is prone to decomposition during vacuum deposition. However, the increase in V_{oc} of the Cl_4 derivatives is consistent with current understanding of the factors affecting V_{oc} in OPVs[18-20] since the ionisation potential of the tetra-chlorinated derivatives is significantly (~0.3 eV) larger than TIPSEpent. The improved performance in devices employing chlorinated derivatives results primarily from an increase in the short-circuit current density (J_{sc}). This improvement is consistent with more favourable alignment of the donor HOMO with the Fermi level of the PEDOT:PSS hole-extraction layer, since the latter is ~ 5.1 eV below the vacuum level (**Figure 4.3**).[18, 24-26] This is also potentially shown in the dark curves of the chlorinated derivatives as with barrierless contacts there is the potential to pass a small amount of charge even at negative bias. The J_{sc} in the chlorinated derivatives is dramatically increased when compared to TIPSEpent, but it is less than a quarter of that achieved when using unsubstituted pentacene.[5, 19]

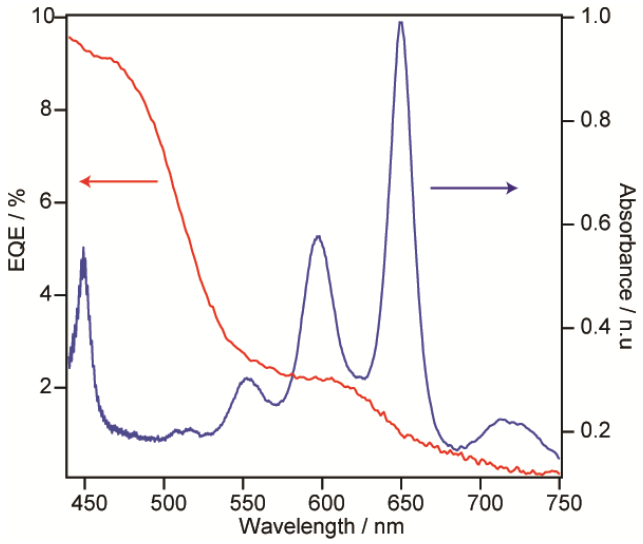

Figure 4.11 EQE for an OPV device employing a TIPSEpentCl_4A donor layer (red line, left hand axis); Normalised UV-Vis absorption spectra of TIPSEpentCl_4A film (blue line, right hand axis).

It is evident from the external quantum efficiency (EQE) data (**Figure 4.11**) that this stems from the failure of the intense vibronic absorptions, common to acenes, in TIPSEpentCl$_4$A to contribute to photocurrent generation. This effect is common to all the other derivatives studied here and has been seen previously by Lane *et al.*[23]

Schumann *et al.*, when using the soluble TS-CuPc as the donor material, also witnessed a similar EQE which predominantly displays only a C_{60} contribution. In both the TSCuPc and TIPSE derivatives, the "donor" layer seems to be merely providing a favourable interface for C_{60} exciton dissociation. Shown in **Figure 4.12** is a C_{60} only device, (device structure: ITO / PEDOT:PSS / C_{60} / BCP / Al), which displays, albeit with poorer device performance due to a lack of D / A interface, an extremely similar EQE. There is a marginal difference between 550 – 650 nm which could be potentially down to an extremely small contribution from the TIPSEpentacene. Though as it is present in the C_{60} absorption (Figure 1.23) it must be due to the actual dissociation and has been seen previously by Tang *et al.*[38]

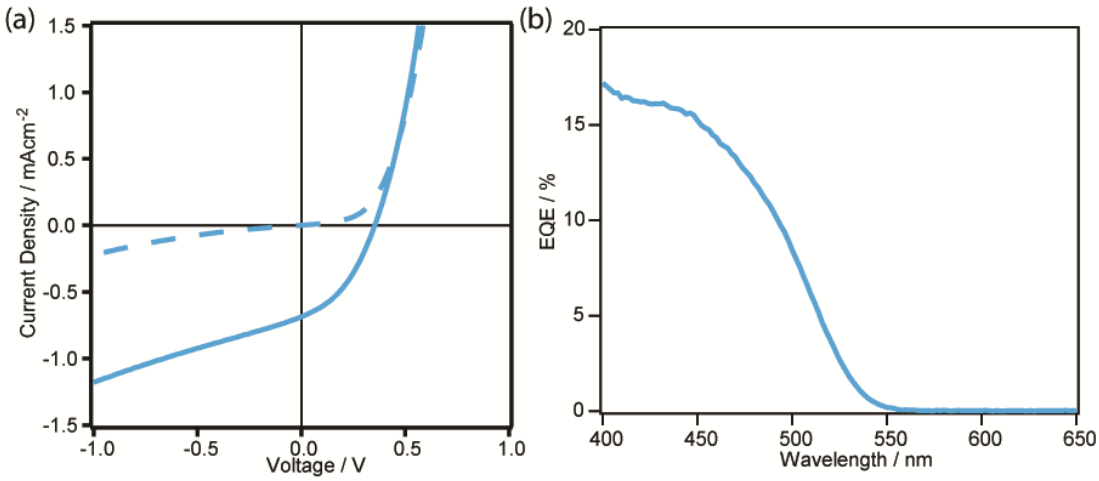

Figure 4.12 (a) *J-V* characteristics and (b) EQE of aC_{60} only device

Consequently, we conclude that the TIPSE moieties are responsible for rendering the lowest energy optical absorption inactive for light harvesting. Recently a study on energy level alignment of interfaces determined that the low hole mobility in TIPSEpent devices was a prime reason for the lack of contribution to photocurrent in both bilayer cells and in bulk heterojunctions.[27] For OPV applications, the advantage of solution processability imparted by the TIPSE moieties is outweighed by a reduction in relatively long-lived free excitons in the solid phase and a lower hole mobility. As a consequence, OPV device perfomance suffers.

4.3. Conclusions

The use of synthesised chlorinated TIPSEpent derivatives and their characteristics in solution, thin film and when incorporated into devices have been discussed. Chlorination of the molecular semiconductor TIPSEpentacene has been shown to be an effective means of tuning the molecular frontier orbitals with minimal change in band gap. Upon chlorination it has a greater stability towards reactions with fullerenes in solution and improved device parameters such as the J_{sc} and V_{oc} are also observed.

To investigate the change in ionisation potential with regards to chlorination, cyclic voltammetry was used to determine the oxidation potentials and via a method by D'Andrade *et al*, the HOMO levels were established. They were found to increase by ~ 150 meV for every two chlorines added to the ring – with both the symmetric and asymmetric tetrachlorinated derivatives resulting in an IP of 5.3 eV.

As acenes are known to react in a diels alder like fashion with fullerenes, through the modification of the IP an increase in stability towards fullerenes was expected. Acenes typically react across the central ring resulting in a colourless solution. Through comparing the absorption spectra of the TIPSEpent in solution over time it was found to decrease, but on the addition of fullerenes the decrease in absorption was much more rapid implying a reaction between the two molecules. The tetrachlorinated derivative is much more stable in solution over the 15 hours with minimal change to the absorption spectrum, and is inherently much more stable on the addition of the fullerene, indicating that the lower IP can indeed increase the stability of the molecules and slow down degradation pathways via unwanted reactions.

Although TIPSEpent and TIPSEpentCl_2 are solution proccessable, it was found that the addition of more Cl atoms resulted in insoluble derivatives only amenable to vacuum deposition. Devices containing the TIPSEpent only achieved an efficiency of 0.1 % (0.41 V, 0.9 mA cm^{-2} and 0.38 FF), which is quite low compared to literature on previous TIPSEpent devices (0.4 %). On the addition of two chlorines the J_{sc} and V_{oc} were improved to 1.51 $mAcm^{-2}$ and 0.44 V respectively. The addition of two more chlorines (symmetric or asymmetric) resulted in further improvements in all parameters resulting in an efficiency of 0.4 %. The systematic increase in V_{oc} can be explained by the increase in electron withdrawing groups (2 – 4 Cl atoms) increasing the ionisation potential. This deepening of the HOMO increases the interface gap at the donor / C_{60} interface, which is known to be the main determinant of the $V_{oc.}$

Although the improvements in the cell parameters correlate with increasing chlorination, the overall current for all the TIPSEpent devices is extremely low in comparison to standard Pent / C_{60} cells (< 25 %). To explain the lack of J_{sc}, the EQE of the devices was examined and it was found that none of the TIPSEpent derivatives contribute to the photocurrent – the only contributor appears to be C_{60}. This has been seen previously in literature for TIPSEpent devices as well as other solution processable donor materials such as TSCuPc. This is thought to be due to the low hole mobility in films when used in a device configuration though in this case, it appears to also be due to the low absorption of the TIPSE derivative thin films.

Although the TIPSE moieties appear to render the donor material inactive within the device in regards to photocurrent contribution there are promising aspects of chlorination as a route to tuning energy levels, modifiying the processesbility, improving cell performance and increasing the inherent stability of the molecule as well as in devices which resulted in the successful chlorinatation and use of Cl_6-SubPc.[15]

4.4. Extra Experimental

Cyclic Voltammetry (CV). CV was performed with CHI model 8.14 using a scan rate of 50 mV s^{-1}. TIPSEpent and the chlorinated derivatives were dissolved in dry acetronitrile with tetrabutylammonium hexafluorophosphate salt (TBAPF6) as the supporting electrolyte. Extremely low concentrations of the insoluble materials were used and to dissolve the tetrachlorinated semiconductors, the solutions were warmed and sonicated and the measurements undertaken quickly. The oxidation potentials were measured with respect to a

Ferrocene / Ferrocene^{+} (Fc / Fc^{+}) reference and the HOMO energy of the molecule was calculated using a previously established method by D'andrade *et al.*

OPV Device Fabrication. The OPV devices were fabricated on commercially available ITO-coated glass (Psiotec, 100nm thick, $R_s < 15$ mΩ sq^{-1}) after cleaning by sonication in acetone, detergent, water and isopropanol immediately prior to treatment with UV/O_3 to remove carbon residues. A 40 nm film of poly (3,4-ethylenedioxythiophene):poly (styrenesulfonate) (PEDOT :PSS) was spin cast onto the clean ITO glass substrates and annealed at 110 ^{o}C for 10 mins. TIPSEpent and TIPSEpentCl_2 were spin cast from 25 mg ml^{-1} solutions in toluene and 1,2-dichlorobenzene respectively. The substrates were then transferred to the vacuum chamber for deposition of the C_{60} (40 nm) and bathocuproine (BCP) (8 nm) layers followed by the aluminium top electrode (100 nm). The organic materials: C_{60} (Nano-C Inc – 99.5%)) were purified using thermal gradient sublimation before deposition and BCP (Aldrich) used as received. TIPSEpentCl_4A and TIPSEpentCl_4S were deposited at 0.1 nm s^{-1}. C_{60} and BCP were deposited at 0.08 nm s^{-1}. The device area was nominally 0.16 cm^2.

4.5. References

1. J. E. Anthony, *Ang. Chem. Int. Edn.* **2008**, *47*, 452.
2. S. Yoo, B. Domercq, B. Kippelen, *Appl. Phys. Lett.* **2004**, *85*, 5427.
3. P. Sullivan, T. S. Jones, T. S. *Org. Electron.* **2008**, *9*, 656.
4. H. Ishii, K. Sugivame, E. Ito and K. Seki, *Adv. Mater.* **1999**, *11*, 605.
5. K. V. Chauhan, R. Hatton, P. Sullivan, T. Jones, S. W. Cho, L. Piper, A. deMasi and K. Smith, *J. Mater. Chem.* (**2010**), *20*, 1173.
6. J. E. Anthony, J. S. Brooks, D. L. Eaton, S. R. Parkin. *J. Am. Chem. Soc.* **2001**, *123*, 9482.
7. M. L. Tang and Z. Bao. *Chem. Mater*. **2011**, *23*, 446.

8. F – R. Schmidt, M. M. Ling, H. J. Oh, M. Winkler, M. Konemann, N. Z. Bao, F. Wurthner *Adv. Mater.* **2007**, *19*, 3692.
9. B. A. Jones, M. J. Ahrens, M. H. Yoon, A. Facchetti, T. J. Marks, M .R. Wasielewski,. *Angew. Chem., Int. Ed.* **2004**, *43*, 6363.
10. M. H. Yoon, S. A. DiBenedetto, A. Facchetti, T. J. Marks.. *J. Am.Chem. Soc.* **2005**, *127*, 1348.
11. M. H. Yoon, A. Facchetti, C. E. Stern, T. J. Marks, *J. Am. Chem.Soc.* **2006**, *128*, 5792.
12. H. Peisert, M. Knupfer, T. Schwieger, G. G. Fuentes, D. Olligs, J. Fink and Th. Schmidt, *J. Appl. Phys.* **2003**, *93*, 9863.
13. A. R. Murphy, J. M. Frechet, J. *Chem. Re*V. **2007**, *107*, 1066.
14. Z. N. Bao, M. L. Tang, J. H. Oh, A. D. Reichardt. *J. Am. Chem. Soc.* **2009**, *131*, 3733.
15. P. Sullivan, A. Duraud, I. Hancox, N. Beaumont, G. Mirri, J. H. R. Tucker R. A. Hatton, M. Shipman, T. S. Jones, *Adv. Energy Mater.* **2011**, *1*, 352.
16. Previously synthesised by an alternative route 14
17. C. R. Swartz, S. R. Parkin, J. E. Bullock, J. E. Anthony, A. C. Mayer, G. G. Malliaras. *Org. Lett.* **2005**, *7*, 3163
18. J. E. Anthony, J. S. Brooks, D. L. Eaton, S. R. Parkin.. *J. Am. Chem. Soc.* **2001**, *123*, 9482.
19. J. E. Anthony, D. L. Eaton, S. R. Parkin. *Org. Lett.* **2002**, *4*, 15.
20. M. L. Tang, J. H. Oh, A. D. Reichardt and Z. Bao, *JACS*. **2009**, *131*, 3733.
21. L. C. Palilis, P. A. Lane, G. P. Kushto, B. Purushothaman, J. E. Anthony and Z. H. Kafafi, *Org. Elec*. **2008**, *9*, 747.
22. B. W. D'Andrade, S. Datta, S. R. Forrest, P. Djurovich, E. PolikarpM .E. ov, Thompson, *Org. Electron.* **2005**, *6*, 11.
23. J. Gierschner, B. Milian Medina, J. E. Anthony.. *ChemPhysChem* **2008**, *9*, 1519.
24. N. Sato, Y. Saito, H. Shinohara. *Chem. Phys.* **1992**, *162*, 433.
25. I. G. Hill and A. Kahn *J. Appl. Phys.* **1999**, *86*, 4515.
26. P. Heremans, D. Cheyns, B. P. Rand. *Acc. Chem. Res.* **2009**, *42*, 1740.
27. B. Kippelen, B., W. J. Potscavage, A. Sharma. *Acc. Chem. Res.* **2009**, *42*, 1758.
28. K. V. Chauhan, R. Hatton, P. Sullivan, T. S. Jones, S. W. Cho, L. Piper, A. deMasi, K. E. Smith, *J. Mater. Chem.* **2010**, *20*, 1173.
29. G. P. Miller, J. B. Briggs, *C. R. Chim.* **2006**, *9*, 916.
30. G. Miller, I. Kaur, *New J. Chem.* **2008**, *32*, 459.
31. J. Han, I. Bae and I Chung. *Ecs. Trans.* **2011**, *33*, 101.
32. P.A. Lane, L. C. Palilis, G. P. Kushto, B. Purushothaman, J. E. Anthony, Z. H. Kafafi, *Org. Electron.* **2008**, *9*, 747.
33. M. G. Helander, Z. B. Wang, M. T. Greiner, Z. W. Liu, K. Lian, Z. H. Lu, *Appl. Phys. Lett.* **2009**, *95*, 173302.
34. M. Kemerink, A. M. Nardes, M. M. de Kok, E. Vinken, K. Maturova, R. A. Janssen, J. *Org. Electron.* **2008**, *9*, 727.
35. N. Beaumont, I. Hancox, P. Sullivan, R. A. Hatton, T. S. Jones, *Energy Environ. Sci.* **2011**, *4*, 1708.
36. S. Schumann, R. A. Hatton and T. S. Jones. *J. Phys. Chem. C.* **2011**, *115*, 4916.
37. R. J. Davis, M .T. Lloyd, S. R. Ferreira, M. J. Bruzek, S. E. Watkins, L. Lindell, P. Sehati, M. Fahlman, J. E. Anthony, and J. W. P. Hsu. *J. Mater. Chem.* **2011**, *21*, 1721.
38. M. Zhang, H. Wang, H. Tian, Y. Geng and C. W. Tang. *Adv. Mater.* **2011**, *23*, 4960.

Acceptors

Introduction

Understanding organic semiconductors on a fundamental level is extremely important not only to understand device parameters once a device has been made, but to predetermine how well a cell will work, and why certain materials are better in some configurations than others. Although designing new materials is a promising (potentially the most important) route forward for OPVs, understanding the materials we currently use, and utilising them to their full potential is also important.

Until now, new acceptors, unless they are fullerene based have had minimal success in small molecule OPVs as previously discussed. The need to move beyond fullerenes is due to their limited light absorption and high cost and although OPVs have moved forward, the acceptor layer has not changed in the past two decades and has partially held the community back. A recent article by Liu *et al.* discusses the inherent qualities of fullerenes (PCBM and $PC_{70}BM$ specifically) that make them such impressive acceptor materials and gives views on potential synthetic equivalents that are not necessarily fullerene based.[1] Using quantum chemical calculations, PCBM (and $PC_{70}BM$) were found to contain extra low lying electronic states, separate to the ground anionic state which could accept electrons. This results in a ten-fold increase in charge separation with little to no effect on charge recombination and to move acceptors forward, synthetic efforts need to include this property when designing new acceptor materials. They showed this further by comparing five new acceptors from a recent review[2] (and five of their own acceptors) and showed that none of the review acceptors synthesised contained the low lying states and therefore predicted poor acceptor performance in comparison to the fullerene – which was indeed the case. They proposed their own conjugated acceptors complete with low lying states and are in the process of working with

experimentalists to prove this route as viable for the synthesise of successful acceptors.[3]

One of the main processes in OPV operation is charge dissociation of the exciton and it is believed that before full dissociation the exciton migrates near the interface to a charge transfer (CT) state, some whom believe this state is bound, others a more delocalised state. This dissociation typically requires an offset and in OPVs this is created via the use of a heterojunction. As excitons are coloumbically bound and have low dielectric constants, it is thought that at least 0.3 eV is needed to separate them and this is extremely important for efficient dissociation. Unfortunately, many device systems have a much larger offset than necessary and this minimises the open circuit voltage achieved due to the small interface gaps created.

Typical exciton transfer is via FRET, a dynamic quenching mechanism, and it is extremely dependant on the emission of the emitter and absorption of the receiver overlap as well as the distance between them. Photoluminescence is an extremely underused technique and can give a welcome insight into the exciton quenching abilities of acceptors which is related to a charge transfer process. Fluorescence quenching is the basis of FRET and has been used here to convey the use of typical donor materials as acceptors by investigating their quenching ability of the excitons in the donor material in comparison to fullerenes.

Once the charges have dissociated, the next process, charge transport and collection, is very much dependant on the charge carrier mobility of the semiconductor. The mobility is dependent on many factors including conjugation, structure (morphology) and purity of the semiconductor. Typically in inorganic semiconductors, due to the large concentration of charge carriers, the Hall effect is

used to measure the mobility, with mobilities reaching 450 - 1500 $cm^2 V^{-1}s^{-1}$ for single crystal Si.[4] In organic semiconductors, the concentration of charge carriers is several magnitudes lower and therefore other techniques are needed to measure the mobility and unfortunately, are generally indirect measurements, such as ToF, SCLC, and CELIV.[5] Typically, in small molecule organic semiconductors single crystal acenes can reach > 1 $cm^2 V^{-1}s^{-1}$,[6] whereas thin films characteristically have mobilities with magnitudes between 10^{-8} - 10^{-2} $cm^2 V^{-1}s^{-1}$.[7]

Understanding interfaces and how materials behave when they come into contact with each other is imperative in OPVs as this determines many of the device parameters, e.g; the electrode / organic interface determines charge injection (extraction) and the organic / organic interface determines recombination (dissociation). Due to dipoles, common vacuum levels are unlikely and band bending can also occur. Both depend on the specific material systems and therefore case by case studies are necessary. Material properties such as work function, IP and EA determine the built in field, V_{oc}, and successful charge transfer and charge separation (as mentioned previously) and therefore it is critical to determine the energetics of the materials and device systems.[8,9,10] Through utilising techniques such as ultra violet photoelectron spectroscopy (UPS) and kelvin probe (KP), band diagrams of device systems can be devised which allow deeper insight into the energetics of organic layers when in contact in various configurations and explain certain cell parameters.[10]

The main goal for PV technology is to fulfil what is known as the unification challenge,[11] as shown in **Figure II.1** by the Venn diagram:

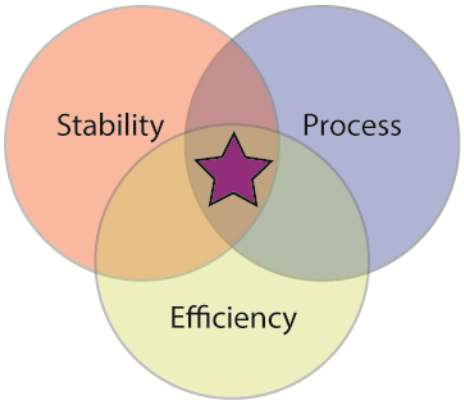

Figure II.1 Venn diagram summarising the Unification Challenge

Only when all aspects are satisfied will current OPVs be suitable for commercial applications and to move forward, degradation mechanisms is one of the understudied aspects of solar cells at present.

Life expectancy indirectly determines cost and currently OPVs fall very far behind inorganic PVs not only in terms of efficiency but also stability, with inorganic cells having lifetimes of ~ 25 years.[12] Knowledge of the degradation mechanisms is paramount if understanding how to prevent them is going to be achieved and as cells will be used in ambient atmosphere currently barrier technology has been invested in to reduce O_2 and moisture diffusion into cells. As it has been shown that metal electrodes are permeable to gas and moisture current OLEDs generally use thin non – organic (nitrides , oxides) as encapsulating layers which typically have H_20 and O_2 transmission rates of 10^{-6} – 10^{-4} $gm^{-2}day^{-1}$ and 10^{-3} $cm^3m^{-2}day^{-1}atm^{-1}$ respectively.[13] Unfortunately, physical / chemical degradation generally splits into two main catergories:

1. Extrinsic – caused by external factors such as water, O_2, electromagnetic radiation, quality of encapsulants *etc.*
2. Intrinsic – dependant purely on materials and interfaces.

There are a number of cell degradation mechanisms and generally more than one will contribute to the same trend (as shown in Table i).

Table i Correlation between main OPV degradation pathways and their impact of OPV cell characteristics. Information taken from N.Grossiord *et al.*[14]

Parameter affected (reduced) and key factors determining it	Possible causes
FF Serial resistance (R_s) Shunt resistance (R_{sh})	Reduced interfacial charge transfer efficiency Deterioration of charge transport in the layers Presence of shunts and shorts
V_{oc} Energy difference between the $HOMO_D$ and $LUMO_A$	Reduction of the active layer / electrode interface Lowering of the Interface gap of the active layers Electrode work function change Presence of shorts
J_{sc} – Light absorption Molecular architecture of the material (band gap) Thickness of active layer (AL)	Chemical degradation of the AL Loss of transparency preventing photons reaching AL
J_{sc} – Exciton dissociation efficiency, ηED Match of the band gap	Decrease of the D / A interface area (if in codeposited / blend ALs)
J_{sc} – Carrier transport and collection efficiency ηCC	Loss of perculating pathways (if codep / blend) due to reorganisation Degradation of the electrode / AL interface Change in energy levels of the cell components
Percolation pathway to electrodes (if blends) Organisation of transportation pathways (e.g. crystallinity) Device architecture	Cracks Layer delamination Degradation of material leading to decrease of charge carrier mobilities / formation of traps

When the J_{sc} decreases this is due to the number of charges collected at the electrodes decreasing. This is possibly one of the most complicated trends to nail down as it has an extremely large amount of potential contributors such as, degradation affecting absorption, dissociation, transport and the active layer / electrode interface. The V_{oc} is generally controlled by the $HOMO_D$-$LUMO_A$ gap and

electrode work functions and therefore degradation that changes any of these properties will affect the V_{oc}. Recombination and temperature are also known to affect the open circuit voltage. The fill factor is an ideality factor which is mainly affected by R_{sh} and R_s and FF degradation generally means there has been a change in the recombination and (or) space – charge effects resulting in imbalanced transport throughout the cell.

The following two chapters will discuss the use of a variety of typical donor materials as acceptors in Tetracene and Pentacene based devices and investigate their potential as ambipolar semiconductors.

References

1. T. Liu and A. Troisi, *Adv. Mater.* (2012),
2. P. Sonar , J. P. F. Lim and K. L. Chan, *Energy Environ. Sci.* **2011**, *4*, 1558.
3. Article:http://esciencenews.com/articles/2012/12/11/alternative.fullerenes.organic.solar.cells.just.exciting
4. J.B. Casady and R.W. Johonson, *Solid State Electronics* **1996**, *39*, 1409.
5. S. Tiwari and N.C. Greenham, *Opt. Quant. Electron*. **2009**, *41*, 69.
6. C. Goldmann, S. Haas, C. Krellner, K. P. Pernstich, D. J. Gundlach and B. Batlogg, *J. Appl. Phys.* **2004**, *94*, 2080.
7. B. P. Rand, J. Xue, S. Uchida and S. R. Forrest J. Appl. Phys. **2005**, *98*, 124902.
8. R. Schlaf, B. A. Parkinson, P. A. Lee, K. W. Nebesny, N. R. Armstrong, *J. Phys. Chem. B.* **1999**, *103*, 2984.
9. H. Ishii, K. Sugivame, E. Ito and K. Seki, *Adv. Mater.* **1999**, *11*, 605.
10. K. V. Chauhan, R. Hatton, P. Sullivan, T. Jones, S. W. Cho, L. Piper, A. deMasi and K. Smith, *J. Mater. Chem.* **2010**, *20*, 1173.
11. M. Jorgensen, K. Norrman and F. C. Krebs, *Sol. Energy. Mat. Sol. Cells* **2008**, *92*, 686.
12. www.renewableenergyworld.com/rea/news/article/2009/12/pv-durability-and-reliability-issues
13. L. Moro, R.J. Visser, Barrier Films for Photovoltaics, in: C.J. Brabec, V.Dyakonov, U. Scherf (Eds.), Organic Photovoltaics – Materials, Device Physics, and Manufacturing Technologies, Wiley-VCH, Weinheim, **2008**.
14. N. Grossiord, J. M. Kroon, R. Andriessen, P. W. M. Blom, *Org. Electron.* **2012**, *14*, 432.

Chapter 5.

Subphthalocyanines as Electron Acceptors in Tetracene Photovoltaics

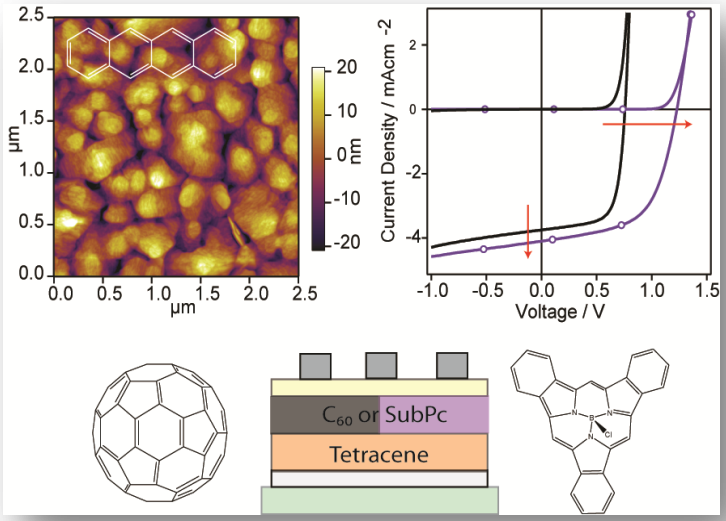

In this chapter the optimisation of tetracene thin films and the use of the typical donor material, SubPc, as an acceptor in SHJ OPVs using Tc as the donor is discussed. The electronic structure and energy levels of Tc / C_{60} and Tc / SubPc heterojunctions are studied using soft x – ray photoelectron spectroscopy (PES) and the performance of OPV devices based on these two donor / acceptor combinations optimised with regards to Tc and SubPc thickness. Through the replacement of C_{60} with SubPc we show significant improvements in V_{oc}, J_{sc} and η_p. Studies with Cl_6SubPc as an acceptor are also included as a comparison with SubPc and C_{60}. The

degradation of these cells has also been investigated in air and show a reduction in degradation when C_{60} is replaced.

5.1. Results: Tetracene solution and thin film properties.

Figure 5.1 is the chemical structure of Tc which compromises of 4 fused benzene rings. This section will discuss the optimisation of this molecule in thin films and the photophysical, structural and morphological properties that result in various difficulties when optimising this underused acene in devices.

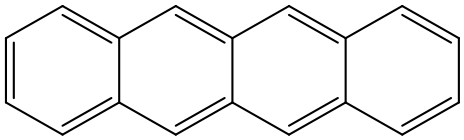

Figure 5. 1 Chemical structure of Tc

5.1.1. Photophysical properties

Shown in **Figure 5.2** is the normalised UV-Vis absorption spectra of tetracene in solution and as a vacuum deposited thin film. As previously mentioned it has distinctive peaks due to accessible vibrational levels and there is a clear red – shift when in solid form. This arises from the 2D π–π stacking present in tetracene crystals and films. The Davydov splitting of the main transition occurs, similar to Pentacene films and is indicative of different dimers / aggregates in the crystalline vacuum deposited film.[1]

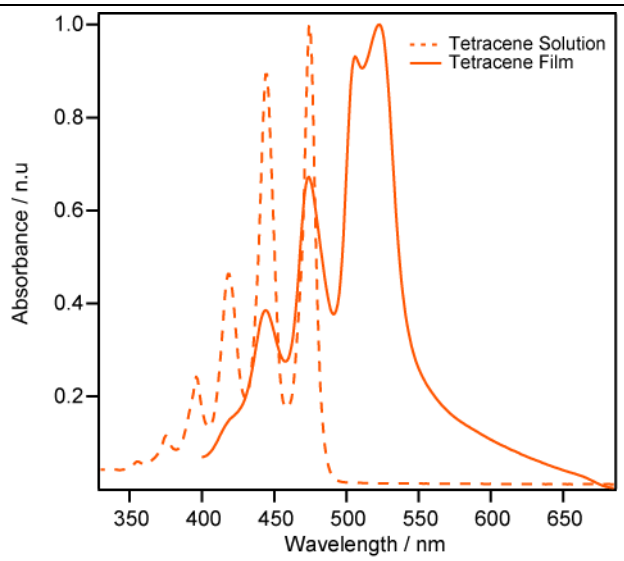

Figure 5. 2 Normalised UV – Vis absorption of both a solution ($1x10^{-3}$ $moldm^{-3}$) and a 60 nm OMBD grown film of Tc.

Unlike pentacene, which doesn't exhibit significant fluorescence (further discussed in **Chapter 6**) the emission spectra of a tetracene film is shown in **Figure 5.3** and has a λ_{max} at 547 nm (55 nm red shifted compared to the solution emission).

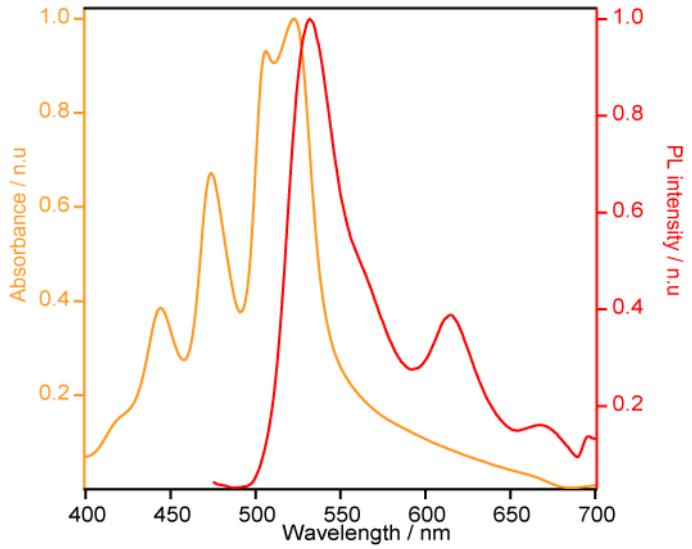

Figure 5. 3 Normalised absorbance and PL spectra of a 60 nm film of Tc

It displays a Stoke's shift of ~10 nm. Although Tc exhibits a strong red emission, there are few published reports of their use in OLEDs due to the poor oxidative stability.[2] In 2003, some Tc derivatives were synthesised making use of their emissive properties and indeed showed promise for use in OLEDs.[3]

5.1.2. Morphology and structure

One of the fundamental interests in organic semiconductors is the possibility of controlling the properties. The final device performance is heavily determined by the bulk structural properties of the films as well as the interfaces created. In the case of small molecules, vacuum deposition onto ITO leaves for various points to be considered:

- The early stages of growth are the basis for the final film morphology. This can be extremely important as layer by layer growth from monolayers (MLs) results in large crystal grains and non-detrimental grain boundaries whereas 3D island growth tend to form smaller grains and detrimental grain boundaries which can limit current flow (as seen in transistors).
- The orientation that the molecules assume influences successive layers and can have a heavy influence on the charge transport characteristics as well as HOMO / LUMO levels.

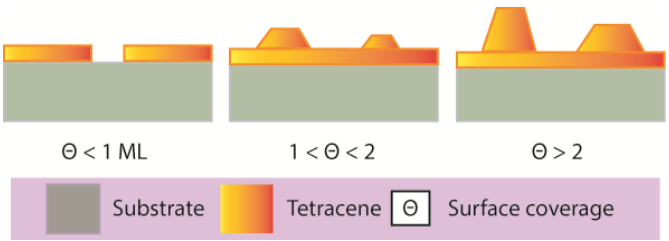

Figure 5. 4 Cross section views of Stranski – Krastanov growth for different surface coverages.

Tetracene is known to exhibit a Stranski-Krastanov growth mechanism on Ag (111) substrates which is characterised by both 2D and 3D island growth, indicated in **Figure 5.4** for various surface coverages (Θ).[4] Langner *et al.* investigated the growth of tetracene using high resolution low energy electron diffraction (LEED) and temperature programmed desorption (TPD) and found two long-range ordered monolayer phases (α, β).[5] Tetracene has also been previously investigated on ITO substrates and is found to exhibit the same growth behaviour.

Various thicknesses of Tc films were grown on ITO substrates and the morphology studied using both SEM and AFM. **Figure 5.5a**, which was taken from a 5 nm Tc film, reveals large voids between the half-micron-sized crystals. As more Tc is deposited onto the substrate the crystals tend to get closer together but the voids still partially exist in the thicker 25 nm films (**Figure 5.5d**).

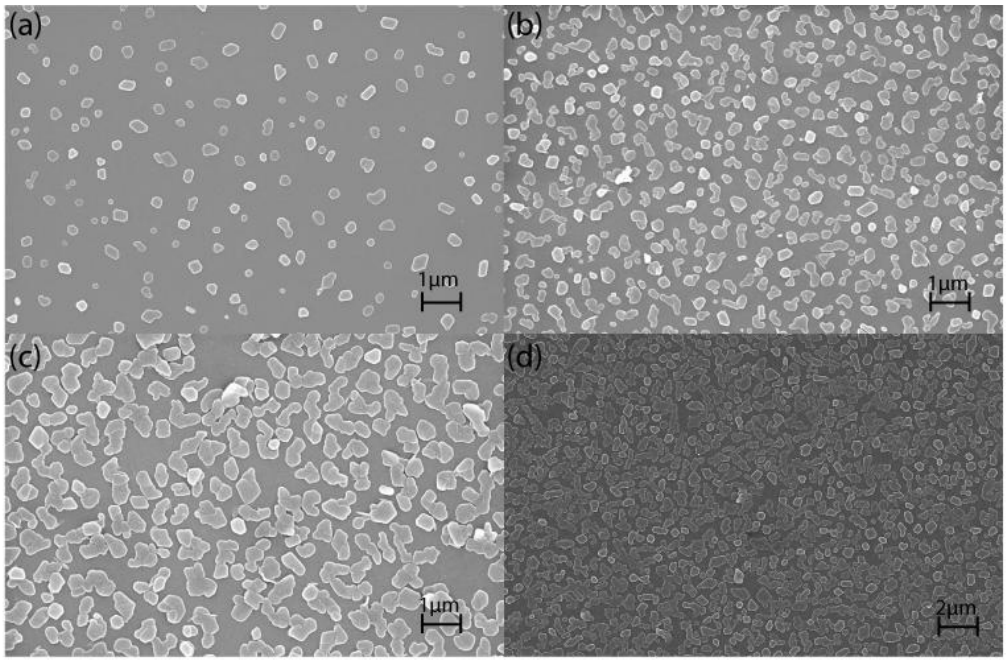

Figure 5. 5 SEM images of (a) 5 nm, (b) 10 nm, (c) 15 nm and (d) 25 nm films of Tc grown on ITO.

The AFM image in **Figure 5.6** shows the crystals on a smaller scale and the voids are still present up to ~ 40 nm (QCM measured) thicknesses, consistent with previous reports by Chu *et al.*[6] Unfortunately, voids to the substrate would be extremely detrimental for device performance as a complete layer is necessary to provide good contact for charge collection.

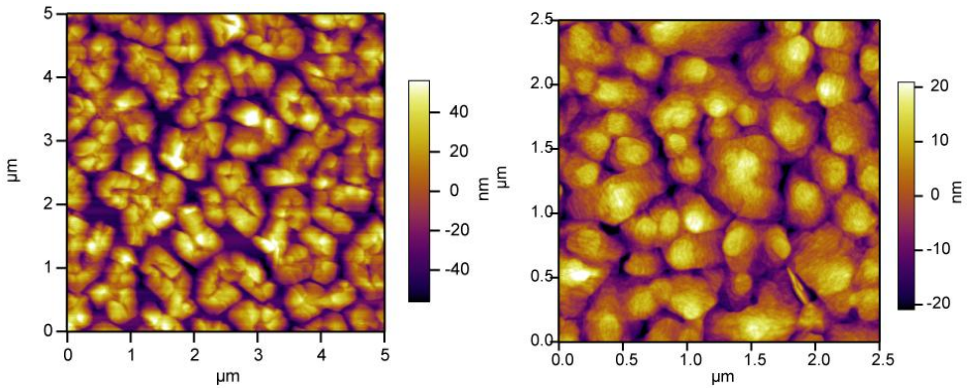

Figure 5.6 AFM images of (a) a 40 nm Tc film and (b) a 60 nm Tc film on ITO.

AFM image **Figure 5.6b,** indicate that island type growth is evident in the 60 nm film, with multilayers apparent in the 2.5 µm scan shown. Complete films began to form at measured thicknesses (d_T) > 40 nm, putting a lower limit on the thickness required for use as a donor layer in OPVs. The root mean square roughness, R_q, of the 60 nm films was found to be 8.5 nm which is higher than other more commonly used donor materials, e.g. chloroaluminium phthalocyanine (ClAlPc), which has an R_q ~ 4 nm.[7]

5.1.2.1. Thin film crystal structure

Tetracene, similar to pentacene, has been shown in the literature to stack perpendicular to the substrate due to strong intermolecular interactions along the conjugated molecule.[8] As shown in the XRD trace (**Figure 5.7**), a 100 nm vacuum deposited tetracene film on ITO has been investigated. Although it has a 001 peak

present at $2\theta = 7^{o}$ to indicate some crystallinity along the c – axis, the 002 peak is hidden by a broadness associated with more amorphous type layers when compared to the single crystal XRD (**Figure 5.7b**) taken from Yang.[9]

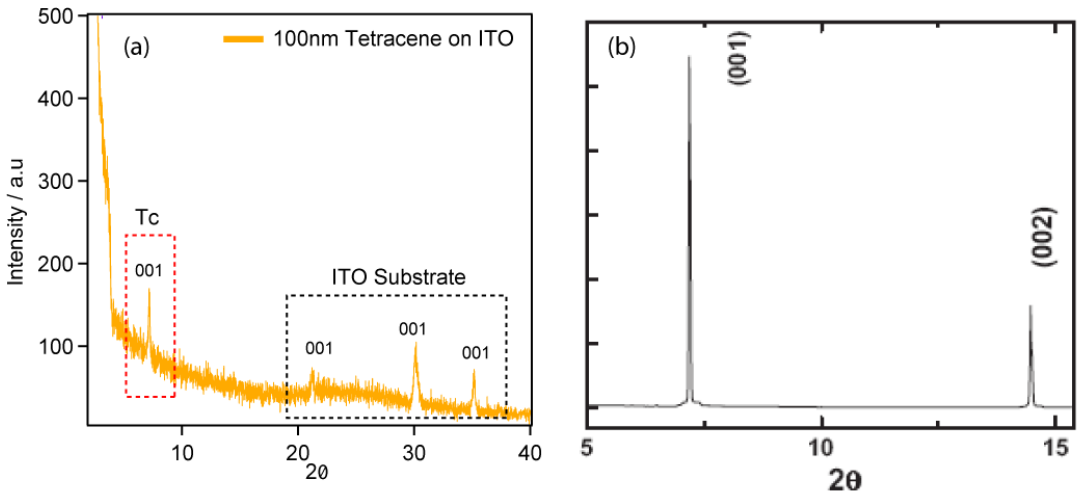

Figure 5. 7 (a) XRD trace of a 100 nm OMBD grown tetracene film on ITO; (b) XRD trace of a tetracene single crystal[9]

5.2. Results: Subphthalocyanines as electron acceptors.

5.2.1. Photophysical characterisation

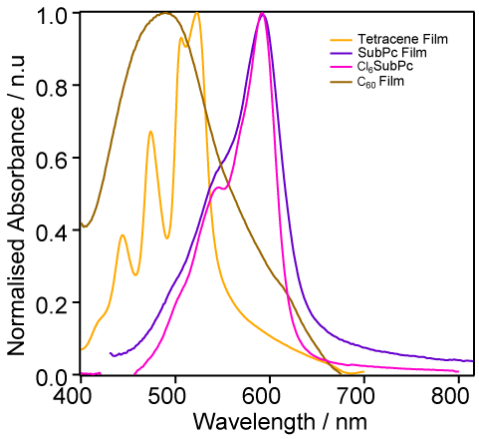

Figure 5. 8 Normalised UV-Vis absorption spectra of the thin films of the semiconductors used within this study.

The absorption of all the layers used within this chapter are shown in Figure 5.8. The overlap in absorption between Tc and C_{60} is large in the 400 -550 nm region and therefore limits the J_{sc} potentially obtained in a conventional SHJ device. (Cl_6-) SubPc has the potential to replace C_{60} as the acceptor material due to the reported energy levels of the material and its strong absorption between 500 - 600 nm, allowing for a greater percentage of the solar spectrum to be harvested

The PL quenching of tetracene emission by (Cl_6-)SubPc was investigated with comparison to C_{60} (**Figure 5.9**) to indicate the acceptor character of the subphthalocyanines.[10] Tetracene has a strong emission at 540 nm and as quenching of this emission is indicative of a charge transfer process bilayers were investigated. A thin layer (5 nm) of acceptor was deposited on top of the tetracene layer (typically 60 nm to ensure complete coverage) and the bilayer excited through the quartz using an excitation wavelength of 465 nm.

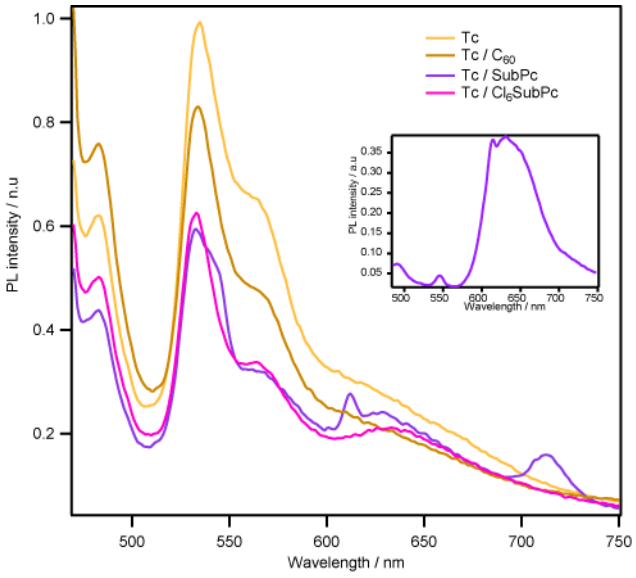

Figure 5.9 PL emission spectra of Tc and Tc / (C_{60} / SubPc / Cl_6 - SubPc) bilayers at an excitation wavelength of 465 nm. Inset: PL emission of a 20 nm pristine SubPc layer at an excitation wavelength of 465 nm.

In the bilayer structure, the tetracene emission is quenched to ~ 40 % of the original emission of the pristine film at 540 nm when using either of the SubPc materials as the acceptor, whereas C_{60} quenches ~ 18 % of the peak. This suggests that there is indeed a charge transfer occurring between the Tc layer and the SubPc, perhaps more efficiently than the C_{60}. This could possibly be partially due to the transfer mechanism, FRET, which is dependent on the emission of the donor and absorption of the acceptor overlap – the greater this overlap, the greater the transfer.[11] As you can see from **Figure 5.10** the Förster overlap is indeed larger for the Tc / (Cl_6)SubPc system in comparison to Tc / C_{60} and therefore could also be participating as well as charge transfer. The peak at ~ 620 nm shows a decrease in PL intensity (~ 15%) due to the quenching effect of C_{60} but there is an increase with the Tc / SubPc bilayer. This is due to the emission of the SubPc layer itself confirmed in the PL for a pristine 20 nm SubPc layer (as shown in the inset **Figure 5.9**). This could be the re-emission of SubPc after FRET from the Tc layer.

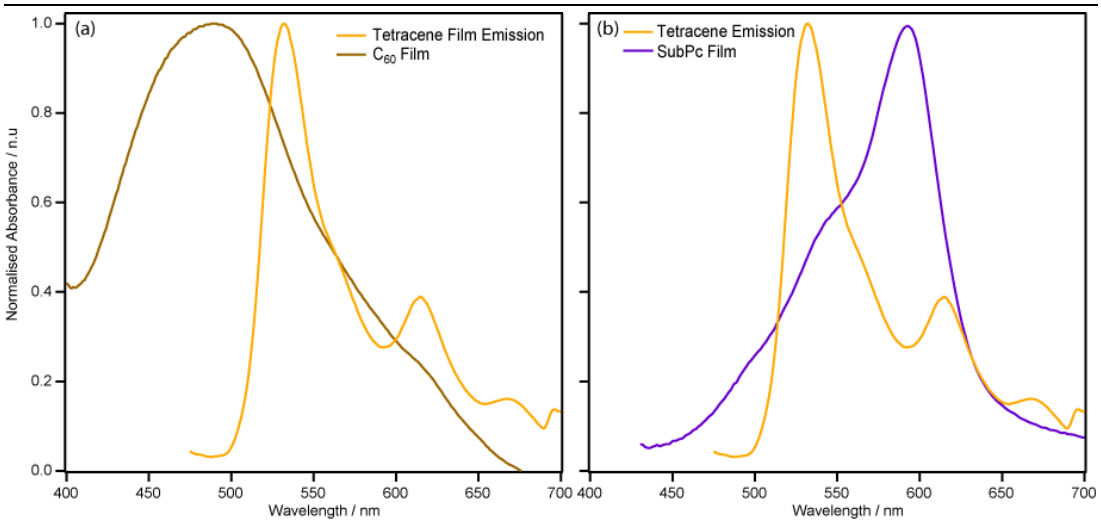

Figure 5.10 PL and UV-Vis absorption spectra of the D / A respectively for (a) Tc / C_{60} and (b) Tc / SubPc indicating the Förster overlap.

With solutions and codeposited films (1:1 ratio) the emission is completely quenched indicating an expected increase in charge transfer. This data suggests that SubPcs are as effective at quenching as C_{60} (perhaps more so) and therefore are a viable potential to replace C_{60} as acceptors.

5.2.2. Mobility

Another important physical property in photovoltaics is the charge mobility. To assess the dual donor/acceptor character, the charge mobilities of (Cl_6-) SubPc were obtained. For the mobility measurements we model the *J-V* characteristics using the space – charge limited current (SCLC) theory (see **Chapter 3**) under the assumption that in devices holes are only transported in tetracene and electrons in the acceptor material (C_{60}, SubPc or Cl_6SubPc depending on device structure).

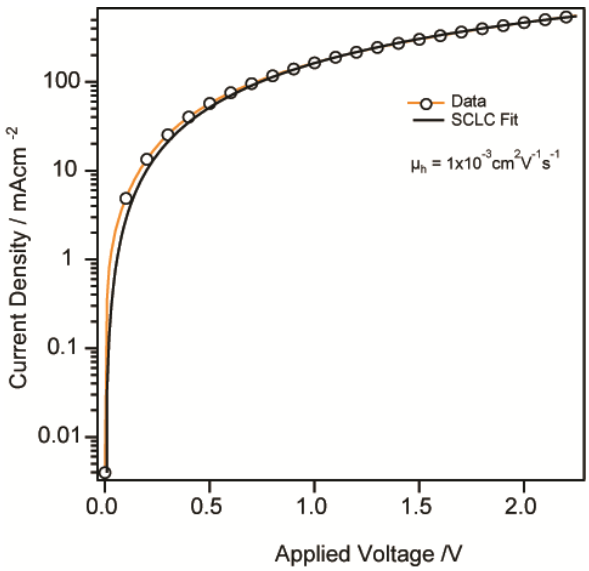

Fgure 5.11 Log *J – V* plot to extract the hole mobility of a thin Tc film (100nm) (circles) and the corresponding fit (solid)

Hole only devices have the structure:

ITO / MoO_x (5 nm) / Donor (100 nm) / MoO_x (5 nm) / Al

Electron only devices have the following structures:

ITO / Ca (8 nm) / Cl_6(SubPc) Material (100 nm) / Ca (8 nm) / Al

ITO / Ag (8 nm) / C_{60} (200 nm) / Ag (8 nm) / Al

Tc thin films (100 nm) show rather high hole mobilities of (μ_h) ~ 1 x 10^{-3} cm^2 V^{-1} s^{-1} when fit, shown in **Figure 5.11**. In comparison to other donor materials such as CuPc, which has μ_h ~ 10^{-5} cm^2 V^{-1} s^{-1},[12] it is relatively high for organic thin films. By contrast in Tc single crystals the mobilities have been found to be as high as 1 cm^2 V^{-1} s^{-1}.[13]

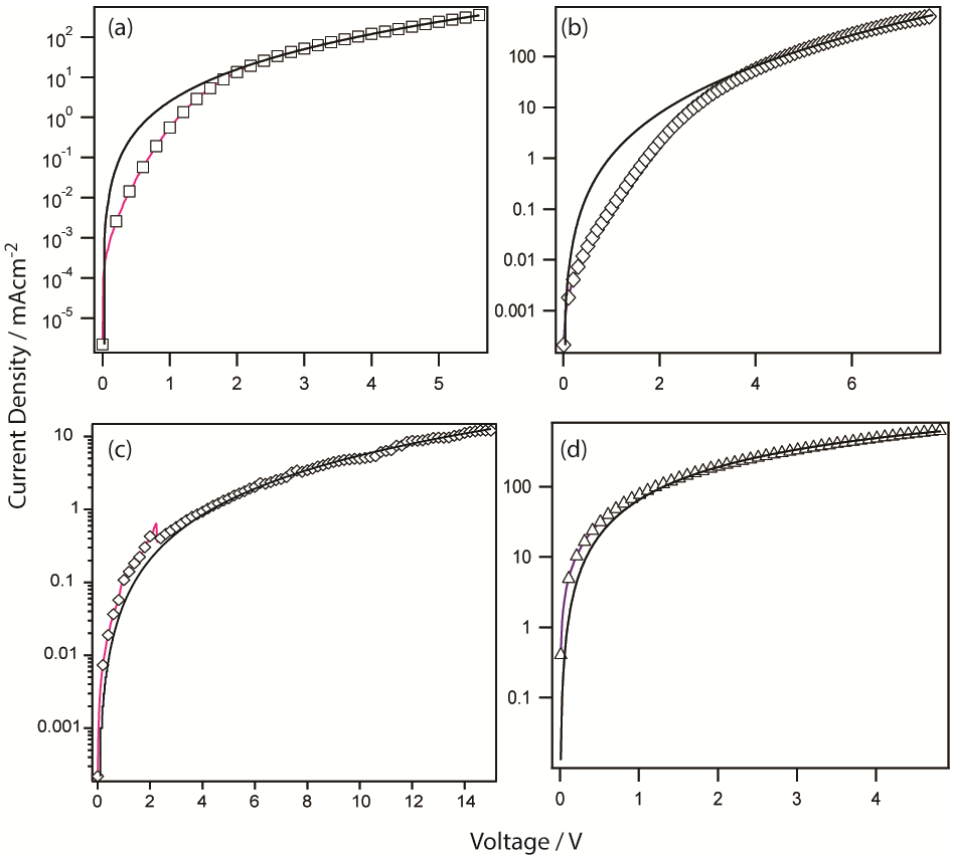

Figure 5.12 Log *J* – *V* data for (a) Cl_6SubPc, and (b) SubPc hole mobilities and (c) Cl_6SubPc, and (d) SubPc electron mobilities and the corresponding fits (solid line).

Shown in **Figure 5.12** are the log *J-V* characteristics for both hole and electron mobilities for the SubPcs. The hole mobilities were found to be 1.01 x 10^{-6} and 2.82 x 10^{-6} cm^2 V^{-1} s^{-1} for SubPc and Cl_6SubPc respectively with poor fitting to the Mott Gurney equation at lower voltages. The electron mobility of Cl_6SubPc was found to have a mobility value which is not unrealistic of 1.64 x 10^{-7} cm^2 V^{-1} s^{-1}. The electron mobility of SubPc was found to be 4.60 x 10^{-4} cm^2 V^{-1} s^{-1} which is a promising indication of its potential use as an acceptor. Although the μ_e of SubPc is almost two orders of magnitude smaller than that measured for $C_{60,}$ it is still comparable to other OPV materials (particularly hole mobility in donors) and we can therefore assume that it can transport charges sufficiently well when used as an acceptor in devices.

Table 5.1. Zero-field mobility, μ_o, for holes and electrons in various samples.

Semiconductor	Hole mobility / V cm^2 s^{-1}	Electron mobility / V cm^2 s^{-1}
Tc	1 x 10^{-3}	-
SubPc	1.0 x 10^{-6}	4.6 x 10^{-4}
Cl_6-SubPc	2. 8x 10^{-6}	1.6 x 10^{-7}
C_{60}*	-	1 x 10^{-2}

5.2.3. AFM of bilayers

In order to exclude morphological factors affecting the replacement of C_{60}, bilayer structures were imaged using atomic force microscopy (AFM). A pristine film of Tc is shown in **Figure 5.10a** for comparison of the underlying morphology. After the deposition of (b) C_{60}, (c) SubPc and (d) Cl_6 - SubPc onto the Tc layer small features appear on the Tc crystallites. Generally the 5 nm of acceptor coats the underlying

morphology with a relatively uniform film. As in previous literature, when a thin film of C_{60} is deposited on top of an organic, for example pentacene, small crystallites form across the surface, rather than filling the gaps in between the crystals, and this is also observed when the SubPcs are deposited on top of the acene layer.[14, 15]

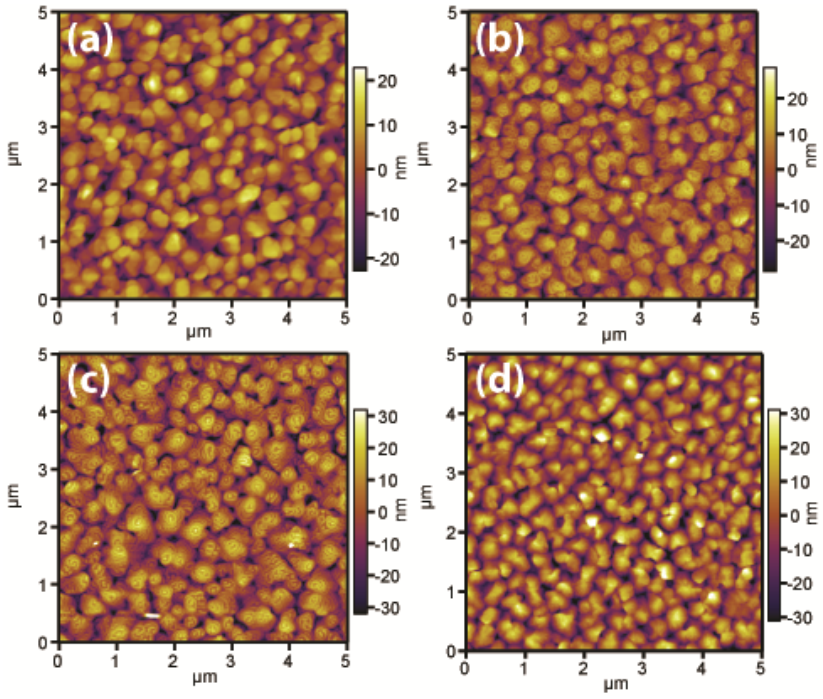

Figure 5.10 AFM images of (a) Tc, (b) Tc / C_{60}, (c) Tc / SubPc, and (d) Tc / Cl_6 – SubPc films.

As there are no obvious morphological differences between the acceptors due to the large influence of the underlying crystalline layers, (the morphology of the acenes has a larger influence over device performance) any change in performance is not attributed to the layer morphology.

5.2.4. Energetics

As previously discussed, although the I_g is extremely important when achieving a larger V_{oc} in OPV cells, the magnitude of the $HOMO_D$-$HOMO_A$ and $LUMO_D$-

$LUMO_A$ offsets are vital to achieving efficient dissociation at the heterojunction interface since too small an offset can result in low charge separation and hence have a detrimental effect on device performance. PES studies of the Tc / C_{60} and Tc / SubPc systems were therefore used to obtain quantitative information on the energy level structure of the two organic heterojunctions. The HOMO energies and shifts in vacuum level and work function were determined using the standard method given by Schlaf *et al.*[16] **Figure 5.11 (LHS)** shows the work function and the valence band spectra after deposition of a MoO_x (5 nm) film on ITO and subsequent growth of both Tc (1 – 15 nm) and C_{60} (5 – 15 nm).

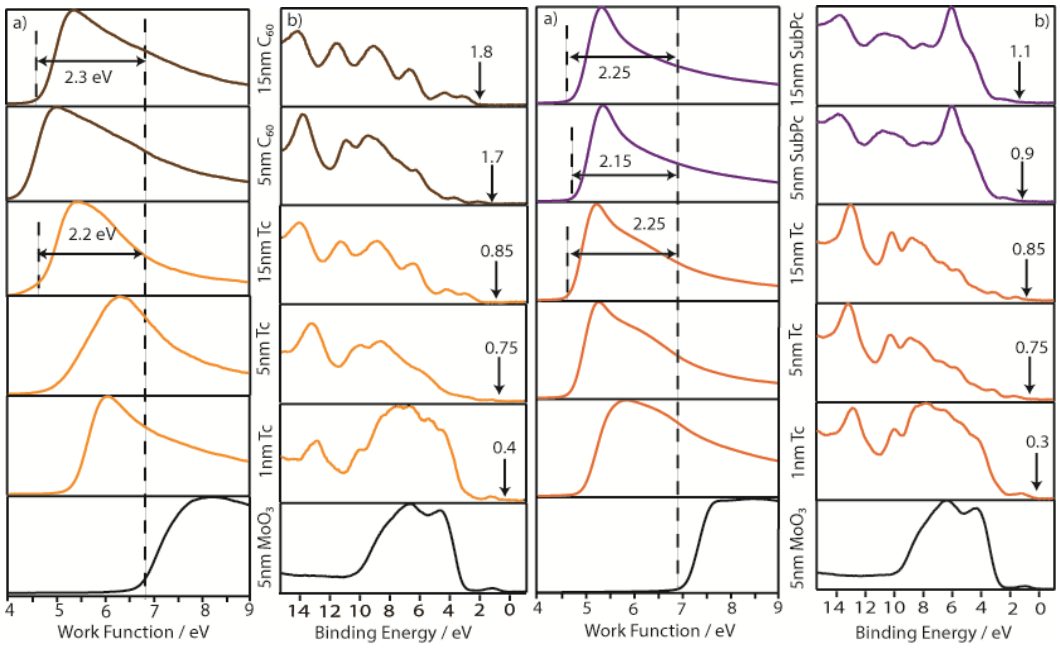

Figure 5.11 LHS: (a) Change in onset of secondary electron PES spectra after sequential deposition of Tc and C_{60} on ITO / MoO_x and (b) Valence band PES spectra recorded near E_f after the deposition of each layer. **RHS:** (a) Change in onset of secondary electron PES spectra after sequential deposition of Tc and SubPc on ITO / MoO_x and (b) Valence band PES spectra recorded near E_f after the deposition of each layer.

The work function (measured from the E_{cutoff} in PES) changes significantly by ~ 2 eV when Tc is deposited onto the MoO_x layer due to the large interface dipole created. The large dipole at the MoO_x / Tc interface is clearly seen by the band bending observed in the Tc films in the range 1 – 15 nm, whereas at the interface between Tc and C_{60} there is only a small change in work function of 0.1 eV. The Tc HOMO onset saturates at around 0.85 eV below E_f giving an IP of 5.4 eV, which compares well to previous literature.[17] C_{60} was found to have an IP of 6.3 eV with the measured HOMO onset at 1.8 eV below the E_f. **Figure 5.11 (RHS)** shows the PES spectra after deposition of Tc and SubPc on ITO / MoO_x. As seen in the Tc / C_{60} system there is a large change in the work function after deposition of the Tc layer onto MoO_x with a small change in work function at the Tc / SubPc interface. The SubPc HOMO saturation occurs around 1.1 eV below E_f and, simliar to previous work, has an IP of 5.6 eV. [18]

The energy level diagrams of the two different heterojunctions are summarised in **Figure 5.12**.

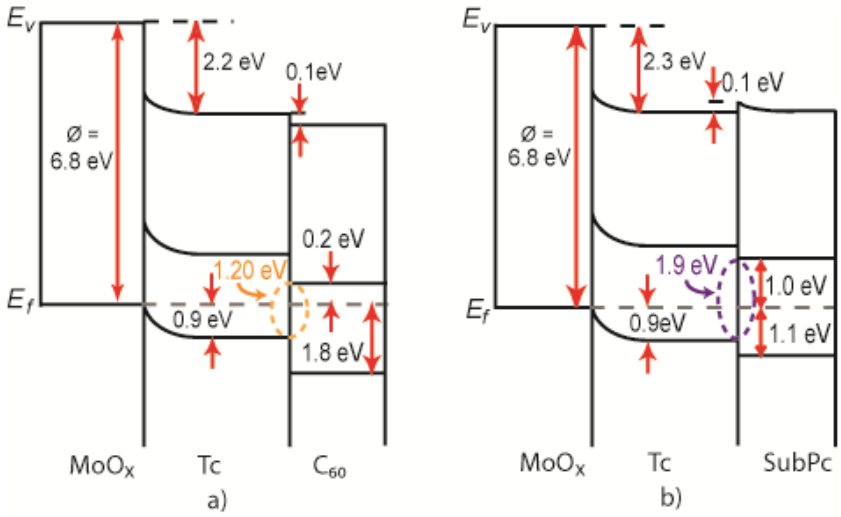

Figure 5.12 Energy level diagrams of a) ITO / MoO_x / Tc / C_{60} and b) ITO / MoO_x / Tc / SubPc

This diagram was derived using the data shown in **Figures 5.11** and the optical gaps of Tc, C_{60} and SubPc which are 2.2 eV, 2.0 eV and 2.1 eV respectively. The main difference between the two systems is the interface gap (I_g) which in the Tc / SubPc heterojunction was found to be 0.7 eV larger than the Tc / C_{60} system. This should allow for a much larger V_{oc} to be achieved in OPV cells containing SubPc as the acceptor, provided efficient exciton dissociation occurs. The $HOMO_D$ – $HOMO_A$ and $LUMO_D$ – $LUMO_A$ offsets are 0.25 eV and 0.3 eV respectively for Tc / SubPc, considerably smaller than the 1.1 eV and 0.9 eV found in Tc / $C_{60.}$ This would suggest that in the Tc / SubPc system there may not be a sufficient offset to separate the charges in the SubPc layer and therefore devices may be expected to have a low photocurrent as well as minimal contribution from the SubPc layer. Although the band diagrams imply an increase in interface gap, there are a few concerns with forming band diagrams of organic materials from UPS data such as; the error introduced in the fitting process, rough initial materials making the formation of a complete sequential layer unlikely, beam damage and charging which should all be taken into account when quoting values and shifts of these materials.

5.3. Results: Device characterisation

5.3.1. Current – density characteristics

To optimise the Tc / C_{60} system a set of planar heterojunction OPV cells were evaporated with varying Tc thickness (d_T). The thickness of C_{60} was kept constant at 40 nm as this was found to be optimum. *J-V* characteristics in the dark and under 1 sun illumination for these cells are shown in **Figure 5.14** with key device parameters listed in **Table 5.2** for the device structure ITO / MoO_x (5 nm) / Tc (d_T nm) / C_{60} (40 nm) / BCP (8 nm) / Al. The insertion of the 5 nm MoO_x interlayer allows for

improved energy level alignment at the electrode / Tc interface. This allows for ohmic contact at this interface and as mentioned previously, will reduce losses caused by offsets at the electrodes in the V_{oc}.[19] A MoO_x free device is shown for comparison (Device E in **Table 5.2**).

Table 5.2. Parameters obtained from OPV devices. Devices A-D have the structure: ITO / MoO_x (5 nm) / Tetracene (d_T nm) / C_{60} (40 nm) / BCP (8 nm) / Al.

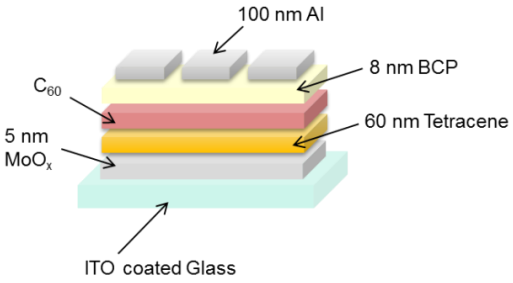

d_T/nm	J_{sc} / mA cm^{-2}	V_{oc} / V	FF	η_p / %
A: 50	3.06	0.65	0.58	1.15
B: 60	3.57	0.76	0.68	1.83
C : 70	3.26	0.74	0.64	1.52
D:100	2.67	0.72	0.60	1.12
E: 60	2.40	0.55	0.54	0.72

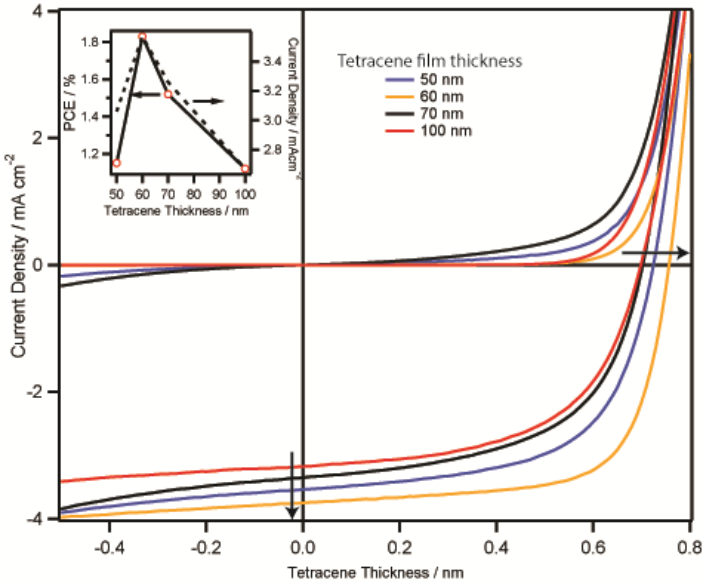

Figure 5.14. *J-V* data under 1 sun illumination for planar Tc/C_{60} heterojunction OPV devices with the illuminated currents (black) and dark currents (grey). Inset: Shows the change in power conversion efficiency (η_p) and current density with respect to Tc thickness, d_T.

It is clear that the optimal Tc thickness is 60 nm, with a J_{sc} of 3.57 mA cm^{-2}, a V_{oc} of 0.76 V, and a FF and n_p of 0.68 and 1.83 % respectively. Below this thickness (d_T < 60 nm) there is a decrease in both J_{sc} and V_{oc}. The reduction in J_{sc} is probably due to reduced exciton formation from the thinner Tc layer. The J_{sc} decreases with d_T > 60 nm, consistent with the creation of an increased number of non-dissociated excitons, and a reduction in charge collection efficiency. There is little change in the V_{oc} past the optimum thickness indicating that the maximum V_{oc} achievable has been reached.

To optimise the Tc / SubPc planar heterojunction OPV devices a set of cells were grown with varying SubPc thickness (d_S). The Tc thickness was maintained at its optimal value of 60 nm. *J-V* characteristics in the dark and under 1 sun illumination for the optimised Tc / SubPc device with structure ITO / MoO_x (5 nm) / Tc (60 nm) / SubPc (35 nm) / BCP (8 nm) / Al are shown in **Figure 5.15** with key device parameters for the series of thicknesses listed in **Table 5.3.** Data for the optimized Tc / C_{60} OPV device is also shown for direct comparison.

Table 5.3: Parameters obtained from OPV devices. Devices E - I have the structure: ITO / MoO_x (5nm) / Tetracene (60 nm) / SubPc (d_S nm) BCP (8 nm) / Al.

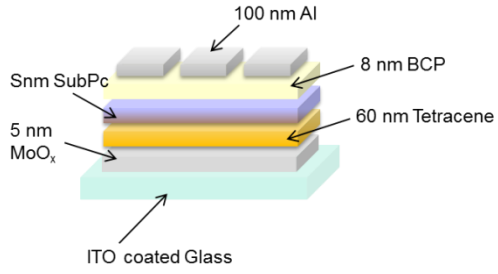

d_S / nm	J_{sc} / mA cm^{-2}	V_{oc} / V	FF	η_p / %
E = 14	2.58	1.06	0.43	1.17
F = 20	3.16	1.19	0.52	1.95
G = 28	3.35	1.23	0.58	2.37
H= 35	4.01	1.24	0.58	2.89
I = 40	3.80	1.24	0.49	2.30

Through the replacement of C_{60} with a 35 nm layer of SubPc, the J_{sc} is improved to 4.01 mA cm^{-2} and the V_{oc} and η_p both increase significantly to 1.23 V and 2.89 % respectively.

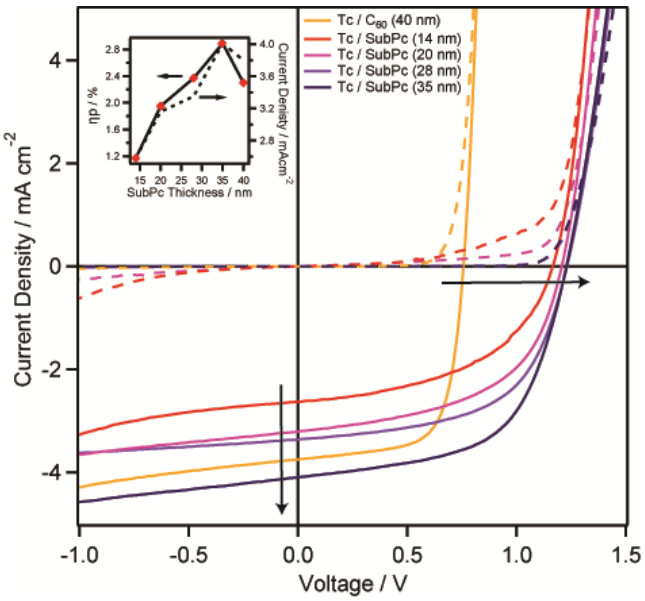

Figure 5.15. *J-V* data for planar Tc / SubPc heterojunction device with the illuminated currents (solid) and dark currents (dotted) with results from a Tc / C_{60} device included as a reference (orange). Inset: Change in power conversion efficiency and current density with respect to SubPc thickness, d_S

There is only a very small corresponding drop in FF. The devices incorporating SubPc as the acceptor material exhibit a much higher V_{oc} over the range of thicknesses studied with a maximum of 1.24 V compared to the 0.76 V achieved using C_{60}. This is due to the increase in the I_g. The reduction in FF in the SubPc cells is thought be due to the amorphous character of the film. When using C_{60} the close packed hexagonal / cubic crystal phases improve the π– π stacking resulting in a higher electron mobility and allow for higher FFs.[20] Although the FF has decreased it is still comparable to other small molecule OPVs.

Below and above the optimal thickness there is a decrease in J_{sc} for reasons similar to the Tc / C_{60} system. Interestingly, the optimum thickness, d_s, of 35 nm is much

thicker than when using SubPc as a conventional donor material,[21] where the best η_p is typically achieved using films as thin as 14 nm due to the short exciton diffusion length which has been measured anywhere from 8 – 28 nm.[22-24] Comparing the L_D measurements to the devices results when in a donor configuration the L_D of 8 nm seems plausible. To explain the use of 35 nm in the Tc / SubPc cells understanding the optical field in the device is necessary. The acceptor / Al interface largely determines the distribution of the optical field within the device and previously Halls *et al.* demonstrated that an acceptor layer, in their case C_{60}, could also be used as a spacer layer to enhance the optical electric field within the device.[25] Through varying the thickness of the acceptor layer the optical electric field at the heterojunction increases, allowing for greater photovoltaic efficiency due to a larger percentage of excitons created close to the interface where they can be easily dissociated.[26, 27] This has also been seen by others for various other spacing layers. For example, Kim *et al.* reported both an increase in photocurrent and V_{oc} in their polymer devices when incorporating a TiO_2 layer in between the active polymer and the Al cathode.[27] We believe that that the SubPc is self – spacing when using thicker layers, pushing the contributing layers further into its absorption maxima.

To cement this concept further, cells were grown using the Cl_6SubPc derivative as the acceptor. Using the literature values for Cl_6SubPc (determined by cyclic voltammetry)[28] the Tc / Cl_6SubPc I_g falls between the two shown previously (**Figure 5.16a**) and therefore should improve the V_{oc} in comparison to C_{60}, but not quite as high as the SubPc. As expected through the replacement of C_{60} with Cl_6-SubPc there is an increase in both V_{oc} to 0.85 V and J_{sc} to ~ 3 mA cm^{-2} and the resulting PCE is improved to 1.7 %. When compared with the two reference devices the V_{oc} falls between the Tc / C_{60} and Tc / SubPc devices (due to the I_g falling

between these two extremes) whereas the current is similar to the Tc / SubPc cell due to similar quenching abilities, mobilities and efficient dissociation.

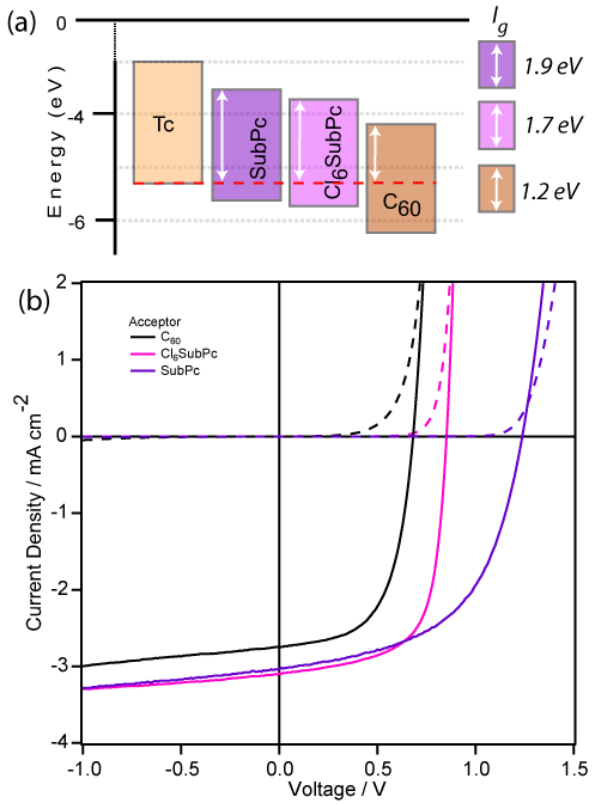

Figure 5.16 (a) Energy levels of the materials in this system and with their interface gaps highlighted **(b)** *J-V* data for planar Tc / Cl_6-SubPc heterojunction device (pink) with the illuminated currents (solid) and dark currents (dotted) with results from a Tc / C_{60} device (B) and Tc / SubPc (H) included as a reference (black and purple respectively).

Table 5.4 Device parameters obtained from OPV devices. Devices have the structure: ITO / MoO_x (5nm) / Tetracene (60 nm) / Acceptor (x nm) BCP (8 nm) / Al. **(N.B** the overall lower efficiency here of Tc / C_{60} and Tc / SubPc cells is lower here due to batch variability in the Tc supplied by Acros.)

d_T / nm	J_{sc} / mAcm^{-2}	V_{oc} / V	FF	η_p / %
J: C_{60} (40 nm)	2.75	0.68	0.59	1.11
K: Cl_6 - SubPc (35 nm)	3.14	0.85	0.63	1.67
L: SubPc (35 nm)	3.04	1.24	0.55	2.11

The implication of the reasonable FFs achieved in the cells suggests that the mobility perhaps may not be such as important factor after a certain point. A poor mobility should cause a charge carrier build up and would result in a poor FF in the organic counterparts. In this case, even though the electron mobility of SubPc is two magnitudes smaller than C_{60} and almost five magnitudes smaller for the Cl_6-SubPc there seems to be minimal to no effect on the FF in Tc / SubPc and even increases when using the Cl_6-SubPc as a replacement. This is quite an important discovery and may relax some of the restraints on materials design that were previously suggested.

5.4.2. Light Intensity Measurements

Light intensity measurements can be an indicator of the recombination mechanisms within devices. Typically, the J_{sc} is proportional to P_{inc} as follows:

$$J_{sc} \alpha P_{inc}^{\gamma} \qquad \textbf{Equation 5.1}$$

Typically, if $\gamma = 1$, the J_{sc} is independent to the light intensity and implies that recombination is localised within the layers and attributed to geminate (monomolecular) recombination. A $\gamma = 0.5$ value implies a bimolecular recombination mechanism and the cell is clearly affected by charge carrier build – up and is typical behaviour in a BHJ device. As shown in **Figure 5.17** as the light intensity increases from 0.25 to ~ 1.5 suns both the J_{sc} and V_{oc} increase. Through plotting a log – log plot of the J_{sc} vs P_{inc}, the relationship between J_{sc} and P_{inc} is established with $\gamma = 1$ for all three acceptor based cells. This implies that the cells indeed behave as bilayer devices, with a discrete interface and that monomolecular recombination dominates. Through changing the acceptor layer we have not introduced any bulk recombination via defects or impurities as they all display a

unity value of ~ 1 and this is promising for the use of phthalocyanines as acceptors as they behave similarly to fullerenes.

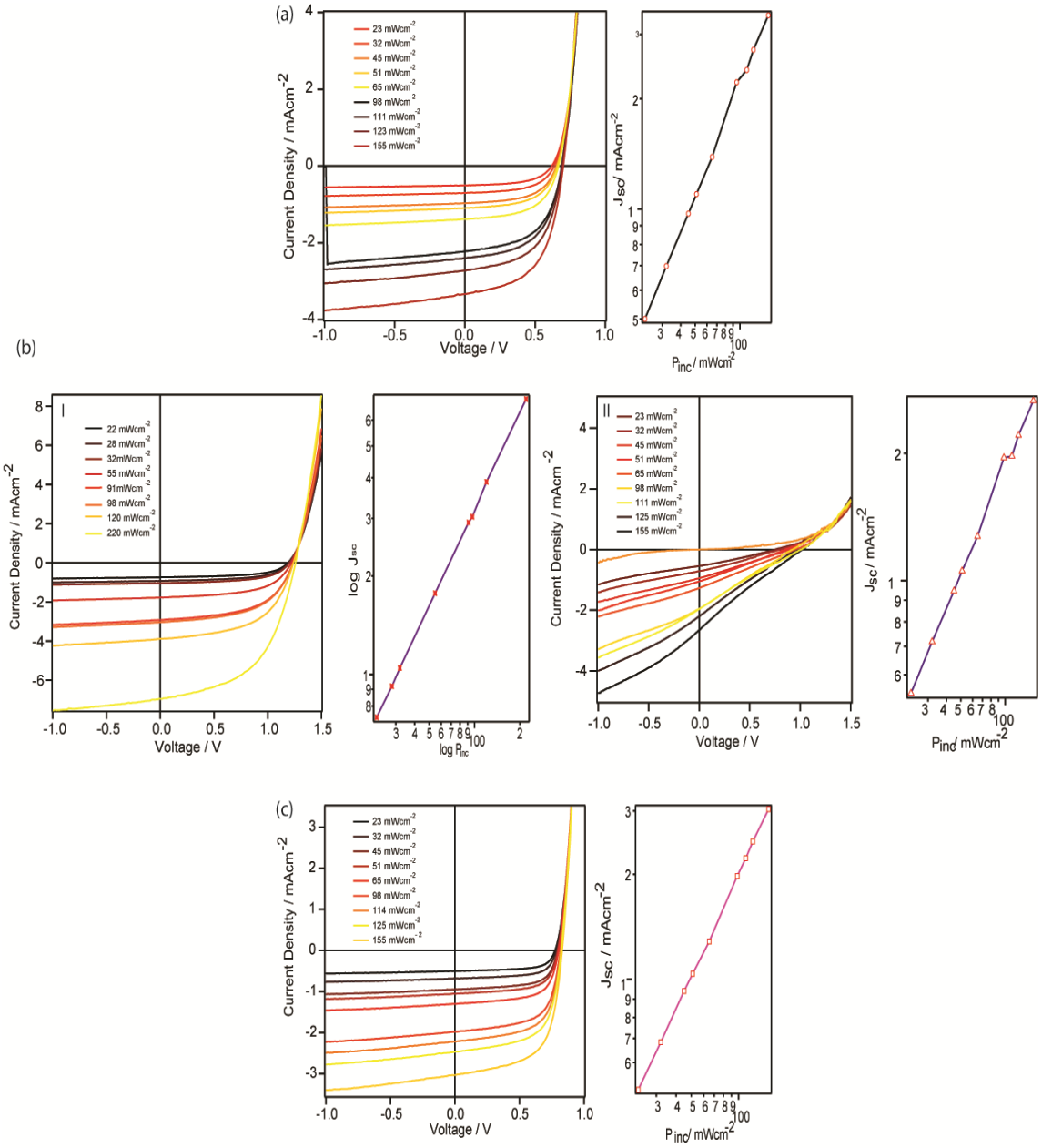

Figure 5.17 LHS: J-V curves for cells device under various illumination intensitys and **RHS:** log – log plot of J_{sc} as a function of P_{inc} for (a) Tc / C_{60} (b) Tc / SubPc I – initial testing II – day later and (c) Tc / Cl_6SubPc

One interesting factor to notice is the appearance of s – shaped kinks in the Tc / SubPc devices. On initial testing, the *J-V* curves (shown in **Figure 5.17**bII) are kink

free but further testing results in a kink as the V_{oc} is approached – limiting both the FF and the V_{oc}. This is likely to be due to a degradation of the SubPc layer resulting in a lower mobility. Although Cl_6SubPc may be expected to behave in a similar fashion it in fact does not and remains kink – free possibly another indication of greater overall stability for chlorinated molecules.

5.3.3. EQE

The external quantum efficiency (EQE) of the Tc / C_{60} and Tc / SubPc OPV cells are shown in **Figure 5.18.**

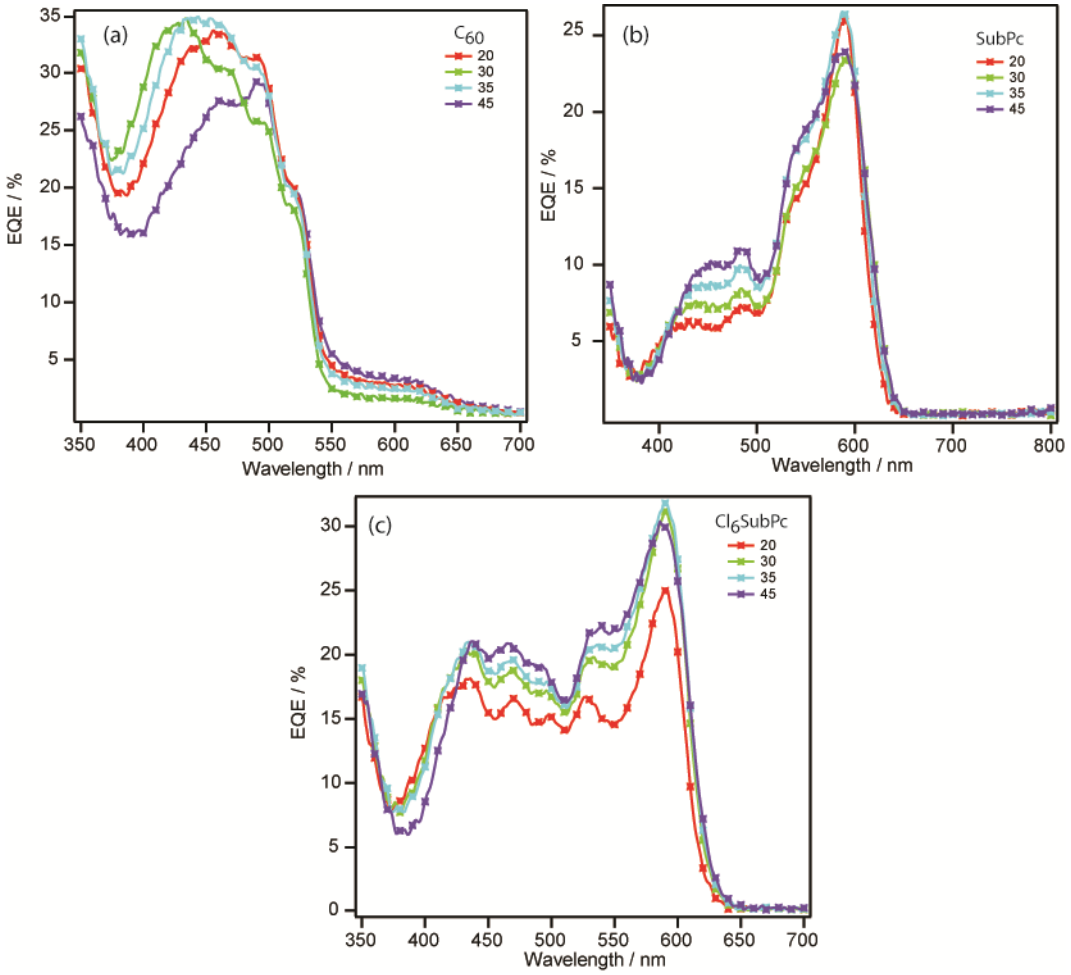

Figure 5.18 EQE of (a) Tc / C_{60}, (b) Tc / SubPc, and (c) Tc / Cl_6SubPc devices with varied acceptor thicknesses (see key).

Although there is a distinct overlap in absorbance, the Tc and C_{60} both show a contribution to the photocurrent in the Tc / C_{60} device as can be seen by the distinct Tc peaks between ~ 450 and 500 nm and the overall broadness consistent with a C_{60} contribution. Previous studies have indicated that a minimum $HOMO_D$ – $HOMO_A$ and $LUMO_D$ – $LUMO_A$ separation energy at the heterojunction for efficient dissociation is 0.3 – 0.4 eV[18, 29] although in the Tc / SubPc case the $HOMO_D$ – $HOMO_A$ separation is only 0.25 eV, and therefore only a small contribution to the photocurrent would be expected from the SubPc. Although only a small contribution is expected, it does in fact contribute quite significantly compared to the Tc layer as can be seen by the strong peak at λ = 595 nm.

This indicates that although the $HOMO_D$ – $HOMO_A$ gap is small, there is still a sufficient energy offset to efficiently separate the exciton and allow a significant contribution from this layer. Cl_6SubPc is also shown to contribute to the photocurrent in a similar fashion though the tetracene peaks are more defined and there is a more equal contribution compared to the Tc / SubPc. When changing the thickness of the acceptors from 20 – 45 nm, the maximum EQE occurs at an acceptor thickness of 35 nm in all three cases (comparative to the *J-V* data).

5.3.4. Degradation

Previously in literature, with the replacement of C_{60} an improvement has been seen in cell stability.[2] Each device was tested under constant illumination of 100 mW cm^{-2} for 1100 minutes at AM1.5G in air. **Figure 5.19** shows the change in device parameters for Tc / SubPc and the C_{60} counter cells with MoO_x in air. In both cases the cells degrade in air, the most dramatic of which is the Tc / C_{60} device which drops to 0 % PCE after 850 minutes. The main decrease is due to a fast degradation in J_{sc} and FF partially due to photobleaching

of the Tc and possibly due to the C_{60} oxidation which previously has been shown to result in a decrease in conductivity.[30]

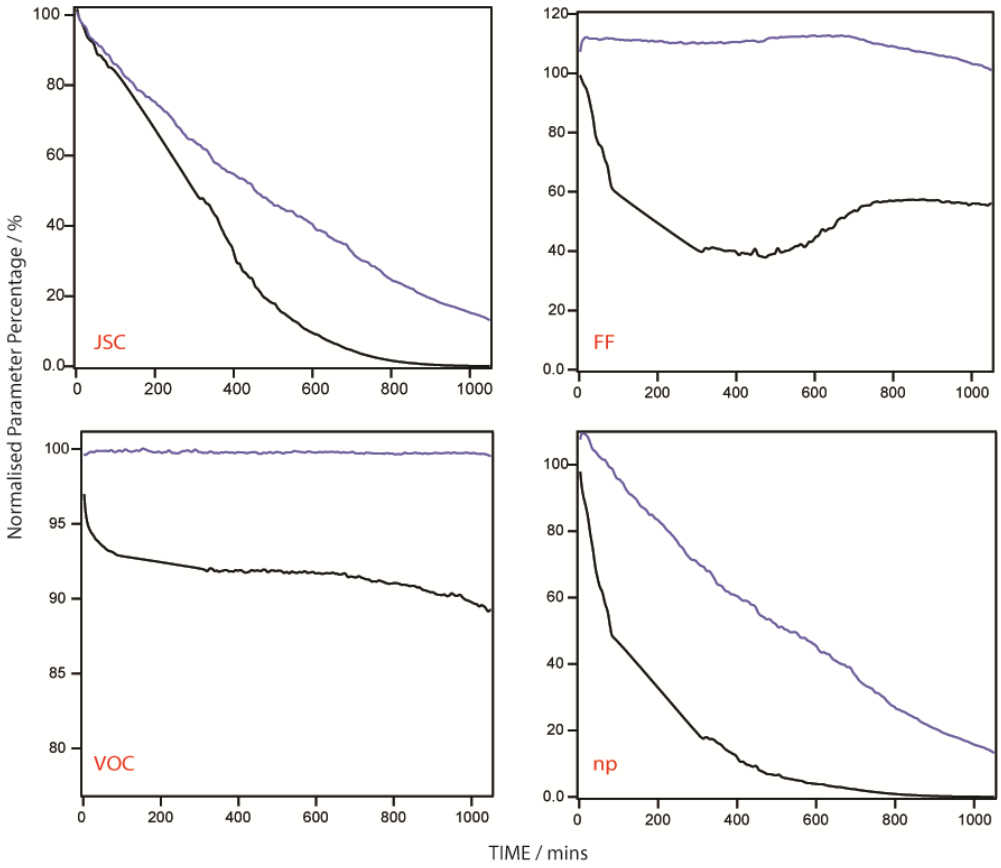

Figure 5.19. Device parameters of Tc / C_{60} (black) and Tc / SubPc (purple) (blue) cells under constant illumination over 1100 minutes.

When replacing the acceptor layer with SubPc, the cells are more stable than their C_{60} counter parts in all parameters and reaches 20 % of the original efficiency at ~ 1000mins (compared to 0 % at 800 mins with Tc / C_{60}). The Tc / SubPc cell is inherently more stable, with no change in V_{oc} over the 1000 mins and the main cause in the degradation is due to the decrease in J_{sc}. Although the degradation of the photocurrent is slower than the other systems it still shows the poor stability of these small molecules. As the decrease in J_{sc} occurs in all systems, it is probably partly down to the Tc layer as it the [4+2] cycloaddition of singlet oxygen is the main degradation pathway for the material and renders the material

colourless over time. This reinforces the need for good encapsulants to remove the possibility of O_2 degradation in cells.

5.4. Conclusion

The optimisation of Tetracene thin films has been demonstrated here for use in OPVs as an efficient donor material. Vacuum deposited thin films were found to form large crystals (~ 500 nm size) investigated by SEM and AFM at thicknesses of 5 – 40 nm, leaving large voids between crystals direct to the substrate – not necessarily ideal for OPV applications. Complete films were found to form at > 40 nm thicknesses and when optimising Tc / C_{60} cells, 60 nm was found to be ideal which is close to the predicted diffusion length of the acene.

Due to the overlap in absorption between Tc and C_{60} and the small interface gap created between them, SubPc and Cl_6-SubPc were investigated as potential replacements for C_{60} as the acceptor due to their red shifted absorption and higher LUMO levels (resulting in larger interface gaps). As Tc films have a large red emission at 547 nm, through using photoluminescence spectroscopy the (Cl_6)SubPcs quenching ability could be investigated in comparison to C_{60}. All three materials were found to quench the Tc emission, indicative of a charge transfer reaction occurring with the SubPcs actually having a larger quenching effect. This could possibly be due to a larger Forster overlap between the Tc and (Cl_6)SubPc. To rule out any morphological differences contributing to any device improvements, AFM was used to image the bilayers and show all acceptors merely following the underlying acene morphology and therefore any performance changes could not be attributed to a change in morphology.

Another apparent important factor in organic semiconductors is the charge mobility, and although SubPc is typically used as a donor material, it was crucial to know the electron mobility of the layer. SCLC was used to determine the hole mobility of tetracene, SubPc and Cl_6SubPc and the electron mobility of the SubPcs. The μ_hs of Tc, SubPc and Cl_6SubPc were found to be 1 x 10^{-3}, 1.01x10^{-6} and 2.82 x10^{-6} $cm^2 V^{-1} s^{-1}$ respectively, and are comparable to literature measurements of these materials. The μ_es of SubPc and Cl_6SubPc were found to be 4.6 x10^{-4} and 1.64 x10^{-7} $cm^2 V^{-1} s^{-1}$ were found to be magnitudes lower than C_{60} (1x$10^{-2}$$cm^2 V^{-1} s^{-1}$). Although seemingly appearing to have mobilities magnitudes slower than C_{60} and causing a mismatch of mobility in the device (as Tc has a high hole mobility 1 x 10^{-3} $cm^2 V^{-1} s^{-1}$) there seemed to be no detrimental effect on the solar cell performance. A low FF was expected (due to an increase in carrier build up due to the slow carriers) yet in the case of Tc / Cl_6SubPc it obtained a larger FF than the C_{60} reference cell. This raises the issue over the importance of mobility in organic small molecule devices and perhaps implies a move away from assumptions due to their inorganic counter parts.

One of the main reasons for investigating other acceptors was to improve the interface gap and hence the open circuit voltage of the devices. To fully understand whether this was indeed possible and to be sure of ohmic contacts at electrodes, soft x – ray spectroscopy at BNL was undertaken to investigate the energetics of the two device systems, MoO_x / Tc / C_{60} and MoO_x / Tc / SubPc. This did indeed show a large improvement in interface gap from 1.2 e V to 1.9 eV but did reveal a very small (0.25eV) $HOMO_D$ – $HOMO_A$ offset between Tc and SubPc which may have translated into poor photocurrent contribution from the SubPc layer.

Once the Tc / C_{60} was optimised, we demonstrated the use of SubPc as an efficient electron accepting material when used in single junction OPV cells in conjunction with tetracene as the donor material. By investigating the replacement of C_{60} with SubPc, significant improvements in V_{oc} and η_p have been demonstrated due to the increase in the interface gap, I_g. Although the diffusion length of SubPc is thought to be $\leq$ 15 nm, thicker layers can be utilised due to an optical spacing effect which allows for a large contribution to the photocurrent from the SubPc acceptor.

Degradation is also largely important for the future of OPVs and through replacing C_{60} in these cells, the stability can be improved due to a greater stability of phthalocyanines to O_2 which is a known contributor to C_{60} degradation. Unfortunately, in air, the Tc / SubPc cells still degrade due to the low stability of tetracene to oxygen and encapsulated cells are therefore necessary to begin to understand other mechanisms of degradation.

Although organic semiconductors show a preference for having donor or acceptor character, we have shown that provided the offsets at the heterojunction are sufficient to dissociate charges efficiently and mobilities are sufficient, a typical donor material can be utilized as an acceptor. We also show that through replacing C_{60} in devices, the stability can be improved. This leads the way for interesting donor – acceptor material combinations allowing for increased harvesting of the solar spectrum and improved device performance.

5.5. Extra experimental

OPV devices were fabricated on commercially available indium tin oxide (ITO) - coated glass substrates (Thin Film Devices, 145 nm thick, R_s < 15 Ω sq^{-1}) after

cleaning by sonication in acetone, detergent, water and isopropanol, and an ultraviolet / ozone treatment decontamination system to remove carbon residues (Novascan PSD-UVT). The OPVs were fabricated using a Kurt. J. Lesker Spectros vacuum evaporation system. The organic materials, Tc (Acros, 98%), SubPc (Aldrich, 85%), C_{60} (Nano-C Inc., 99.5%), were purified using thermal gradient sublimation before deposition and bathocuproine (BCP, Aldrich, 96%) and molybdenum oxide (MoO_x, Aldrich) were used as received. The aluminium electrodes were deposited *in situ* by evaporation through a shadow mask to a thickness of 100 nm to give an active pixel area of 0.16 cm^2. Atomic force microscopy (AFM) images were obtained using an Asylum research MFP-3D in AC mode. Current density - voltage (*J-V*) characteristics were recorded using a Keithley 2400 sourcemeter with simulated AM 1.5 G solar illumination at 100 mW cm^{-2} (1 sun) from a Newport Oriel solar simulator. External quantum efficiency (EQE) measurements were obtained using a Scienetech SF150 xenon arc lamp and a PTI Monochromator. The monochromatic light intensity was calibrated with a Si photodiode (Newport 818-UV) and chopped at 500 Hz. Signal detection was performed with a current-voltage amplifier (Femto DHPCA-100) and lock-in amplifier (Stanford Research SR 830 DSP).

XPS measurements were carried out at the soft X –ray undulator beamline X1B at the National Synchrotron Light Source (NSLS), Brookhaven National Laboratory. Thin films of Tc/ C_{60} were grown in situ in an ultra high vacuum (UHV) organic molecular beam deposition (OMBD) custom chamber, attached to a multi-technique soft X – ray spectroscopy system. Clean ITO surfaces were obtained via Ar^+ ion sputtering and annealing in UHV, and the film deposition rate was monitored using a quartz crystal microbalance (QCM). The secondary electron cut – off and valence

band spectra were recorded using an incident photon energy of 260 eV and the sample work function was measured with an applied bias voltage of – 9 V. Spectra obtained are referenced to the Fermi level (E_f) of atomically clean gold foil in contact with the sample.

5.6. References

1. O. K. Lee and T. T. Gan. *Chemical Physics Letters*, **1977,** *51*, 120.
2. (a) E. A. Venedictov, and E. Tulikova *J.Tetrahedron Lett.* **2003**, *44*, 3215.(b) M. T. Cicerone, and M. D. Ediger *J. Phys. Chem.* **1993**, *97*, 10489.
3. S. A. Odom, S. R. Parkin and J. E. Anthony, *Org. Lett.* **2003**, *5(23)*, 4245.
4. F. Schreiber *Phys. Stat. Sol. (a)* **2004**, *6*, 1037.
5. A. Langner, A. Hauschild, S. Fahrenhoz, M. Sokolowski, *Surf. Sci.* **2005**, *574*, 153.
6. C. W. Chu, Y. Shao, V. Shrotriya, Y. Yang, *Appl. Phys. Lett.* **2005**, *86*, 243506.
7. I. Hancox, K. V. Chauhan, P. Sullivan, R. A. Hatton, A. Moshar, C. P. A. Mulcahy, T. S. Jones, *Energ. Environ. Sci.* **2010**, *3*, 107.
8. D. J. Gundlach, J. A. Nichols, L. Zhou, T. N. Jackson, *Appl. Phys. Lett.* **2002**, *80*, 2925.
9. R. J. Tseng R. Chan, V. C. Tung and Y. Yang *Adv. Mater*. **2008** *20*, 435.
10. Z. R. Hong, R. Lessmann, B. Maennig, Q. Huang, K. Harada, M. Riede and K. Leo *J. Appl. Phys.* **2009**, *106*, 064511.
11. J. R. Lakowicz, *Principles of Fluorescence Spectroscopy, 3rd Edtn.* **2006**
12. B. P. Rand, J. Xue, S. Uchida and S. R. Forrest *J. Appl. Phys.* **2005**, *98*, 124902.
13. J. E. Anthony, *Ang. Chem. Int. Edn.* **2008**, *47*, 452.
14. P. Sullivan, T. S. Jones, *Org. Electron.* **2008**, *9*, 656.
15. K. Cnops, B. P. Rand, D. Cheyns and P. Heremens, *Appl. Phys. Lett.* **2012**, *101*, 143301.
16. R. Schlaf, B. A. Parkinson, P. A. Lee, K. W. Nebesny, N. R. Armstrong, *J. Phys. Chem. B.* **1999**, *103*, 2984.
17. Y. Shao, S. Sista, C. W. Chu, D. Sievers, Y. Yang, *Appl. Phys. Lett.* **2007**, *90*.
18. S. W. Cho, L. F. J. Piper, A. DeMasi, A. R. H. Preston, K. E. Smith, K. V. Chauhan, P. Sullivan, R. A. Hatton, T. S. Jones, *J. Phys. Chem. C.* **2010**, *114*, 1928.
19. I. Hancox, P. Sullivan, K. V. Chauhan, N. Beaumont, L. A. Rochford, R. A. Hatton, T. S. Jones, *Org. Electron.* **2010**, *11*, 2019.
20. H. Gommans, T. Aernouts, B. Verreet, P. Heremans, A. Medina, C. G. Claessens, T. Torres, *Adv. Funct. Mater.* **2009**, *19*, 3435.
21. K. V. Chauhan, R. Hatton, P. Sullivan T. S. Jones, S.W Cho, L. Piper, A. deMasi, and K. E. Smith *J. Mater. Chem.*, **2010**, *6***,** 1173.
22. W. A. Luhman, R. J. Holmes, *Adv. Funct. Mater*, **2011**, *21*, 764.
23. H. Gommans, S. Schols, A. Kadashchuk, P. Heremans, S. C. J. Meskers, *J. Phys. Chem. C*, **2009**, *113*, 2974.

24. J. J. M. Halls, K. Pichler, R. H. Friend, S. C. Moratti, A. B. Holmes, *Synth. Met.* **1996**, *77*, 277.
25. L. A. A. Pettersson, L. S. Roman, O. Inganas, *J. Appl. Phys.* **1999**, *86*, 487.
26. T. Stubinger, W. Brutting, *J. Appl. Phys.* **2001**, *90*, 3632.
27. J. Y. Kim, S. H. Kim, H. H. Lee, K. Lee, W. L. Ma, X. Gong, A. J. Heeger, *Adv. Mater.* **2006**, *18*, 572.
28. P. Sullivan, A. Duraud, l. Hancox, N. Beaumont, G. Mirri, J. H. R. Tucker, R. A. Hatton, M. Shipman, T. S. Jones, *Adv. Energ. Mater.* **2011**, *1*, 352.
29. K. Schulze, C. Uhrich, R. Schuppel, K. Leo, M. Pfeiffer, E. Brier, E. Reinold, P. Bauerle, *Adv. Mater.* **2006**, *18*, 2872.
30. T. Asakawa, M. Sasaki, T. Shiraishi and H. Koinuma, Jpn. *J. Appl. Phys*, **1995**, *34*, 1958.

Chapter 6.

Phthalocyanines as Electron Acceptors in Pentacene cells

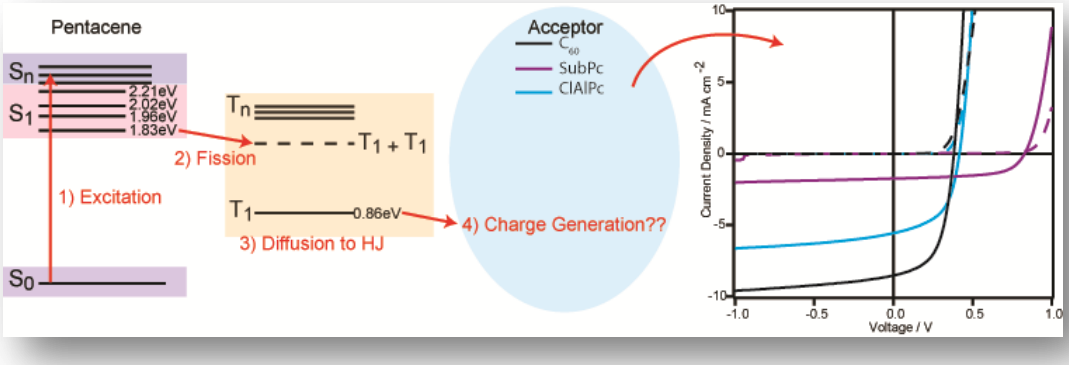

In this chapter the use of (sub)phthalocyanines as acceptors in Pentacene based heterojunctions is discussed. As previously discussed, there are many problems associated with C_{60}, one being the limitations on the interface gap of the system which limits the V_{oc} in particular cells. With Pentacene, although optimum devices have a large J_{sc}, the V_{oc} is $\leq$ 0.4V. Through the use of SubPc and ClAlPc as acceptor materials, the *J-V* characteristics are discussed and the stability of devices also investigated.

6.1. Results: Pentacene

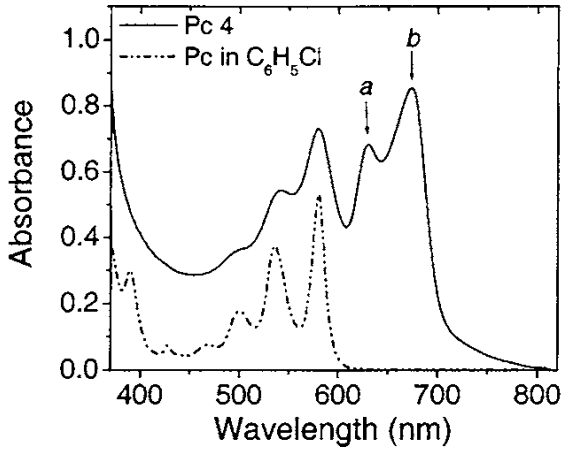

Figure 6.1 UV-Vis absorption spectra of a pentacene solution and vacuum deposited thin film.[2]

Pentacene has been studied extensively as a thin film, and incorporated into OTFTs and OPV devices with promising results.[1-4] It is highly insoluble but a low concentration absorption spectra in dichlorobenzene is shown in **Figure 6.1** and is compared to a thin film.[2] The solid state red shift is approximately 90 nm and the Davydov splitting of the 0 → 0 peak is clearly apparent indicating the high crystallinity of the film (~ 48nm split is seen in single crystals).[5] Thin films of pentacene typically reveal large crystallites, as shown in **Figure 6.2** for a 60 nm vacuum deposited film grown at 1 Å s^{-1}. As seen previously, this deposition rate of growth for Pentacene causes the formation of islands with the potential to form large dendritic grains.[3] This is due to the molecules arriving at the surface with increased opportunity for the strong Pentacene – Pentacene interactions to overcome any surface interaction. This results in increased crystallinity and favourable island growth and at faster rates (1.5 Å s^{-1}) much smaller crystallites have been observed.[4]

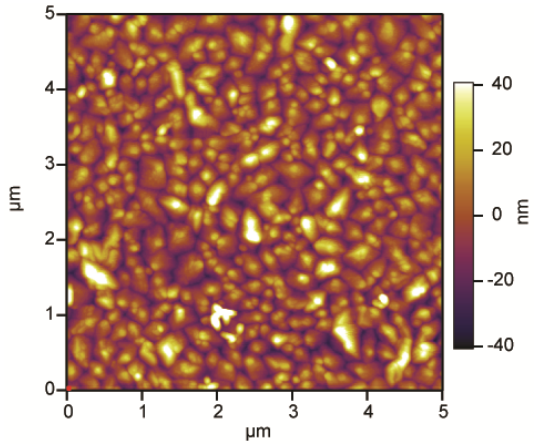

Figure 6.2 5µm AFM topographic image of a vacuum deposited thin film of Pentacene.

6.2. Pentacene / Acceptor Bilayers

6.2.1. Photophysical properties and energetics

The normalised UV-Vis absorption spectra of the layers used within this chapter are shown in **Figure 6.3.** The spectra were taken for 20 nm films on quartz. In the Pent / SubPc system there is increased spectral overlap between the donor / acceptor (D/A) between 500 and 650 nm compared to the Pentacene / C_{60} layers which could result in a decrease in short circuit current as much of the solar spectrum isn't harvested.

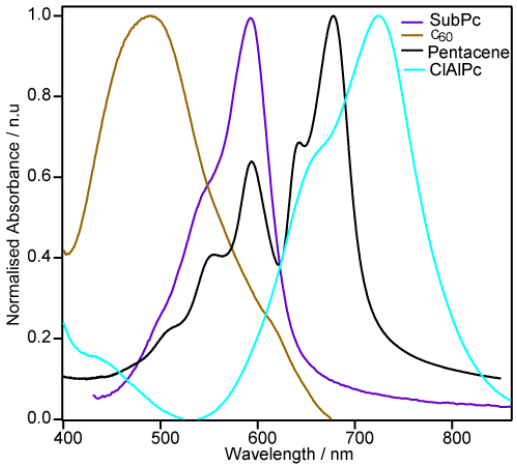

Figure 6.3 UV-Vis absorption spectra of Pentacene, C_{60}, SubPc and ClAlPc thin films.

The peak absorbance of ClAlPc is further red shifted in comparison to Pentacene and therefore a smaller overlap is observed athough the ClAlPc shoulder does overlap. Photoluminescence of pentacene monolayers has been studied at temperatures < 8K, and a strong peak is observed at 1.88eV with emerging peaks at 1.66 and 1.44 eV as thicker films are created.[6] There have been a few other studies at various low temperatures, but at room temperature there is a rapid relaxation of the initial excited state to a non-emissive species and therefore the films of Pentacene exhibit an extremely low photoluminescence.[7] The quenching abilities of the C_{60}, SubPc and ClAlPc could not therefore be determined in this case.

From the energy levels in the Pent / C_{60} systems, by replacing C_{60} with SubPc or ClAlPc there is an increase in the interface gap from 0.7 eV to 1.3 eV and 1.2 eV respectively (summarised in **Figure 6.4**).[8-11]

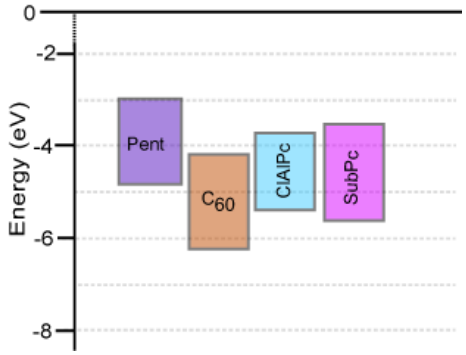

Figure 6.4 Summary of the molecular frontier orbitals of the materials used here. Literature values were used for Pent,[8] C_{60},[9] ClAlPc[10] and SubPc[11]

Due to the large increase in I_g for the Pent / SubPc or ClAlPc system we would assume an increase in V_{oc} for these cells as seen previously in the Tet / (Cl_6) SubPc system.[12]

6.2.2. Morphology

To confirm there were no morphological factors affecting device performance from the replacement of C_{60}, the morphologies of a 5 nm deposit of acceptor atop of a 60 nm pristine pentacene layer (**Figure 6.5a**) are investigated by atomic force microscopy (AFM). **Figure 6.5a** clearly shows the large dendritic Pent crystallites typically present at thicknesses larger than 35 nm.[4]

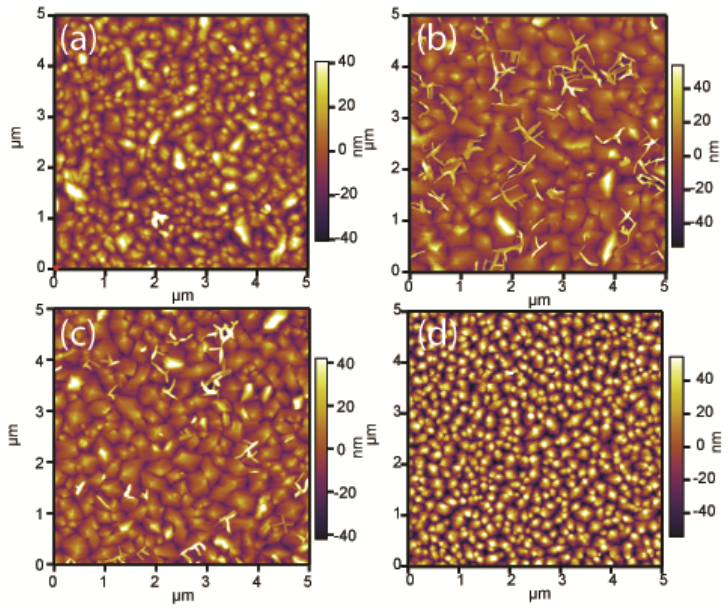

Figure 6. 5 AFM morphology of (a) Pristine pent (b) Pent / C_{60} (c) Pent / SubPc and (d) Pent / ClAlPc films.

With a 5 nm layer of acceptor (C_{60}, SubPc, or ClAlPc) deposited atop of the pentacene layer there is no apparent visual change in morphology or roughness. Due to the large influence of the underlying acene morphology the acceptors overlay the surface with small crystallites rather than fill the gaps, as also seen by Sullivan *et al.*[4] and others.[13] Therefore any performance deviations from the reference is not attributed to the layer morphology.

6.3. Devices

6.3.1. Mobility

As mentioned in **Chapter 5** it is important to check the ambipolar quality of the semiconductors for use as acceptor materials, and therefore mobility measurements were also made on ClAlPc. The device structure for hole mobility was:

ITO / MoO_x (5nm) / ClAlPc (100nm) / MoO_x (5nm) / Al

The corresponding electron mobility structure was:

ITO / Ca (8nm) / ClAlPc (100nm) / Ca (8nm) / Al

The device log *J-V* data is shown in **Figure 6.6** complete with fit and is summarised in **Table 6.1.**

T**able 6.1**. Zero-field mobility, μ_o, for holes and electrons in various samples.

Semiconductor	Hole mobility / V cm^2 s^{-1}	Electron mobility / V cm^2 s^{-1}
Pent	1.2 x 10^{-3}	-
SubPc	1.0 x 10^{-6}	4.6 x 10^{-4}
ClAlPc	6.1 x 10^{-5}	2.3 x 10^{-4}
C_{60}*	-	1 x 10^{-2}

The hole mobility of 1.2 μm thick films of ClAlPc were previously modelled according to the disorder formalism by Bassler and co workers.[14] Using ToF, a further study by Ioannidis and Dodelet discovered an improvement in hole mobility in ClAlPc from low 10^{-4} to 1 x 10^{-3} cm^2 V^{-1} s^{-1} when deposited onto a heated substrate and at a rate of 200 Å min^{-1}.[15] This was due to improved crystallinity when

grown onto a hot substrate (95°C) and similar behaviour was seen with the electron transients.[15]

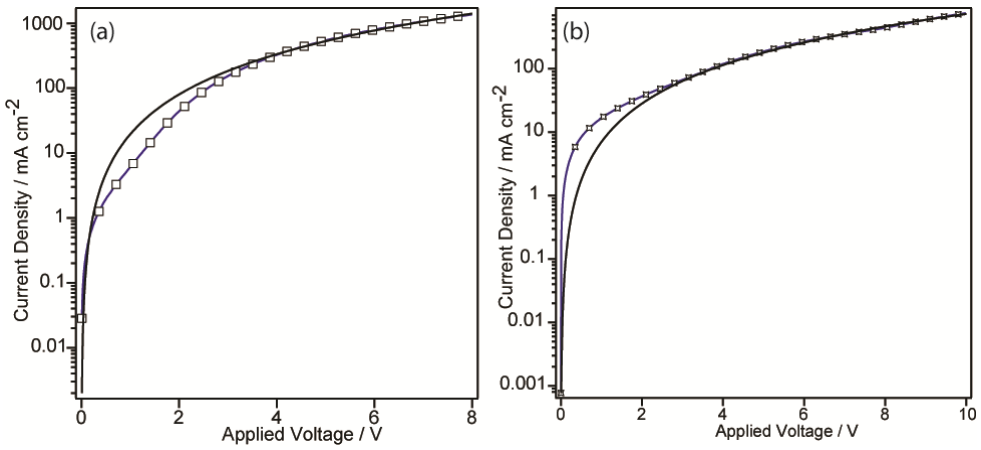

Figure 6.6 log *J-V* characteristic for ClAlPc (a) hole mobility and (b) electron mobility

From SCLC the ClAlPc has a μ_h of 6.1 x 10^{-5} cm^2 V^{-1} s^{-1} and a μ_e of 2.3 x 10^{-4} cm^2 V^{-1} s^{-1}. Although smaller than previous reports, possibly due to the use of a heated substrate, ClAlPc appears to have reasonable μ_h and μ_e mobilities, comparable to SubPc. With the μ_e actually almost a magnitude larger it implies promising acceptor behaviour.

6.3.2. J-V Device characterization

In order to probe the effect of replacing C_{60} with SubPc and ClAlPc in device structures, planar HJ solar cells comprising of ITO / MoO_x (5 nm) / Pent (60 nm) / Acceptor (t_A nm) / BCP (8 nm) / Al were fabricated. The insertion of the 5 nm MoO_x interlayer allows for improved stability of the devices under testing conditions and has no effect on cell performance as shown previously.[16] *J-V* characteristics in the dark and under 1 sun illumination (AM 1.5G) for these cells are shown in **Figure 6.7** with key device parameters listed in **Table 6.2.** With C_{60}, the optimal device has a J_{sc}

of 7.68 mA cm^{-2}, a V_{oc} of 0.43 V, and a FF and n_p of 0.55 and 1.8 % respectively, similar to previous literature.[3,4] Through the replacement of C_{60} with a 35 nm layer of SubPc, the V_{oc} increases significantly to 0.9 V, due to the increase in the I_g, but the resulting n_p drops to 0.9 % due to a large decrease in J_{sc} to 2.00 mA cm^{-2}.

Table 6.2. Device parameters obtained from OPV devices. Devices A-C have the structure: ITO / MoO_x (5 nm) / Pentacene (60 nm) / Acceptor (x nm) / BCP (8 nm) / Al.

Acceptor / t_A nm	J_{sc} / mA cm^{-2}	V_{oc} / V	FF	η_p / %
A: C_{60} (40 nm)	7.68	0.43	0.55	1.8
B: SubPc (35 nm)	2.00	0.90	0.50	0.9
C: ClAlPc (35 nm)	5.56	0.42	0.53	1.26

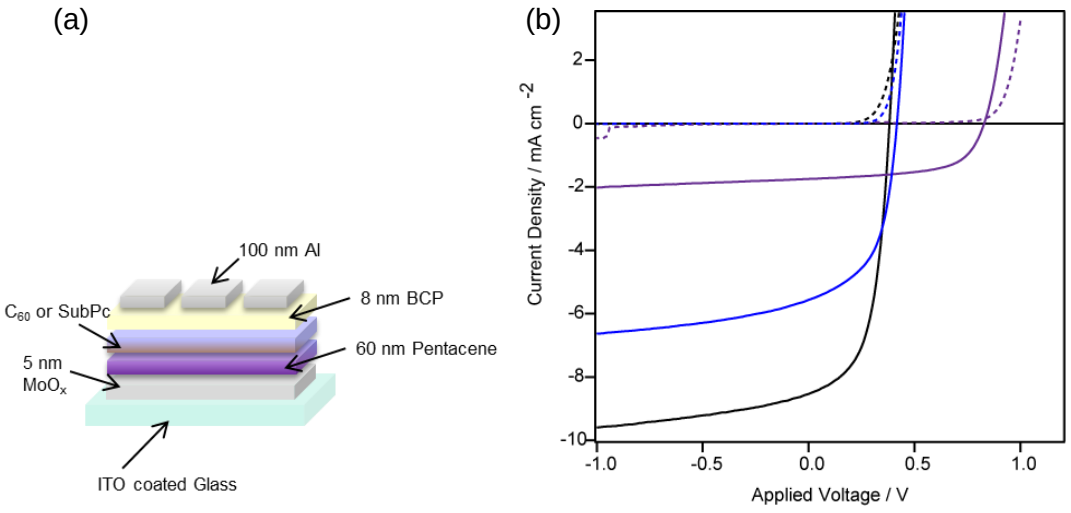

Figure 6.7 (a) Device structure and (b) *J-V* characteristics of optimised Pent / C_{60} (black), Pent / SubPc (purple) and Pent / ClAlPc (blue) devices.

There is only a very small corresponding drop in FF. This is similar to the previous studies with Tc, where although the mobility of the acceptors are two magnitudes smaller than the conventional C_{60}, there is no apparent detrimental

effect. This reinforces the concept that the mobility is perhaps not as important as initially thought. In the previous case of Tc / SubPc there was an increase in J_{sc} due to the reduced spectral overlap in comparison to Tc / C_{60}. Pent / SubPc overlap greatly around the 595 nm peak of SubPc and therefore a small decrease was expected. However, there is a loss of ~ 6 mA cm^{-2} and it seems apparent that there must be another cause for the dramatic loss of photocurrent. When replacing C_{60} with 35 nm of ClAlPc the J_{sc} decreases to 5.6 mA cm^{-2}, the FF decreases marginally and the PCE decreases to 1.26 %. Interestingly, the V_{oc} remains almost entirely unchanged at 0.42 V.

6.3.3. Intensity measurements

Subtle changes in recombination can affect the V_{oc}, and intensity dependant *J-V* measurements can give a clue about the type of dominant recombination mechanism. Intensity measurements were undertaken on the Pentacene cells (shown in **Figure 6.8**). As the light intensity increases from 22 to 200 mW cm^{-2} there is a linear increase in J_{sc} and a small increase in V_{oc} for all Pentacene cells. Through plotting a log – log plot of J_{sc} vs P_{inc}, the power – law relationship between them is established as $\gamma = 1$, which as previously discussed, implies they do indeed show minimal bimolecular recombination as expected in a bilayer structure.

As there is no real deviation from unity, it can be assumed that by changing the acceptor there is no infiltration between the active layers at the interface with a discrete heterojunction formed.

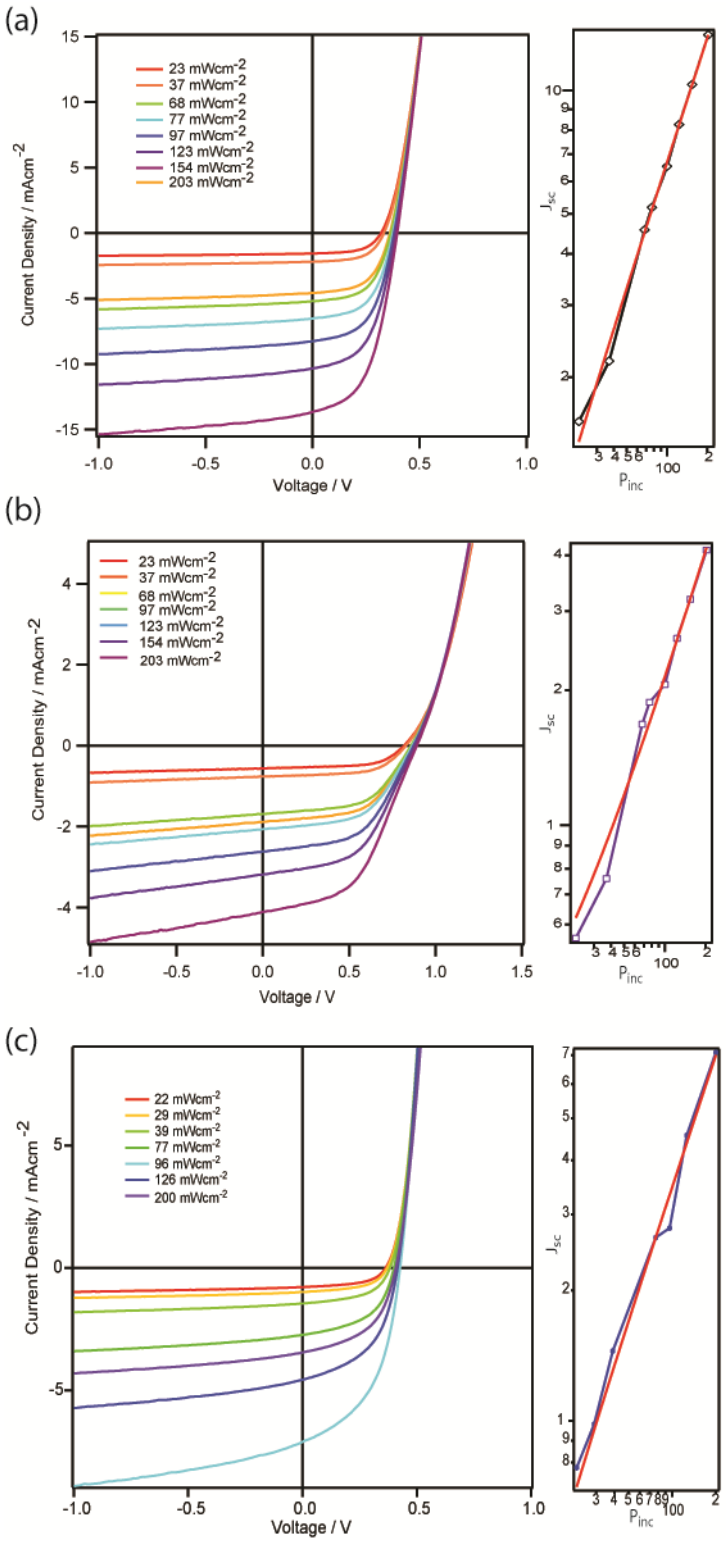

Figure 6.8 *J-V* curves for cells device under various illumination intensitys and **RHS:** log – log plot of J_{sc} as a function of P_{inc} for (a) Pent / C_{60} (b) Pent / SubPc and (c) Pent / ClAlPc

6.3.4. EQE and further discussion

To better understand the decrease in J_{sc} the external quantum efficiencies (EQE) of the Pent OPV cells were recorded and are shown in **Figure 6.9.**

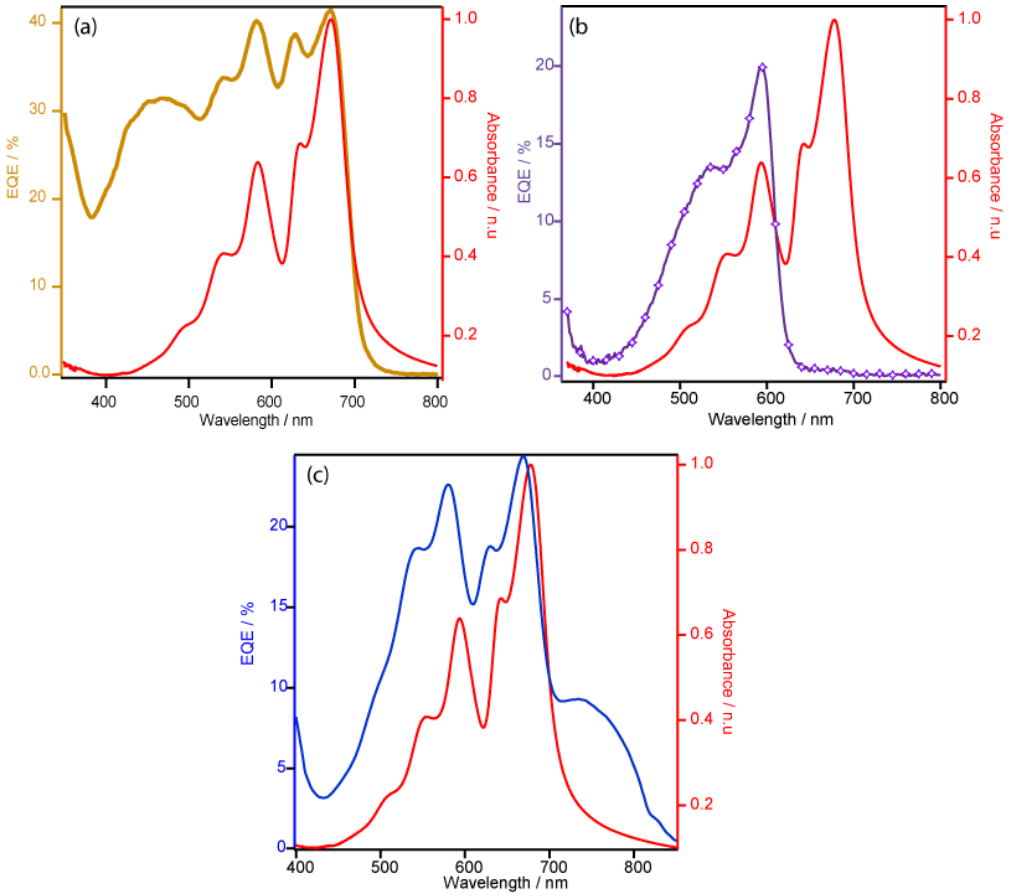

Figure 6.9 EQE (a) Pent / C_{60} (b) Pent / SubPc and (c) Pent / ClAlPc. The red line is a Pent thin film absorption for comparison.

We would expect to see the pentacene contribution between 500 - 700 nm (as shown in the absorption spectra) and a proportion of the photocurrent being attributed to the acceptor. In the Pent / C_{60} case, both the active layers contribute as expected with the distinctive pentacene peaks apparent with a broad contribution between 400 – 500 nm, a peak EQE of 40 % and an associated C_{60} contribution. The only dominant peak present in the Pent / SubPc cell is at 595 nm. This is the main absorption peak

of SubPc and indicates that this layer is the only major contributor to the photocurrent as the pentacene peaks are distinctly lacking. Although the current was expected to be reduced due to the overlap in absorption spectra, we would expect some contribution from the Pent layer at the longer wavelengths. In the case of Pent / ClAlPc, the pentacene contribution is again clearly apparent with a small contribution from the ClAlPc around 750 nm. **Figure 6.10** shows the EQE of the cells with regards to acceptor thickness.

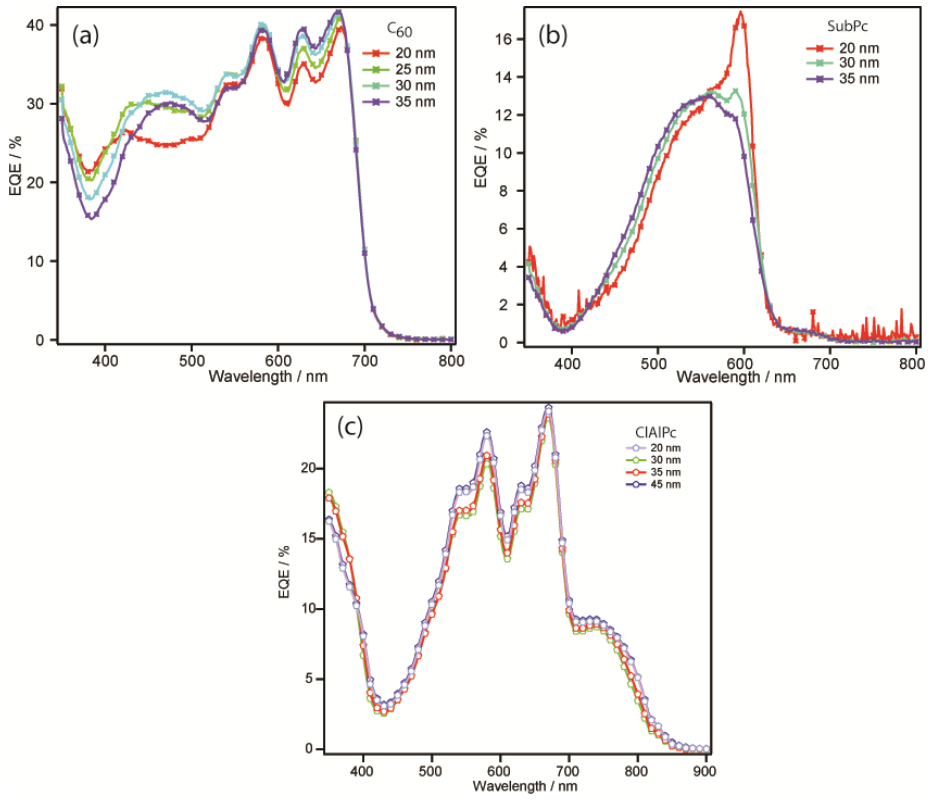

Figure 6.10 EQE of (a) Pent / C_{60} (b) Pent / SubPc and (c) Pent / ClAlPc with varied acceptor thickness (as shown in the key)

The Pent / C_{60} cell behaves as expected with improvements in both the C_{60} region and the Pentacene region (due to a spacing effect). Through increasing the SubPc thickness from 20 nm to 35 nm, the sharp peak normally present in SubPc devices

begins to decrease and a broader EQE is observed but still lacking a contribution from the Pentacene layer. In the case of ClAlPc the change in J_{sc} occurs predominately from the increase in Pent contribution, with little or no change in the ClAlPc contribution. This implies that the ClAlPc is acting as a spacer for the pentacene layer, as seen previously, and its maximum contributing thickness has been reached (which is determined by the L_D of the ClAlPc at ~25 nm[17]).

From the predicted energy levels, the Δ_{LUMO} in both the SubPc and ClAlPc cells is not large enough to efficiently separate the excitons from the pentacene layer due to its large binding energy, E_B, as it has been quoted in some cases to be around 0.5 eV.[18] Though this may explain the Pent / SubPc case, it does not explain the photocurrent contribution from the pentacene in the Pent / ClAlPc case. Looking further into the contributions, the energy levels of the materials must be again addressed and a summary of Pentacene and C_{60} is shown in **Figure 6.11.**

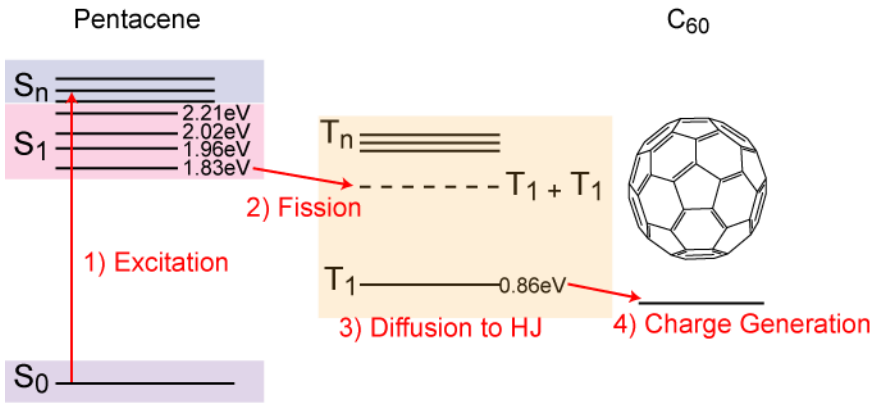

Figure 6.11 Schematic of Singlet – Triplet conversion in Pentacene layers [adapted from ref. 6]

Pentacene is well known for its rapid singlet fission to form two triplet excitons, converting all singlets to triplets in < 80 fs in highly crystalline films.[7] It occurs in pentacene films due to the triplet level existing at less than half the singlet energy

and triplets have been shown to participate in Pent / C_{60} cells as measured using TAS.[7]

In order for triplet excitons to dissociate at the Pent / Acceptor interface the charge separation (CS) state must be lower in energy. E_{CS} can be roughly estimated from the following equation,

$$E_{CS} = IP_{Pent} + EA_{Acceptor} + E\left(\frac{P^+}{A^-}\right) \qquad \textbf{Equation 6.1}$$

where IP_{pent} and $EA_{acceptor}$ are the ionisation potential of pentacene and the electron affinity of the acceptor respectively and $E\left(\frac{P^+}{A^-}\right)$ is the electrostatic stabilization energy between the pentacene cation and the acceptor anion, as discussed by Bredas *et al.*[19] Using IP_{pent}= 4.9 eV,[7] EA_{C60} = 4.2 eV,[8] EA_{SubPc} = 3.6 eV[10] and EA_{ClAlPc} = 3.7 eV[9], the E_{CT}s are 0.7 eV, 1.3 eV and 1.2 eV respectively and are shown schematically in **Figure 6.12**.

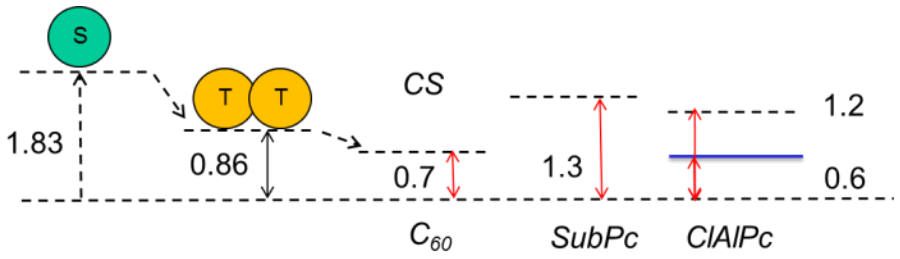

Figure 6.12 Schematic of the energetics from GS to excited state in the device systems.

Initially, the E_{CS} values imply we would expect to see increases in V_{oc} but perhaps little to no current contribution from the pentacene layer due to the triplet state energy of pentacene being much smaller. In the case of the SubPc system there is no dissociation of the Pent triplets due to the E_{CS} being much greater at 1.3 eV (0.44 larger than the Pent triplet state) and hence there is minimal contribution

from the Pent in the EQE and a much lower J_{sc} in the device than expected. As the V_{oc} is determined by the E_{CS} it allows for a larger V_{oc} to be achieved in comparison to C_{60}, hence the improvement from 0.4 V to 0.9 V.

In the case of the ClAlPc system, the E_{CS}ClAlPc calculated is 1.2 eV indicating that it should act in a similar way to the SubPc layer. We propose that there is a lower lying level in ClAlPc (highlighted in blue) by which the excitons can dissociate to allow for photocurrent contribution but still limit the potential voltage (with a level similar to that of C_{60}) resulting in no change in V_{oc}. Schlenker *et al.* previously showed that the cascade cell with structure ITO / Pent / ClAlPc / C_{60} / BCP / Al works due to a transfer of the triplet excitons from pentacene to the ClAlPc triplet state.[20] ClAlPc has a singlet – triplet splitting of ~ 0.6 eV (0.6 eV lower than the E_{CS}ClAlPc)[21] and therefore the triplet state is low enough to allow for a transfer of the triplet exciton to the ClAlPc and separation at the ClAlPc / C_{60} interface. As C_{60} is not present in our devices we assume that due to this lower level the excitons are separated from the Pent layer and converted to free charges (as indicated from the dual contribution in the EQE). As a result of this low lying level, it is clear that Pent / C_{60} and Pent / ClAlPc cells will give similar V_{oc}s, as both systems now have an E_{CT} of ~ 0.6 – 0.7 eV.

6.4. Degradation studies

To investigate the stability of these cells in air the degradation of PV parameters under constant illumination was monitored over 1100 mins (~ 18.3 hours) (shown in **Figure 6.13**) with the *J-V* changes shown in **Figure 6.14.** The cells shown below have the structure: ITO / Pent (60 nm) / Acceptor (25 nm)/ BCP / Al and were tested in air. As seen clearly in **Figure 6.12** the Pent / SubPc (ClAlPc) device is inherently

more stable across all parameters compared to the Pent / C_{60} device. As seen previously, the Pent / C_{60} cell degrades to zero efficiency quite quickly (< 1000 mins).[4] This degradation begins with a fast decline in FF to ~ 40% in 200 minutes and the J_{sc} to less than 40 % of the initial current in less than 400 mins. The V_{oc} also degrades to ~ 60 % of the initial value in the time frame which contributes to the further decay of the efficiency between 300 and 1100 minutes.

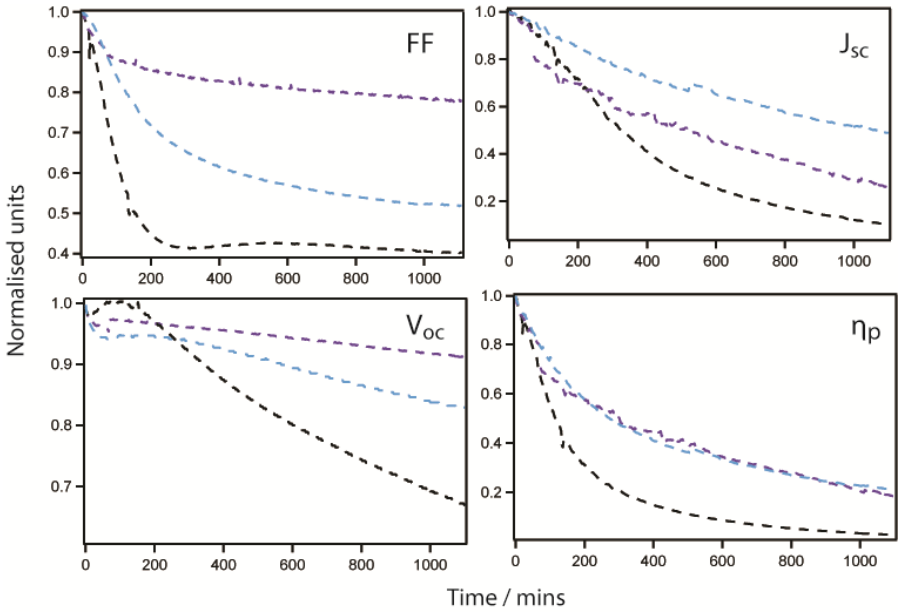

Figure 6.13 Device parameters of Pent / C_{60} (black); Pent / SubPc (purple) and Pent / ClAlPc (blue) cells under constant illumination over 1100 mins.

When replaced with SubPc, the V_{oc} is more stable only losing 10% but 80 % of the J_{sc} is lost over the 1100 mins, with the FF retaining 80 % over the 1100mins. The Pent / ClAlPc cell is again more stable than the Pent / C_{60} cell losing only ~ 30 % of the V_{oc} and 50 % of J_{sc} over the same time frame but loses 50 % of the FF over the time. Although the current in the Pent / ClAlPc is more stable than the Pent / SubPc, due to the decrease in FF and V_{oc}, both systems reach the same change in PCE after degradation.

The Pent / C_{60} *J-V* curves (shown in **Figure 6.14**) explain clearly the fast decrease in FF caused by an s-shaped kink in the *J-V* curve, this also largely affects the J_{sc} and V_{oc} causing the fast degradation. Sullivan *et al.* conveyed this previously, and believed there to be both an O_2 induced and a photo-induced degradation occurring in the cell. The O_2 degradation could be removed by placing the cell under vacuum but the photo-induced degradation was only resolved with the introduction of a UV filter.[4]

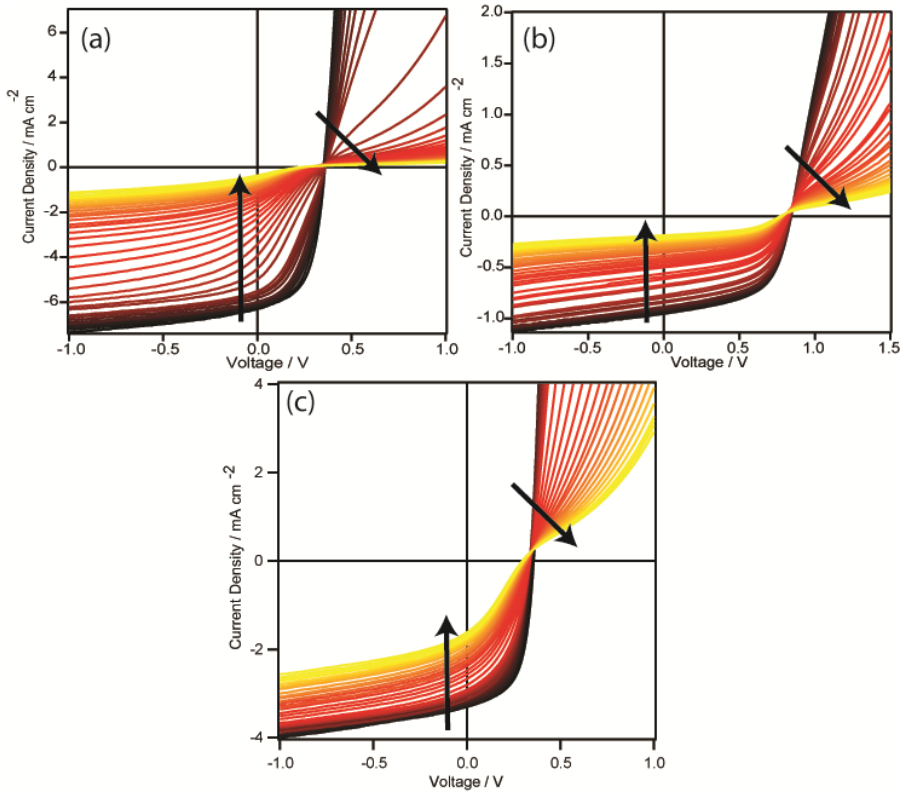

Figure 6.14 *J-V* curves of the (a) Pent / C_{60} (b) Pent / SubPc and (c) Pent / ClAlPc over the degradation time period. Plotted are 0 – 100 mins in 10 minute intervals and then *JV* curves at 50 min intervals. The direction of the arrows indicate from 0 – 1100 mins

Initially, this was thought to be due to a reorganisation of the pentacene molecules at the ITO / Pent interface, introducing a barrier to charge extraction.

More recently, there has been a study on the correlation between the work function of ITO and the resulting device performance affected by UV radiation. They found that through exposure to UV radiation for a period of time the work function of the ITO could change from 4.7 eV to 4.2 eV. In a standard architecture bilayer CuPc / C_{60} cell, this caused a barrier to extraction at the ITO / CuPc interface, allowing for a large charge build up and an s – shape kink to form – similar to what is seen in Pent / C_{60}.[22] They could reverse this behaviour through introducing the cell to air. To prevent this affect, they investigated the use of a surface modifier which was less sensitive to UV radiation. Over the same exposure time, the cell behaviour was unaffected and no kink was seen.[22]

A similar kink is also seen in the ITO / Pent / SubPc and ITO / Pent / ClAlPc cell close to V_{oc} which indicates that the ITO / Pent interface is causing a large part of the overall degradation. One of the first mechanisms of degradation in the Pent cell is reduced on the replacement of C_{60}. The kink near J_{sc} is reduced which improves the stability of the FF over the same period of time. This implies that the Pent / C_{60} interface was a contributor to the degradation and could be due to C_{60}s poor stability in air, as the C_{60} degrades there is a problem with charge transport causing a build up of charges and a kink to form. Although the FF degradation is reduced in the case of Pent / SubPc the Pent / ClAlPc cell is still affected by another degradation mechanism.

Figure 6.15 shows the degradation of cell parameters under constant illumination for 24 hours with the addition of the MoO_x hole transporting layer. These cells have the structure ITO / MoO_x (5nm) / Pent / Acceptor / BCP / Al. All three systems are inherently more stable with the introduction of MoO_x retaining ~ 100 % of the V_{oc} and J_{sc} over the 24 hours. The aforementioned ITO / Pent interface

problem is now heavily reduced, with little effect on V_{oc} over the full 24 hours for all three systems, (<1% loss for C_{60}, (Cl_6)-SubPc systems) with a maximum loss of 9% for Pent / ClAlPc. The J_{sc} is more stable in Pent / ClAlPc and Pent / Cl_6SubPc with Pent / SubPc behaving quite similar to Pent / C_{60}. This indicates that SubPc has a tendency to degrade almost in a similar amount to C_{60} either due to UV light or oxidation which the chlorinated derivative is more stable towards.

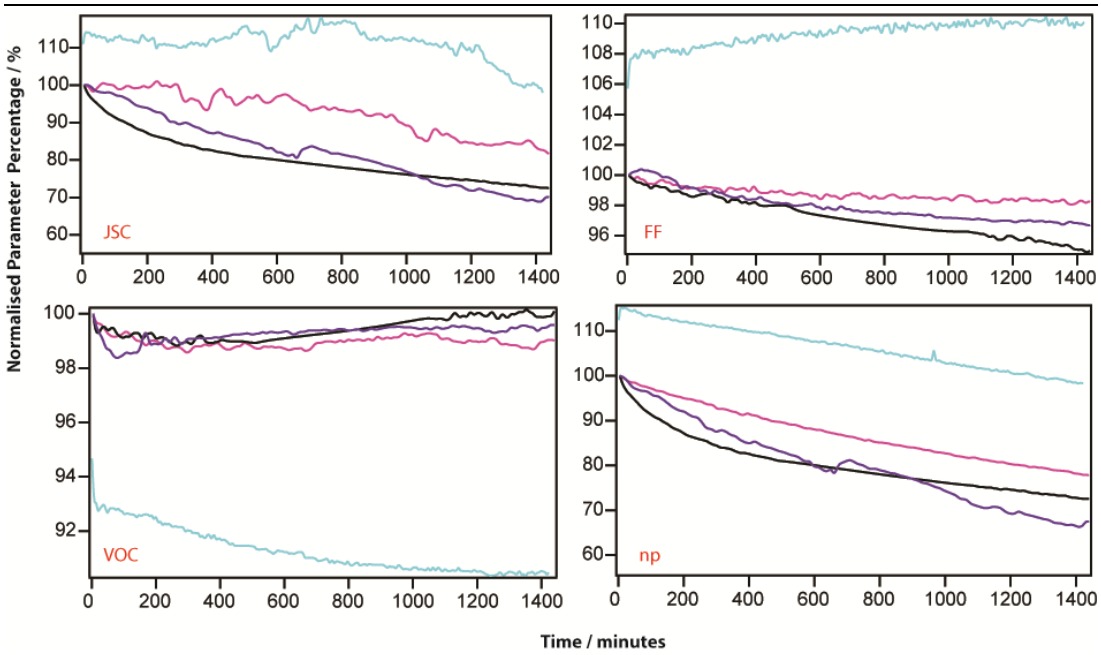

Figure 6.15 Device parameters of Pent / C_{60} (black); Pent / SubPc (purple), Pent / Cl_6SubPc (pink) and Pent / ClAlPc (blue) cells under constant illumination over 1440 minsttr

The kink caused by this interface previously seen in the cells now does not occur over time, shown in **Figure 6.16** which corroborates that the problem was more likely to be due to a change in the ITO work function over a reorganisation of the Pentacene layer.

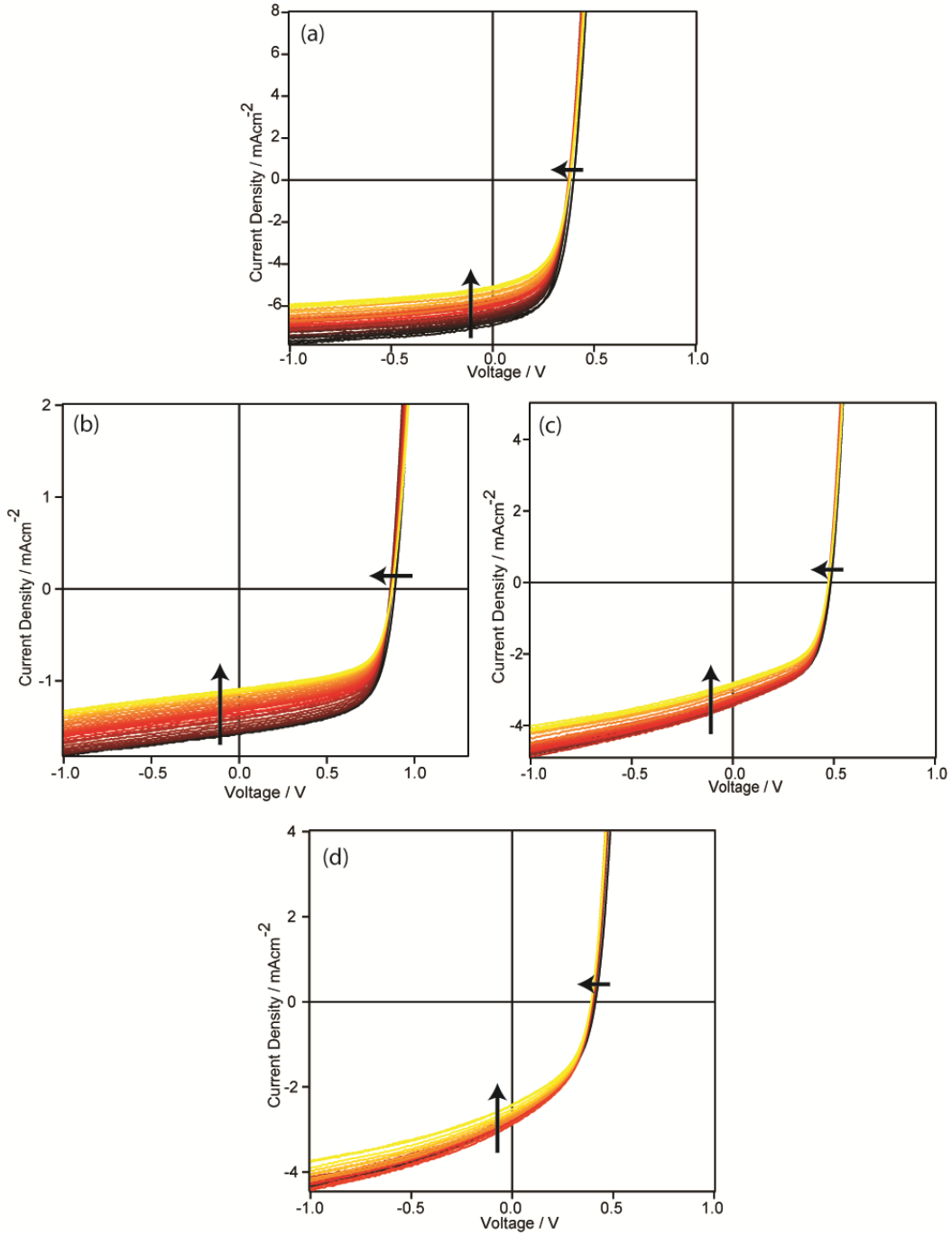

Figure 6.16. *J-V* curves of the (a) Pent / C_{60} (b) Pent / SubPc (c) Pent / Cl_6SubPc and (c) Pent / ClAlPc over the degradation time period on ITO / MoO_x. Plotted are 0 – 100 mins in 10 minute intervals and then *JV* curves at 50 min intervals. Direction of the arrows indicate from 0 – 1440 minutes.

There is also a problem with the Pentacene triplets quenching at the ITO interface which has now been prevented. Unfortunately, however there is still a reduction in current for all three systems with the largest change occurring in the Pent / C_{60} cell for reasons mentioned previously. This is again could be due to O_2 causing degradation of the layers which would reduce conductivity or photobleaching.

This highlights the further need for good encapsulants as although the stability can be improved with ITO surface modifications and the replacement of $C_{60,}$ O_2 infiltration and moisture is still a problem.

6.5. Conclusion

As an extension to the previous work demonstrating the use of SubPcs as acceptors, ClAlPc was also investigated as a suitable replacement for C_{60} in Pentacene based cells. The molecular frontier energy levels of both SubPc and ClAlPc indicate compatibility with Pentacene and there is a systematic increase in interface gap which would hopefully translate to an increase in V_{oc}. The absorption spectra of ClAlPc in particular allows for extended coverage into the infra-red, whereas Pent / SubPc encounters a large overlap in absorption in the 500- 600 nm region, which could be detrimental to the short circuit current in comparison to Pent / $C_{60.}$ ClAlPc again showed promise with a high electron mobility of 2.3×10^{-4} $cm^2 V^{-1} s^{-1}$ comparable to the SubPc electron mobility, indicating its ambipolar qualities.

Bilayers were again investigated to rule out any morphological differences between the acceptor layers accounting for any change in performance, with SubPc behaving similarly to C_{60} and ClAlPc, forming small clusters atop of the Pentacene underlying layer, similar to earlier literature reports and the previous chapter.

Unfortunately, photoluminescence quenching of these bilayers could not be determined due to the lack of emission from Pentacene at room temperature.

Pentacene / C_{60} cells were optimised on MoO_x resulting in an η_p of ~ 1.8 %. Through replacing C_{60} with 25 nm of SubPc the V_{oc} is indeed increased from 0.4 V to 0.9 V. However, there was an extremely detrimental effect of the J_{sc} and it decreased from 9 $mAcm^{-2}$ to 2 mA cm^{-2}. When replacing C_{60} with ClAlPc, the J_{sc} was again reduced by a much smaller amount, whereas the V_{oc} remained unchanged. Although a decrease in current was expected in the Pent / SubPc system, such a large reduction was not and therefore it seemed indicative that there was more than an absorption overlap problem.

To investigate this further, both intensity dependant *J-V* and EQE measurements were undertaken. The intensity measurements revealed no change in recombination mechanisms, with all systems behaving as a bilayer with $\gamma \sim 1$. In the case of Pent / SubPc the EQE revealed that there is only photocurrent contribution from the SubPc layer, with no distinctive peaks present from the Pentacene. On the other hand, with the Pent / ClAlPc system, the majoritive contributor is the pentacene layer, with a small contribution from the ClAlPc. Through investigating various thicknesses of acceptor layer, the current can vary due to spacing of the pentacene layer and normal optimisations of current thickness (dependant on L_D) but the lack of contribution from the Pent layer in the Pent / SubPc cell does not change.

To explain these unusual results, a further look into the excitons created in the pentacene cell was needed. In pentacene, singlets rapidly convert to triplet excitons due to the triplet energy level existing at less than half of the singlet excitation. If the CS states are roughly calculated, C_{60} can dissociate the excitons as

it is below this triplet level. The excitons encounter a barrier at the Pent / SubPc interface of ~ 0.44 eV which they cannot overcome to dissociate. This results in a lack of contribution from the Pent layer but still allows for a large V_{oc} (as the energy from the GS is 1.3 eV compared to the initial 0.7 eV for Pent / C_{60}). Investigating the ClAlPc, initial calculations suggest there is still a barrier at the interface but as we do see a contribution from the Pent layer, and have a low V_{oc}, there must be a lower lying LUMO level where the triplets can dissociate.

Investigation into the stability of the devices revealed sharp kinks in the Pent / C_{60} devices which resulted in a fast decrease in PCE over a 24 hr period. On replacing C_{60}, the reduction in FF, J_{sc} and V_{oc} could be retarded due to the improved stability to oxygen as well as any potential diels alder reactions as a route to degradation. A sharp decrease in V_{oc} occurs quickly due to the sensitivity of ITO to UV illumination, and this can be entirely stopped through the introduction of a MoO_x HTL. Although replacing C_{60} in both cases results in a more stable cell, the need for encapsulation of devices is crucial to retain useable devices over extended periods of time.

In summary, we have demonstrated that the archetypal donor materials SubPc and ClAlPc have ambipolar characteristics due to the reasonable electron mobility, energy levels and previously seen quenching abilities. When SubPc is incorporated into devices in conjunction with Pentacene as the donor material although there is a decrease in J_{sc} and PCE the voltage can be dramatically increased due to the increase in interface gap. However when using ClAlPc, although there was an expected increase in V_{oc} it in fact remains unchanged due to dissociation of the triplet excitons at the triplet level in ClAlPc. With intelligent device engineering ambipolar

phthalocyanines could be used in a variety of configurations to achieve high efficiency OPVs.

6.6. References

1. A. Di Carlo, F. Piacenza, A. Bolognesi, B. Stadlober, and H. Maresch *Appl. Phys. Lett.* **2005**, *86*, 263501.
2. O. Ostroverkhova, S. Shcherbyna, D. G. Cooke, R. F. Egerton and F. A. Hegmann. *J. Appl. Phys.* **2005,** *98,* 033701.
3. B. Kippelen, W. J. Potscavage, and A. Sharma, *Acc. Chem. Res.* **2009**, *42*, 1758.
4. P. Sullivan and T. S. Jones, *Org. Electron.* **2008**, *9*, 656.
5. A. F. Prikhotko, A.F. Skorobogat'ko, and L. I. Cikora, *Optika I Spektroskopiya*, **1969**, *26*, 214.
6. R. He, N. G. Tassi, G. B. Blanchet, and A. Pinczuk, *Appl. Phys. Lett.* **2010**, *96*, 263303.
7. A. Rao, M. W. B. Wilson, J. M. Hodgkiss, S. A – Seifried, H. Bassler and R. H. Friend, J.A.C.S. **2010**, *132*, 12698.
8. S. Yoo, B. Domercq, B. Kippelen, *Appl. Phys. Lett.* **2004**, *85*, 5427.
9. N. Sato, Y. Saito, and H. Shinohara, H. *Chem. Phys.* **1992**, *162*, 433.
10. S. W. Cho, L. F. J. Piper, A. DeMasi, A. R. H. Preston, K. E. Smith, K. V. Chauhan, P. Sullivan, R. A. Hatton, T. S. Jones, *J. Phys. Chem. C.* **2010**, *114*, 1928.
11. V. Chauhan, R. Hatton, P. Sullivan, P, T. Jones, S. W. Cho, L. Piper, A. deMasi, K. Smith, *J. Mater. Chem.* **2010**, *20*, 1173.
12. N. Beaumont, S. W. Cho, P. Sullivan, D. Newby, K. E. Smith and T. S. Jones *Adv. Funct. Mater.* **2011**, *22*, 561.
13. K. Cnops, B. P. Rand, D. Cheyns and P. Heremens, *Appl. Phys. Lett.* **2012**, *101*, 143301.
14. H. Bassler, *Phys. Status. Solidi*. **1993**, *B175*, 16.
15. A. Ioannidis and J. P. Dodelet, *J. Phys. Chem. B.* **1997**, *101*, 5100.
16. I. Hancox, K. V. Chauhan, P. Sullivan, R. A. Hatton, A. Moshar, C. P. A. Mulcahy, T. S. Jones, *Energ. Environ. Sci.* **2010**, *3*, 107.
17. R. F. Bailey-Salzman, B. P. Rand and S. R. Forrest, *Appl. Phys. Lett.* **2007**, *91*, 013508.
18. P. K. Nayak and N. Periasamy, *Org. Elec.*, **2009**, *10*, 101396.
19. Y. Yi, V. Coropceanu, and J – L. Bredas, *J. Am. Chem. Soc*.**2009**,*131*,15777.
20. C. W. Schlenker, V. S,. Barlier, S. W. Chin, M. T. Whited, R. E. McAnally, S. R. Forrest and M. E. Thompson. *Chem. Mater.* **2011**, *23*, 4132.
21. J. R. Darwent, P. Douglas, A. Harriman, G. Porter, M. C. Richoux, *Coord Chem. Rev.* **1982**, *44*, 83.
22. Y. Zhou, J. W. Shim, C. Fuentes-Hernandez, A. Sharma, K. A. Knauer, A. J. Giordano, S. R. Marder and B. Kippelen *Phys. Chem. Chem. Phys.*, **2012**, *14*, 12014.

Chapter 7.

Conclusions and Future Work

7.1. Overview

Although OPVs are steadily increasing in efficiency many more improvements are necessary before commercialisation can be reached. Research into extending device lifetimes, encapsulation, the use of flexible substrates, alternate electrodes to ITO, improving current materials and finding new materials is necessary for future progression and until more of the concerns have been answered, commercialisation will be a hard struggle. To start answering some of these concerns more fundamental studies have to be undertaken to understand the underlying mechanisms of the organic semiconductors and their interfaces.

7.1.1. TIPSEpentacene derivatives

Chapter 4 discussed the use of TIPSEpentacene and chlorinated derivatives for use as novel donor materials in combination with C_{60} as an acceptor material. TIPSEpentacene was first introduced to the PV community as a soluble pentacene derivative for low cost, easily processable devices. Through the use of successive chlorination, the molecular frontier orbitals of the TIPSEpent could be tuned from 5 eV for the parent acene to 5.2 eV for dichlorinated and 5.3 eV for the two tetrachlorinated derivatives. As acenes are known to readily undergo cycloaddition

reactions with fullerenes, preventing this reaction is paramount for improved cell stability. The bulky addition of the TIPSE moieties is not enough to slow this reaction but as the $HOMO_{(diene)}$–$LUMO_{(dienophile)}$ gap controls the rate, through increasing the IP of the acene the stability towards fullerenes is greatly improved in solution.

When incorporated into devices, with increasing chlorination (and hence IP) η_p is increased from 0.14 % for TIPSEpent / C_{60} to 0.4 % for the TIPSEpentCl_4 / C_{60} cells. As the interface gap is increased from 0.8 eV to 1.1 eV the V_{oc} increases from 0.41 V to 0.57 V as expected with increased chlorination. Unfortunately, although the J_{sc} increases to near double for the TIPSEpentCl_4A device in comparison to the TIPSEpent, it is less than a quarter of the best performing Pent / C_{60} cells (~ 9 $mAcm^{-2}$). Further investigation into the photocurrent contribution of the layers through measuring external quantum efficiency revealed a lack of contribution from the TIPSEpent layer – common to the parent acene and all derivatives, with only the C_{60} layer contributing. The TIPSE moieties render the acene unable to contribute to the photocurrent due to poor absorption and possibly a lack of good charge mobility in device configuration.

Although the future of OPVs will not be utilising TIPSEpent based semiconductors as donor layers, the use of chlorination to tune the molecular orbitals was shown as a viable route to improve stability of the material as well as tune the molecular orbitals. This in turn modified the interface gap of the TIPSEderivative / C_{60} heterojunctions to improve the open circuit voltage.

7.1.2. Subphthalocyanines as Acceptors in Tetracene OPVs

The typically underused acene Tetracene was discussed in **Chapter 5** and the optimisation of its use as a donor material in conjunction with C_{60} was shown. The use of (Cl_6)-SubPc as a replacement for C_{60} is also examined within this chapter.

Thin films of tetracene were found to form ~ 500nm size crystals when vacuum deposited with large voids to the substrate. Tetracene typically grows following an island growth mechanism with complete films formed only above 40 nm thickness. The XRD revealed the 001 crystalline peak present in the vacuum deposited films and also broadness associated with amorphous type films. This may indicate the mixture of both crystalline and amorphous phases present in the OMBD grown film.

When investigating its use in OPVs, it exhibits a large absorption range from 400 to 550 nm (with a small tail absorbing to 650 nm) which significantly overlaps with C_{60}. Through replacing this layer with an absorber out of this range, the J_{sc} could potentially be increased due to increased solar harvesting. SubPc and the chlorinated derivative Cl_6-SubPc were chosen due to their absorption around 600 nm and suitable energy levels predicting their compatibility with Tc. Photoluminescence studies also indicated their potential as use as acceptors. The Tc emission at 547 nm was quenched by ~ 40 % (compared to ~ 20 % when using C_{60}) when using (Cl_6)SubPc signifying a charge transfer taking place.

Charge mobility was initially thought to be an important material property and to demonstrate the SubPc's ambipolar quality, both the electron and hole mobility were measured using SCLC theory. The electron mobility values were promising with magnitudes $x10^{-4}$ – $x10^{-5}$ cm^2 V^{-1} s^{-1} and although slower than C_{60},

there appeared to be no detrimental effects on FF or device performance. This implied that mobility is perhaps not as important as it is in inorganic devices and was later reinforced again with Pentacene devices in **Chapter 6**.

The energetics of these systems were investigated using soft x-ray photoelectron spectroscopy and the HOMO onsets and work function changes were used to determine the band structures of the Tc / C_{60} and Tc / SubPc cells. It showed a large increase in interface gap from 1.2 eV to 1.9 eV which would predict an increase in V_{oc}. It also highlighted a potential issue with the $HOMO_D$-$HOMO_A$ offset of only 0.25 eV (where 0.3 eV is thought to be necessary to separate excitons). This would suggest a reduced J_{sc} and a minimal contribution from the SubPc layer.

The optimum Tc / C_{60} device achieved was found to occur at a Tc thickness of 60 nm with a V_{oc}, J_{sc}, FF and η_p of 0.74 V, 3.57 $mAcm^{-2}$, 0.68 and 1.8% respectively. Through replacing the C_{60} with a 35 nm layer of SubPc, the V_{oc} indeed increased dramatically to 1.24 V. The J_{sc} was increased by ~0.5 $mAcm^{-2}$ and the FF remained reasonable at 0.58 resulting in an increase in η_p to 2.9 %. This trend was also reinforced through using the Cl_6SubPc as it has energy levels between the C_{60} and SubPc, the trend in V_{oc} would be C_{60} < Cl_6SubPc < SubPc and this was indeed seen with the devices. Intensity measurements also indicated promising results as the new acceptors did not introduce increased recombination via defects and/or impurities.

Due to the concerns over the SubPc contribution from the soft x-ray spectroscopy, EQE measurements were undertaken to determine the contributions from the individual layers. SubPc was shown to generously contribute in the EQE of

the Tc / SubPc devices and therefore the 0.25 eV offset is sufficient to separate the SubPc exciton (Cl_6SubPc was also shown to contribute to the photocurrent).

The stability of organic photovoltaics is extremely important and as the degradation of C_{60} has been well established, the cells were investigated under constant illumination. On replacing the C_{60} with SubPc there is an improvement in the stability in terms of both J_{sc} and FF. The reference Tc / C_{60} device reached 0% after 800 mins whereas the Tc / SubPc cell retains 25 % of the initial efficiency at this time. Both cells do degrade (primarily due to the sharp reduction in J_{sc}) due to the presence of oxygen and moisture and therefore good barrier technology needs to be developed.

7.1.3. Typical Donor Materials as Acceptors in Pentacene OPVs

As an extension to **Chapter 5**, the use of (sub)phthalocyanines as acceptor materials in Pentacene devices was discussed. Although Pentacene devices are typically well performing with short circuit currents above 9 mA cm^{-2} one of the limiting factors is the low V_{oc} when using C_{60} as the acceptor material. To find a replacement for C_{60}, (sub)phthalocyanines were investigated in terms of suitable energy levels and absorption overlap with both SubPc and ClAlPc considered.

SubPc was found in the previous chapter to have reasonable ambipolar qualities in terms of mobility and ClAlPc was also found to exhibit a relatively good electron mobility (10^{-4} $cm^2V^{-1}s^{-1}$) implying its suitability for use as an acceptor in Pent cells and with no detriment to device FF, reinforced the issues raised in **Chapter 5**. Unfortunately, due to extremely low photoluminescence of Pentacene the quenching abilities of the acceptors in this case could not be determined.

When investigating the *J-V* characteristics of the Pentacene / acceptor cells a few interesting characteristics were noticed. In the case of Pent / SubPc a larger V_{oc} was achieved but an extremely detrimental decrease in J_{sc} was also obtained, whereas in the Pent / ClAlPc case there was a small decrease in J_{sc} but a similar V_{oc} to the reference cell (where an increase would be expected). On further investigation into the photocurrent contribution using EQE both active layers were found to contribute in the Pent / ClAlPc (C_{60}) cells whereas only the SubPc "acceptor" layers were found to contribute in those devices.

Although this explains the low J_{sc} in the SubPc acceptor based devices, it does not explain the strange observation in the V_{oc} in the Pent / ClAlPc. It implies there is a barrier to exciton separation in Pent / SubPc cells which doesn't occur in Pent / ClAlPc. By calculating the charge separation (CS) state there is a clear barrier to separation of the Pent triplet excitons in Pent / SubPc cells which doesn't occur in the case of Pent / C_{60}. Due to the larger CS in comparison to the reference device, a larger V_{oc} can be achieved. Unfortunately, through the same method, the CS state for the Pent / ClAlPc device should also have a barrier to separation and indeed a larger V_{oc}. As the devices clearly show a strong pentacene contribution and a low V_{oc}, the only potential explanation is that there is a low lying LUMO level in ClAlPc that is aiding charge separation and limiting the V_{oc}. Previous work by Forrest *et al.* demonstrated a transfer of the Pentacene triplet excitons to ClAlPc and further dissociation at a C_{60} heterojunction in a cascade (or ternary) device, but as there is no C_{60} in these devices we can only assume separation at the Pent / ClAlPc interface.

In terms of degradation, the ITO / Pent / C_{60} devices, over a 24 hour period, degrade to 0 % efficiency due to large kinks appearing causing a fast degradation in all parameters. On replacing the C_{60}, the decrease in all parameters is reduced (quite

significantly when replaced with ClAlPc) but degradation in all parameters still occurs. The reduction in V_{oc} is predominately caused by a change in the work function of the ITO due to UV degradation. On introducing MoO_x as an interlayer, the kink near V_{oc} is removed and the overall degradation is slowed down. Unfortunately, the Pentacene layer and (sub)phthalocyanines are still affected by oxygen, moisture and heat and therefore methods of encapsulating are still crucial to solving the long term stability problems associated with OPV.

7.2. Future work

Currently the limitations in achieving much greater efficiencies in OPVs are small diffusion lengths, limited organic semiconducting materials, and the current electrodes as well as device stability. Through fully characterising the semiconductors, a variety of different device heterojunctions can be made with ideal parameters to manufacture high performance devices, whether that be single or multi – junction cells, to realistically achieve commercialisation.

Chlorination was shown to be a viable method to modifying the frontier orbitals and stability of current materials and although modification is a route forward, the need for new material classes should be priority. This work has also shown the use of typical donor (sub)phthalocyanines as acceptors, the need for a greater range of materials is paramount and to be sure of obtaining successful materials, fully understanding the current materials is vital.

An in depth study of mobility in small molecule semiconductors could shed some light on whether this factor should be considered in material design, perhaps trying to obtain high charge mobility materials is unnecessary? Investigating the charge carrier density, mobility vs field, thickness and temperature via different

techniques as well as device manufacture with a range of semiconductors with varied mobility would begin to answer this question.

The factors behind the V_{oc} in the pentacene cells discussed earlier (Pent / ClAlPc) are not yet fully understood and therefore more experiments are needed to determine the reasons behind this. Investigations into the triplet levels created in Pentacene, and the possibility of accessible levels in ClAlPc can be made using modelling techniques and rates of charge separation can be computed. The use of transient absorption spectroscopy (TAS) to investigate the emergence of singlet fission to create two triplets and the subsequent dissociation (or not so in some cases) would be extremely revealing and lend to explaining the strange behaviour of the Pent / ClAlPc cell and confirm the lack of contribution in Pent / SubPc cells. Through the use of careful optimization singlet fission devices with suitable acceptors could also potentially be used to improve J_{sc} and EQE efficiencies. Understanding our materials in greater detail is needed, as well as how they perform in devices under testing conditions. Transient photocurrent(voltage) measurements can provide insight into trapping / detrapping of charges in cells, and can also aid in explaining strange *J-V* behaviour, such as s-shaped kinks.

Improvements in cell stability were realised on the replacement of C_{60} with the (sub)phthalocyanines but the degradation mechanisms are not fully understood. Further work into oxygen and humidity testing as well as longer life time tests are necessary in order to understand the complex nature of the degradation. There is also a need for more realistic lifetime studies where the conditions are closer to actual outdoor testing conditions. The mechanisms in OPVs are still fruitfully discussed almost three decades after their initial invention and further information is needed in order to improve cell efficiencies past their theoretical limits.

THE END